Hydrocarbon Activation via Reversible 1,2-RH-Elimination from (^{t}Bu$_3$SiNH)$_3$ZrR: Synthetic, Structural, and Mechanistic Investigations

Christopher P. Schaller, Christopher C. Cummins, and Peter T. Wolczanski*

Contribution from the Department of Chemistry, Cornell University, Baker Laboratory, Ithaca, New York 14853

Received August 2, 1995[⊗]

Abstract: Hydrocarbyl complexes, (^{t}Bu$_3$SiNH)$_3$ZrR (**1**-R), were prepared via metatheses of (^{t}Bu$_3$SiNH)$_3$ZrCl (**1**-Cl) with RMgX or RLi (R = Me, Et, Cy, CH_2Ph, allyl, CH═CH_2, Ph, $CH_2{}^t$Bu, C≡CPh, C≡C^{t}Bu), through addition of isobutylene, H_2C═C═CMe_2, and acetylene to **1**-H (R = ^{i}Bu, dma, or CH═CH_2), and by CH-bond activation; thermal 1,2-RH-elimination from **1**-R produced putative (^{t}Bu$_3$SiNH)$_2$Zr═NSi^{t}Bu$_3$ (**2**), which was subsequently trapped by R′H. Thermolysis of **1**-R (∼100 °C, R = Me or Cy) in the presence of H_2, c-C_3H_6, and CH_4 in cyclohexane or neat C_6H_6, mesitylene, and toluene afforded **1**-R (R = H, ^{c}Pr, Me, Ph, CH_2-3,5-$Me_2C_6H_3$) and a mixture of **1**-CH_2Ph and **1**-C_6H_4Me, respectively. Exposure of **1**-Cy to C_2H_4 or C_6H_6 in cyclohexane provided **1**-CH═CH_2 or **1**-Ph, respectively, but further reaction produced **1**$_2$-(*trans*-HC═CH) and **1**$_2$-(*p*-C_6H_4) through double CH-bond activation. Thermolysis of (^{t}Bu$_3$SiND)$_3$ZrCH_3 (**1**-$(ND)_3$-CH_3) in C_6H_6 or C_6D_6 yielded CH_3D, and **1**C_6H_5 or **1**-$(ND)_3C_6D_5$, through reversible benzene activation. Thermolysis of **1**-Cy in neat cyclohexane, and with C_2H_6 or CMe_4 present, gave cyclometalation product (^{t}Bu$_3$SiNH)$_2$ZrNHSi^{t}Bu$_2$CMe_2CH_2 (**3**) and **1**-NHSi^{t}Bu$_3$. In THF, thermolysis of **1**-CH_3 afforded (^{t}Bu$_3$SiNH)$_2$-(THF)Zr═NSi^{t}Bu$_3$ (**2**-THF); at 25 °C, **1**-H lost H_2 in the presence of L (L = THF, Et_2O, NMe_3, PMe_3) generating **2**-L; **2**-L (L = Et_2O, py) was also prepared via ligand exchange with **2**-THF. Single crystal X-ray diffraction studies of **2**-THF revealed a pseudotetrahedral core, with a long Zr═N bond distance (1.978(8) Å), normal Zr−N(H) bond lengths (2.028(8), 2.031(8) Å), similar amide (154.7(5), 158.1(5)°) and imide (156.9(5)°) bond angles, and little O(pπ) → Zr(dπ) bonding. Crystal data: monoclinic, $P2_1/n$, a = 13.312(5) Å, b = 18.268(6) Å, c = 20.551(7) Å, β = 92.30(3)°, Z = 4, T = 25 °C. **2**-Et_2O thermally eliminated C_2H_4 to give **1**-OEt through γ-CH activation. Kinetic isotope effects (KIE) on 1,2-RD-elimination from **1**-$(ND)_3$-R (96.7 °C, R = CH_3, z_{Me} = 6.3(1); CH_2Ph, z_{Bz} = 7.1(6); Ph, z_{Ph} = 4.6(4)) and CD_3H loss from **1**-CD_3 ($k(CH_3)/k(CD_3) = (z'_{Me})^3$ = 1.32) revealed a symmetric H-transfer in a loose transition state. 1,2-RH-elimination rates follow: (96.7 °C, k_R ($\times 10^4$ s^{-1}) = 22.6(2), Ph; 15.5(2), ^{c}Pr; 13.2(4), CH═CH_2; 10.4(2), Cy; 3.21(6), Et; 3.2(1), ^{i}Bu; 1.3(1), dma; 1.51(6), H; 1.42(4), $CH_2{}^t$Bu; 1.06(2), Me; 0.34(2), CH_2-3,5-$Me_2C_6H_3$; 0.169(3), CH_2Ph). Competition for (^{t}Bu$_3$SiNH)$_2$Zr═NSi^{t}Bu$_3$ (**2**) by RH/R′H and equilibria provided information about the stabilities of **1**-R relative to **1**-^{c}Pr (R = ^{c}Pr (0.0 kcal/mol) < Ph (0.3) < CH_2Ph (0.7) < Me (1.2) < $CH_2{}^t$Bu (≥7.6) < Et (≥7.8) < Cy (≥10.9)). Transition state energies afforded relative C−H bond activation selectivities ($\Delta\Delta G^‡$ relative to ^{c}Pr-H): ^{c}PrH ≈ ArH (0.0 kcal/mol) > MeH (3.4) > PhCH_2H (4.0) > cyclometalation (≥8.5) > EtH (≥8.9) > ^{t}BuCH_2H (≥9.3) > CyH (≥11.2). A correlation of $\Delta G^‡$(1,2-RH-elimination) with D(R−H) indicated generally late transition states but suggested an earlier composition for the alkyls, as rationalized through a Hammond analysis. Correlation of $\Delta G^‡$(1,2-RH-elimination) with RH proton affinity implicated tight binding of RH in the transition state and possible RH-binding intermediates (**2**-RH). 1,2-HC≡CR-elimination from **1**-C≡CR was not observed, but second-order exchanges of **1**-C≡CPh with ^{t}BuC≡CH, and **1**-C≡C^{t}Bu with HC≡CPh were indicative of an associative pathway. All data can be accommodated by the following mechanism: **1**-R + R′H ⇌ **2**-RH + R′H ⇌ **2**-R′H + RH ⇌ **1**-R′ + RH; a variant where **2** mediates reversible **2**-RH + R′H exchange is less likely.

Introduction

The transition metal-mediated activation of carbon−hydrogen bonds has been a forefront area of organometallic research for over a decade.[1,2] In that time, a variety of electronically unsaturated metal complexes have accomplished the scission of a C−H bond through divergent pathways, which include (1) oxidative addition to late metal centers (i.e., L_nM + RH ⇌ L_n-HMR);[3,4] (2) late metal assisted heterolytic RH cleavage in polar media (i.e., L_nM + RH ⇌ $[L_nMR]^-$ + H^+);[5−7] 3) σ-bond metathesis by early metal,[8] lanthanide,[9−11] and cationic iridium[12]

[⊗] Abstract published in *Advance ACS Abstracts,* December 1, 1995.

(1) (a) *Activation and Functionalization of Alkanes*; Hill, C., Ed.; John Wiley & Sons: New York, 1989. (b) *Selective Hydrocarbon Activation*; Watson, P. L., Ed.; VCH Publishers: Toledo, OH, 1989. (c) Shilov, A. E. *Activation of Saturated Hydrocarbons by Transition Metal Complexes*; Reidel: Boston, 1984.

(2) (a) Crabtree, R. H.; *Chem. Rev.* **1985**, *85*, 245−269. (b) Bergman, R. G. *Science* **1984**, *223*, 902−908. (c) Graham, W. A. G. *J. Organomet. Chem.* **1986**, *300*, 81−91. (d) Green, M. L. H.; O'Hare, D. *Pure Appl. Chem.* **1985**, *57*, 1897−1910. (e) Halpern, J. *Inorg. Chim. Acta* **1985**, *100*, 41−48. (f) Crabtree, R. H.; Hamilton, D. G. *Adv. Organomet. Chem.* **1988**, *28*, 299−338. (g) Jones, W. D.; Feher, F. J. *Acc. Chem. Res.* **1989**, *22*, 99−106.

(3) Jones, W. D.; Hessell, E. T. *J. Am. Chem. Soc.* **1993**, *115*, 554−562 and references therein.

(4) For an example of a new system, see: Wang, C.; Ziller, J. W.; Flood, T. C. *J. Am. Chem. Soc.* **1995**, *117*, 1647−1648.

(5) (a) Lin, M.; Sen, A. *Nature* **1994**, *368*, 613−614. (b) Kao, L.-C.; Hutson, A. C.; Sen, A. *J. Am. Chem. Soc.* **1991**, *113*, 700−701. (c) Sen, A.; Gretz, E.; Oliver, T. F.; Jiang, Z. *New J. Chem.* **1989**, *13*, 755−760. (c) Sen, A. *Acc. Chem. Res.* **1988**, *21*, 421−428.

(6) (a) Luinstra, G. A.; Labinger, J. A.; Bercaw, J. E. *J. Am. Chem. Soc.* **1993**, *115*, 3004−3005. (b) Labinger, J. A.; Herring, A. M.; Lyon, D. K.; Luinstra, G. A.; Bercaw, J. E.; Horváth, I. T.; Eller, K. *Organometallics* **1993**, *12*, 895−905.

(7) Periana, R. A.; Taube, D. J.; Evitt, E. R.; Loffler, D. G.; Wentrcek, P. R.; Voss, G.; Masuda, T. *Science* **1993**, *259*, 340−343.

0002-7863/96/1518-0591$12.00/0

systems (i.e., $L_nMR + R'H \rightleftharpoons L_nMR' + RH$); (4) Hg* ($^3P_1$, $5d^{10}6s^16p^1$) sensitized C−H bond homolysis;[13] (5) attack on RH by Rh(II) porphyrins (i.e., 2(por)Rh + RH ⇌ (por)RhH + (por)-RhR),[14] and related, photochemically generated metalaradicals;[15] (6) H-atom abstractions by metal oxo derivatives,[16,17] including photochemical[18] and bioinorganic systems;[19] and (7) 1,2-RH-additions across M═X (X = O (R = OH, H,[20] R′NH),[21] NR,[21−29] CR_2)[30] multiple bonds.

These disparate systems can be roughly separated into two categories: radical C−H bond scissions with no apparent binding of RH (4, 5, and 6), and concerted processes where RH binding may play a significant role (1,[4,29−34] 2, 3, and 7). Within the latter group, the activation of C−H bonds by d^0 metal imido derivatives[21−27] is most intriguing. Isoelectronic oxo groups exhibit mostly radical-based activations, perhaps because the reactive functionality is typically bound to a coordinatively and/or electronically saturated metal center, and H-atom abstraction must occur at the periphery of the complex. The concerted nature of the metal imido derivatives suggests that their reactivity patterns are more complex and that the electrophilicity of the metal center plays a significant role in the attack of C−H bonds, just as in late metal systems. Adjacent to the reactive imido functionalities of transient $X_{3-n}M(═NSi^tBu_3)_n$ (X = $HNSi^tBu_3$, M = Ti, *n* = 1;[23] M = Zr, *n* = 1;[22,26] M = V,[27] Ta,[24] *n* = 2; X = OSi^tBu_3, M = Ti, *n* = 1)[25] and $Cp_2Zr═NR$[28,29] species are respective d_{z^2}/p_z and "d_{y^2}"/p_y (*z* axis along Zr═N) hybrid, empty orbitals oriented toward the C−H bond of an approaching substrate. Similar orbitals mediate *σ*-bond metathesis pathways in related d^0 and d^0f^n systems, but these second-order exchange processes[9] render possible R−H binding events difficult to detect by indirect methods.[37]

Scheme 1

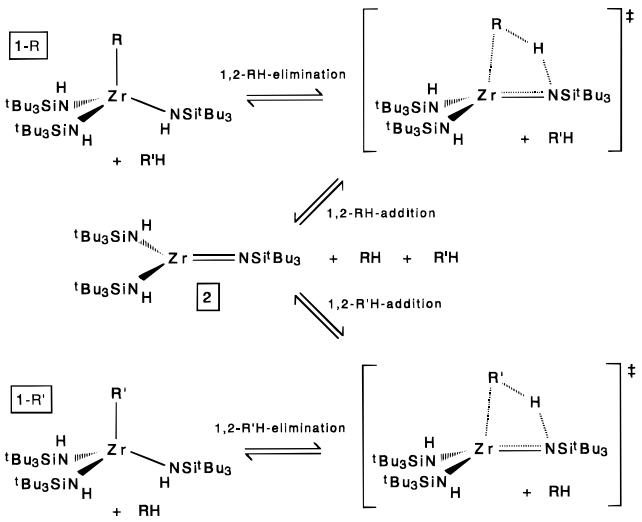

Current research in homogeneous C−H bond activation is proceeding along several fronts,[38] but themes of practical and fundamental nature stand out. In order to make use of a C−H bond activation event, catalysis of this transformation must be coupled with functionalization of the substrate. Radical based oxidations of hydrocarbons are the most common, but inherent problems of selectivity persist.[17] Electrophilic oxidation processes in aqueous and other polar media that provide greater opportunity for selective hydrocarbon conversion are under development,[5−7] and nonaqueous dehydrogenative methods also appear promising.[39] An earlier study featured functionalization of a C−H bond through an intramolecular isonitrile insertion.[40]

A fundamental understanding of the events that govern the activation of a C−H bond in each of the above systems is crucial to the design of future homogeneous, and perhaps heterogeneous, catalysts that can selectively activate hydrocarbons. Typical commercial hydrocarbon activations are autoxidations that are tantamount to a controlled burn.[41] Radical pathways promise some selectivity based on the relative C−H bond strengths, but even the radical-based, heterogeneously catalyzed oxidative coupling of methane is operationally restricted.[42]

Scheme 1 illustrates the general features of the C−H

(8) Guram, A. S.; Jordan, R. F.; Taylor, D. F. *J. Am. Chem. Soc.* **1991**, *113*, 1833−1835.
(9) Thompson, M. E.; Baxter, S. M.; Bulls, A. R.; Burger, B. J.; Nolan, M. C.; Santarsiero, B. D.; Schaefer, W. P.; Bercaw, J. E. *J. Am. Chem. Soc.* **1987**, *109*, 203−219.
(10) Watson, P. L.; Parshall, G. W. *Acc. Chem. Res.* **1985**, *18*, 51−56.
(11) Fendrick, C. M.; Marks, T. J. *J. Am. Chem. Soc.* **1986**, *108*, 425−437.
(12) Burger, P.; Bergman, R. G. *J. Am. Chem. Soc.* **1993**, *115*, 10462−10463.
(13) Muedas, C. A.; Ferguson, R. R.; Brown, S. H.; Crabtree, R. H. *J. Am. Chem. Soc.* **1991**, *113*, 2233−2242.
(14) (a) Wayland, B. B.; Ba, S.; Sherry, A. E. *J. Am. Chem. Soc.* **1991**, *113*, 5305−5311. (b) Zhang, X.-X.; Wayland, B. B. *J. Am. Chem. Soc.* **1994**, *116*, 7897−7898.
(15) Brown, S. N.; Mayer, J. M. *J. Am. Chem. Soc.* **1994**, *116*, 2219−2220.
(16) Cook, G. K.; Mayer, J. M. *J. Am. Chem. Soc.* **1994**, *116*, 1855−1868.
(17) For related oxidation processes, see: Sheldon, R. A.; Kochi, J. K. *Metal Catalyzed Oxidations of Organic Compounds*; Academic Press: New York, 1981.
(18) Jaynes, B. S.; Hill, C. L. *J. Am. Chem. Soc.* **1993**, *115*, 12212−12213.
(19) (a) Watanabe, Y.; Groves, J. T. In *The Enzymes*, 3rd ed.; Academic Press: New York, 1992. (b) Stewart, L. C.; Klinman, J. P. *Annu. Rev. Biochem.* **1988**, *57*, 551−592.
(20) Parkin, G.; Bercaw, J. E. *J. Am. Chem. Soc.* **1989**, *111*, 391−393.
(21) Howard, W. A.; Waters, M.; Parkin, G. *J. Am. Chem. Soc.* **1993**, *115*, 4917−4918.
(22) Cummins, C. C.; Baxter, S. M.; Wolczanski, P. T. *J. Am. Chem. Soc.* **1988**, *110*, 8731−8733.
(23) Cummins, C. C.; Schaller, C. P.; Van Duyne, G. D.; Wolczanski, P. T.; Chan, E. A.-W.; Hoffmann, R. *J. Am. Chem. Soc.* **1991**, *113*, 2985−2994.
(24) Schaller, C. P.; Wolczanski, P. T. *Inorg. Chem.* **1993**, *32*, 131−144 and references therein.
(25) Bennett, J. L.; Wolczanski, P. T. *J. Am. Chem. Soc.* **1994**, *116*, 2179−2180.
(26) Schaller, C. P.; Bonanno, J. B.; Wolczanski, P. T. *J. Am. Chem. Soc.* **1994**, *116*, 4133−4134.
(27) de With, J.; Horton, A. D. *Angew. Chem., Int. Ed. Engl.* **1993**, *32*, 903−905. Upon reassessment of the data in this paper, $\Delta S^{\ddagger}_{elim} \sim 8(23)$ eu, a value lacking the precision necessary for interpretation: Bennett, J. L.; Wolczanski, P. T., unpublished work.
(28) Walsh, P. J.; Hollander, F. J.; Bergman, R. G. *Organometallics* **1993**, *12*, 3705−3723.
(29) Lee, S. Y.; Bergman, R. G. *J. Am. Chem. Soc.* **1995**, *117*, 5877−5878.
(30) (a) McDade, C.; Green, J. C.; Bercaw, J. E. *Organometallics* **1982**, *1*, 1629−1634. (b) Chamberlain, L. R.; Rothwell, I. P.; Huffmann, J. C. *J. Am. Chem. Soc.* **1986**, *108*, 1502−1509. (c) Couturier, J.-L.; Paillet, C.; Leconte, M.; Basset, J. M.; Weiss, K. *Angew. Chem., Int. Ed. Engl.* **1992**, *31*, 628−631. (d) van der Heijden, H.; Hessen, B. *J. Chem. Soc., Chem. Commun.* **1995**, 145−146.
(31) (a) Wasserman, E. P.; Moore, C. B.; Bergman, R. G. *Science* **1992**, *255*, 315−318. (b) Weiller, B. H.; Wasserman, E. P.; Bergman, R. G.; Moore, C. B.; Pimentel, G. C. *J. Am. Chem. Soc.* **1989**, *111*, 8288−8290.
(32) Schultz, R. H.; Bengali, A. A.; Tauber, M. J.; Weiller, B. H.; Wasserman, E. P.; Kyle, K. R.; Moore, C. B.; Bergman, R. G. *J. Am. Chem. Soc.* **1994**, *116*, 7369−7377.
(33) Bengali, A. A.; Schultz, R. H.; Moore, C. B.; Bergman, R. G. *J. Am. Chem. Soc.* **1994**, *116*, 9585−9589.
(34) Periana, R. A.; Bergman, R. G. *J. Am. Chem. Soc.* **1986**, *108*, 7332−7346.
(35) (a) Buchanan, J. M.; Stryker, J. M.; Bergman, R. G. *J. Am. Chem. Soc.* **1986**, *108*, 1537−1550. (b) Bloyce, P. E.; Rest, A. J.; Whitwell, I. *J. Chem. Soc. Dalton Trans.* **1990**, 813−822.
(36) For methane complexes preceding elimination, see: (a) Parkin, G.; Bercaw, J.E. *Organometallics* **1989**, *8*, 1172−1179. (b) Gould, G. L.; Heinekey, D. M. *J. Am. Chem. Soc.* **1989**, *111*, 5502−5504. (c) Bullock, R. M.; Headford, C. E. L.; Hennessy, K. M.; Kegley, S. E.; Norton, J. R. *J. Am. Chem. Soc.* **1989**, *111*, 3897−3908.
(37) (a) Piers, W. E.; Shapiro, P. J.; Bunel, E. E.; Bercaw, J. E. *Synlett.* **1990**, 74−84. (b) Piers, W. E.; Bercaw, J. E. *J. Am. Chem. Soc.* **1990**, *112*, 9406−9407.

activation in the zirconium imido system, where 1,2-RH-elimination occurs from (^{t}Bu$_3$SiNH)$_3$ZrR (**1**-R) to generate the purported three-coordinate (^{t}Bu$_3$SiNH)$_2$Zr=NSi^{t}Bu$_3$ (**2**). The imido can then select to activate RH or R′H via 1,2-RH/R′H-addition across the Zr=N bond.[43,44] Herein is described the culmination of an eight year effort[22] to understand the fundamental nature of this process through synthetic, kinetics, isotope effects, thermodynamics, and structural[45] investigations.

Results and Discussion

Synthesis and Characterization. 1. (^{t}Bu$_3$SiNH)$_3$ZrR (R = H, BH$_4$, Alkyl, Aryl). Three different routes led to the preparation of hydride and hydrocarbyl *tris*-amido zirconium derivatives: metathesis of halides with alkyl anion equivalents, R−H bond activation (alkane/arene/H_2 metathesis), and olefin insertion. The procedures were usually not optimized, except for those that provided critical starting materials (**1**-Me, **1**-Cy) for ensuing mechanistic and reactivity studies. Although many of the reported isolated yields are modest, reactions that were monitored by ^{1}H NMR spectroscopy, typically those involving C−H bond activation or insertion, manifested conversions of >90%. Extreme solubilities of the monomeric hydride and hydrocarbyls have hampered their isolation. Table 1 lists the ^{1}H and ^{13}C{^{1}H} NMR spectral data for **1**-R; ^{1}H NMR spectra typically exhibit a prominent singlet ascribed to the three equivalent ^{t}Bu$_3$Si fragments, a broad singlet due to the amido protons, and resonances attributable to the remaining ligand.

Various hydrocarbyls were synthesized through treatment of (^{t}Bu$_3$SiNH)$_3$ZrCl (**1**-Cl)[45] with appropriate Grignard reagents RMgX in Et_2O at −78 °C, followed by stirring at 25 °C for 6−12 h. Recrystallization from hexanes afforded derivatives (^{t}Bu$_3$SiNH)$_3$ZrR (**1**-R, R = Me,[45] Et, Cy, CH_2Ph, Ph, CH=CH_2,

$$(^t\text{Bu}_3\text{SiNH})_3\text{ZrCl} + \underset{\textbf{1}\text{-Cl}}{} \quad \begin{matrix}\text{RMgX}\\ \text{X = Cl, R = Et}\\ \text{Cy}\\ \text{CH}_2\text{Ph}\\ \text{X = Br, R = Me}\\ \text{CH=CH}_2\\ \text{CH}_2\text{CH=CH}_2\\ \text{Ph}\end{matrix} \xrightarrow[-\text{MgXCl}]{\text{Et}_2\text{O, 25 °C, 6−12 h}} \underset{\begin{matrix}\textbf{1}\text{-Et, 77\%}\\ \textbf{1}\text{-Cy, 46\%}\\ \textbf{1}\text{-CH}_2\text{Ph, 35\%}\\ \textbf{1}\text{-Me, 91\%}\\ \textbf{1}\text{-CH=CH}_2\text{, 56\%}\\ \textbf{1}\text{-allyl, 32\%}\\ \textbf{1}\text{-Ph, 32\%}\end{matrix}}{(^t\text{Bu}_3\text{SiNH})_3\text{ZrR}} \quad (1)$$

allyl = CH_2CHCH_2) as colorless crystalline solids in 32−91% yield (eq 1). Evidence of agostic interactions[46] between the electrophilic zirconium center and any α-protons was not observed in either NMR or IR spectra. Infrared stretching absorptions corresponding to the NH functionality were found in a 3218−3280 cm^{-1} range of the spectrum, consistent with a relatively unperturbed ν(N-H).

Although alkyllithiums generally proved to be less efficient when directly compared with Grignard reagents (e.g., MeLi vs MeMgBr), in certain cases alkylations using RLi were simply more convenient. The addition of 1 equiv of ^{t}BuCH$_2$Li to **1**-Cl in hexanes at −78 °C, followed by stirring for 8 h at ambient temperature, generated colorless, crystalline **1**-CH$_2$^{t}Bu (eq 2).

$$\underset{\textbf{1}\text{-Cl}}{(^t\text{Bu}_3\text{SiNH})_3\text{ZrCl}} + {}^t\text{BuCH}_2\text{Li} \xrightarrow[-\text{LiCl}]{\text{hexanes, 25 °C, 8 h}} \underset{\textbf{1}\text{-CH}_2{}^t\text{Bu, 51\%}}{(^t\text{Bu}_3\text{SiNH})_3\text{ZrCH}_2{}^t\text{Bu}} \quad (2)$$

Similarly, (^{t}Bu$_3$SiNH)$_3$ZrCCPh (**1**-C$_2$Ph) was prepared by combining **1**-Cl and LiC≡CPh in THF at −78 °C then stirring for 8 h at 25 °C; crystallization from hexanes afforded an orange,

$$\underset{\textbf{1}\text{-Cl}}{(^t\text{Bu}_3\text{SiNH})_3\text{ZrCl}} + \text{PhC}{\equiv}\text{CLi} \xrightarrow[-\text{LiCl}]{\text{THF, 25 °C, 8 h}} \underset{\textbf{1}\text{-C}_2\text{Ph, 41\%}}{(^t\text{Bu}_3\text{SiNH})_3\text{ZrC}{\equiv}\text{CPh}} \quad (3)$$

$$\underset{\textbf{1}}{(^t\text{Bu}_3\text{SiNH})_3\text{ZrCl}} + {}^t\text{BuC}{\equiv}\text{CLi} \xrightarrow[-\text{LiCl}]{\text{C}_6\text{H}_6\text{, 25 °C, 4 h}} \underset{\textbf{1}\text{-C}_2{}^t\text{Bu, 81\%}}{(^t\text{Bu}_3\text{SiNH})_3\text{ZrC}{\equiv}\text{C}{}^t\text{Bu}} \quad (4)$$

microcrystalline solid (eq 3). The related yellow *tert*-butyl acetylide, (^{t}Bu$_3$SiNH)$_3$ZrCC^{t}Bu (**1**-C$_2$^{t}Bu), was synthesized from **1**-Cl and ^{t}BuC≡CLi in benzene (eq 4).

Treatment of (^{t}Bu$_3$SiNH)$_3$ZrCl (**1**-Cl) with 1 equiv of LiBH$_4$ at −78 °C in toluene, followed by 7 h at 25 °C, yielded the colorless borohydride complex (^{t}Bu$_3$SiNH)$_3$Zr(η^3-BH$_4$) (**1**-BH$_4$, eq 5). In the ^{1}H NMR spectrum of **1**-BH$_4$, a broad quartet at

$$\underset{\textbf{1}\text{-Cl}}{(^t\text{Bu}_3\text{SiNH})_3\text{ZrCl}} + \text{LiBH}_4 \xrightarrow[-\text{LiCl}]{\text{C}_7\text{H}_8\text{, 25 °C, 4 h}} \underset{\textbf{1}\text{-BH}_4\text{, 56\%}}{(^t\text{Bu}_3\text{SiNH})_3\text{Zr}(\eta^3\text{-BH}_4)} \quad (5)$$

δ 1.67 signified the presence of the BH$_4$ ligand, which was also observed as a quintet (J_{BH} = 81 Hz) in the ^{11}B NMR spectrum at δ −20.48. In the infrared spectrum of **1**-BH$_4$, a single sharp A_1 band in the terminal B−H stretching region at 2530 cm^{-1}, and two absorptions at 2210 and 2150 cm^{-1} due to the bridging B−H A_1 and E stretching modes, characterized the η^3-conformation.[47] Attempts to form a hydride complex from **1**-BH$_4$ through cleavage of the BH$_3$ group upon addition of Lewis bases (e.g., NH_3, NMe_3) were unsuccessful, as were additions of alternative hydride sources to chloride, **1**-Cl.

Activation of solvent cyclohexane by transient imido (^{t}Bu$_3$SiNH)$_2$Zr=NSi^{t}Bu$_3$ (**2**) has not been observed, hence thermolysis of (^{t}Bu$_3$SiNH)$_3$ZrR (**1**-R, R = Me, Cy) in C_6H_{12} permitted metathetical syntheses of new hydrocarbyls and convenient syntheses of several others. In cyclohexane, thermolysis of **1**-Cy at ∼100 °C for 8 h in the presence of ∼20 equiv of cyclopropane

(38) Arndtsen, B. A.; Bergman, R. G.; Mobley, T. A.; Peterson, T. H. *Acc. Chem. Res.* **1995**, *28*, 154−162.
(39) (a) Maguire, J. A.; Petrillo, A.; Goldman, A. S. *J. Am. Chem. Soc.* **1992**, *114*, 9492−9498. (b) Maguire, J. A.; Boese, W. T.; Goldman, A. S. *J. Am. Chem. Soc.* **1989**, *111*, 7088−7093. (c) Maguire, J. A.; Boese, W. T.; Goldman, M. E.; Goldman, A. S. *Coord. Chem. Rev.* **1990**, *97*, 179−192. (d) Sakakura, T.; Sodeyama, T.; Sasaki, K.; Wada, K.; Tanaka, M. *J. Am. Chem. Soc.* **1990**, *112*, 7221−7229.
(40) Jones, W. D.; Hessell, E. T. *Organometallics* **1990**, *9*, 718−727.
(41) Parshall, G. W.; Ittel, S. D. *Homogeneous Catalysis*; Wiley-Interscience: New York, 1992.
(42) Labinger, J. A. *Catal. Lett.* **1988**, *1*, 371−376.
(43) Cundari, T. R. *J. Am. Chem. Soc.* **1992**, *114*, 10557−10563.
(44) Cundari, T. R. *Organometallics* **1993**, *12*, 1998−2000.
(45) Cummins, C. C.; Van Duyne, G. D.; Schaller, C. P.; Wolczanski, P. T. *Organometallics* **1991**, *10*, 164−170.
(46) Brookhart, M.; Green, M. L. H.; Wong, L. *Prog. Inorg. Chem.* **1988**, *36*, 1−124.
(47) Marks, T. J; Kolb, J. R. *Chem. Rev.* **1977**, *77*, 263−293.

Table 1. ^{1}H and ^{13}C{1H} NMR Spectral Data for (^{t}Bu$_3$SiNH)$_3$ZrR (**1**-R) and (^{t}Bu$_3$SiNH)$_2$LZr=NSi^{t}Bu$_3$ (**2**-L) in C_6D_6 Unless Otherwise Noted

	^{1}H NMR (δ, assgmt, mult, J(Hz))			^{13}C NMR (δ, assgmt, J(Hz))		
compound	((H$_3$C)$_3$C)$_3$	NH	R	C(*C*H$_3$)$_3$	*C*(CH$_3$)$_3$	R
(^{t}Bu$_3$SiNH)$_3$ZrCl (**1**-Cl)	1.24	4.89		30.93	23.32	
(^{t}Bu$_3$SiNH)$_3$ZrH (**1**-H)	1.25	4.87	9.60 (H, s)	30.84	22.91	
(^{t}Bu$_3$SiNH)$_3$ZrMe (**1**-Me)	1.24	4.10	0.63 (CH$_3$, s)	30.92	23.24	28.68 (CH$_3$)
(^{t}Bu$_3$SiNH)$_3$ZrEt (**1**-Et)	1.25	3.94	1.77 (CH$_3$, t, 8)	30.92	23.13	43.78 (CH$_2$)
			(CH$_2$ obscured)			15.49 (CH$_3$)
(^{t}Bu$_3$SiNH)$_3$Zr^{i}Bu (**1**-^{i}Bu)	1.25	3.89	2.50 (CH, m)	30.93	23.22	65.17 (CH$_2$)
			1.39 (CH$_2$, d, 7)			31.27 (Me$_2$)
			1.27 (Me$_2$, d, 7)			28.90 (CH)
(^{t}Bu$_3$SiNH)$_3$Zr^{c}Pr (**1**-^{c}Pr)	1.25	3.83	0.75−1.00 (m)	31.23	23.31	
(in C_6D_{12})	1.18	3.77	0.87 (CH$_2$, ddd, 8, 5, 3)	31.21	23.62	34.95 (CH, 131)
			0.74 (CH$_2$, ddd, 10, 5, 3)			9.72 (CH$_2$, 161)
(^{t}Bu$_3$SiNH)$_3$ZrCy (**1**-Cy)	1.26	3.89	2.68 (CH$_2$, dm, 14)	30.92	23.15	68.23 (CH)
			1.98 (CH$_2$, quar d, 13, 3)			36.05 (CH$_2$)
			1.88 (CH$_2$, dt, 13, 3)			31.05 (CH$_2$)
			1.78 (CH, m)			28.02 (CH$_2$)
			1.43 (CH$_2$, quin t, 13, 3)			
			1.35 (CH$_2$, quin t, 13, 3)			
(^{t}Bu$_3$SiNH)$_3$Zr(η^3-H$_2$CCHCH$_2$)	1.23	4.18	6.61 (CH, quin, 11)	30.89	23.18	142.05 (CH, 147)
(**1**-allyl)						
			3.64 ((CH$_2$)$_2$, d, 11)			81.88 (CH$_2$, 136)
(^{t}Bu$_3$SiNH)$_3$Zr(η^3-H$_2$CCH=CMe$_2$)	1.25	4.06	6.08 (CH, t, 9)	31.04	23.23	138.75 (CH)
(**1**-dma)						
			2.22 (CH$_2$, d, 9)			121.41 (CMe$_2$)
			1.90 (Me, s)			54.55 (ZrCH$_2$)
			1.83 (Me, s)			18.24 (Me)
(^{t}Bu$_3$SiNH)$_3$ZrCH$_2$^{t}Bu	1.27	3.79	1.66 (Me$_3$C, s)	31.03	23.23	74.24 (CH$_2$)
(**1**-CH$_2$^{t}Bu)			1.32 (CH$_2$, s)			35.59 ((H$_3$*C*)$_3$C)
						34.48 (Me$_3$*C*)
(^{t}Bu$_3$SiNH)$_3$ZrCH=CH$_2$	1.25	4.34	7.65 (CH, dd, 17, 22)	30.98	23.23	183.54 (CH)
(**1**-CH=CH$_2$)			6.30 (CH$_t$, dd, 4.5, 22)			134.8 (CH$_2$)
			6.63 (CH$_c$, dd, 4.5, 17)			
[(^{t}Bu$_3$SiNH)$_3$Zr]$_2$	1.23	3.94	8.9 (CH, s)			
(μ_2:η^1,η^1-*trans*-C$_2$H$_2$)						
(**1**$_2$-C$_2$H$_2$ in C_6D_{12})						
(^{t}Bu$_3$SiNH)$_3$ZrPh (**1**-Ph)	1.25	4.50	8.28 (Ph(*o*), dm, 7)	31.27	23.67	180.29 (C$_{ipso}$)
			7.31 (Ph(*m*), tm, 7)			138.77 (Ph)
			7.17 (Ph(*p*), tm, 7)			128.60 (Ph)
						127.18 (Ph)
(^{t}Bu$_3$SiNH)$_3$Zr]$_2$	1.16	4.18	7.72 (Ar, s)	31.29	23.65	183.01 (C$_{ipso}$)
(μ_2:η^1,η^1-1,4-C$_6$H$_4$)						136.61 (Ar)
(**1**$_2$-C$_6$H$_4$ in C_6D_{12})						
(^{t}Bu$_3$SiNH)$_3$ZrCH$_2$Ph	1.21	4.14	7.10−7.43 (Ar(2H), m)	30.90	23.15	148.97 (C$_{ipso}$)
(**1**-CH$_2$Ph)			6.81−6.92 (Ar(3H), m)			129.05 (Ar)
			2.83 (CH$_2$, s)			126.87 (Ar)
						121.86 (Ar)
						58.65 (CH$_2$, 119)
(^{t}Bu$_3$SiNH)$_3$Zr-CH$_2$C$_6$H$_3$-3,5-Me$_2$	1.22	4.06	6.96 (Ar(2H), s)	30.93	23.16	148.48 (C$_{ipso}$)
(**1**-Mes)						
			6.50 (Ar(1H), s)			138.16 (Ar)
			2.84 (CH$_2$, s)			124.96 (Ar)
			2.23 (Me$_2$, s)			124.18 (Ar)
						59.89 (CH$_2$)
						21.55 (Me$_2$)
(^{t}Bu$_3$SiNH)$_3$ZrCCPh	1.32	4.86	7.56 (Ph(2H), m)			
(**1**-CCPh)			6.95 (Ph(3H), m)			
(^{t}Bu$_3$SiNH)$_3$ZrCC^{t}Bu	1.29	4.57	1.21 (Me$_3$C, s)	31.03	23.34	117.92 (ZrC)
(**1**-CC^{t}Bu)						104.33 (C^{t}Bu)
						31.44 ((H$_3$*C*)$_3$C)
						30.93 (Me$_3$*C*)
(^{t}Bu$_3$SiNH)$_3$Zr(η^3-BH$_4$)	1.23	4.68	1.67 (BH$_4$, br quar)	30.94	23.33	^{11}B NMR δ −20.48
(**1**-BH$_4$ in C_6D_{12})						(η^3-BH$_4$, quin,
						J_{BH} = 81 Hz)
(^{t}Bu$_3$SiNH)$_3$ZrOCH$_2$CH$_3$	1.25	3.54	4.12 (OCH$_2$, q, 7)	31.03	23.26	67.69 (OCH$_2$)
(**1**-OEt)			1.21 (CH$_3$, t, 7)			19.79 (CH$_3$)
(^{t}Bu$_3$SiNH)$_4$Zr (**1**-NHSi^{t}Bu)	1.28	3.42		31.27	23.34	
(^{t}Bu$_3$SiNH)$_2$ZrNHSi^{t}BuCMe$_2$CH$_2$ (**3**)	1.24	3.97 (2H)	1.57 (Me$_2$, s)	31.04	23.13	74.89 (CH$_2$)
		3.67 (1H)	1.42 (CH$_2$, s)			35.34 (C(*C*H$_3$)$_2$)
			1.22 (Me$_3$C, s)			30.17 ((SiC(*C*H$_3$)$_3$)$_2$)
						23.49 ((Si*C*(CH$_3$)$_3$)$_2$)
						23.32 (*C*(CH$_3$)$_2$)
(^{t}Bu$_3$SiNH)$_2$(THF)	1.29	3.85	4.02 (OCH$_2$, m)	31.16	23.10	76.77 (OCH$_2$)
Zr=NSi^{t}Bu (**2**-THF)	1.44		1.13 (CH$_2$, m)	31.83	24.09	25.22 (CH$_2$)
(^{t}Bu$_3$SiNH)$_2$(Et$_2$O)	1.29	3.83	3.93 (OCH$_2$, quar, 7)	31.14	23.13	69.99 (OCH$_2$)
Zr=NSi^{t}Bu$_3$) (**2**-OEt$_2$)	1.42		0.82 (CH$_3$, t, 7)	31.61	24.10	13.16 (CH$_3$)
(^{t}Bu$_3$SiNH)$_2$(Me$_3$N)	1.27	3.80	2.36 (Me$_3$, s)			
Zr=NSi^{t}Bu$_3$ (**2**-NMe$_3$)	1.42					
(^{t}Bu$_3$SiNH)$_2$(Me$_3$P)	1.26	4.36	1.02 (Me$_3$, d, 7)			
Zr=NSi^{t}Bu$_3$ (**2**-PMe$_3$)	1.42					
(^{t}Bu$_3$SiNH)$_2$(py)	1.30	4.18	8.89 (py(*o*), m)			
Zr=NSi^{t}Bu$_3$ (**2**-py)	1.44		6.69 (py(*p*), m)			
			6.44 (py(*m*), m)			

provided (^{t}Bu$_3$SiNH)$_3$Zr(c-C$_3$H$_5$) (**1**-^{c}Pr, eq 6). Inspection of isolated, colorless **1**-^{c}Pr by ^{1}H NMR spectroscopy revealed

$$(^t\mathrm{Bu_3SiNH})_3\mathrm{ZrCy}\ (\mathbf{1}\text{-Cy}) + \text{c-}C_3H_6\ (\text{excess}) \xrightarrow[100\ ^\circ\mathrm{C},\ 8\ \mathrm{h}]{C_6H_{12}} (^t\mathrm{BuSiNH})_3\mathrm{Zr(c\text{-}C_3H_5)}\ (\mathbf{1}\text{-}^c\mathrm{Pr},\ 35\%) + \mathrm{CyH} \quad (6)$$

$$\mathbf{1}\text{-Cy} + CH_4\ (4\ \mathrm{atm}) \xrightarrow[100\ ^\circ\mathrm{C},\ 8\ \mathrm{h}]{C_6D_{12}} (^t\mathrm{Bu_3SiNH})_3\mathrm{ZrMe}\ (\mathbf{1}\text{-Me}) + \mathrm{CyH} \quad (7)$$

impurities that amounted to ~5% of the ^{t}Bu region; the principal byproduct was determined to be (^{t}Bu$_3$SiNH)$_4$Zr (**1**-NHSi^{t}Bu$_3$). In a sealed NMR tube, **1**-Cy was heated (~100 °C, 8 h) with CH_4 (4 atm) in C_6D_{12} to produce (^{t}Bu$_3$SiNH)$_3$ZrMe (**1**-Me) in essentially quantitative yield (eq 7).

1,2-Elimination of MeH (100 °C, 8 h) from **1**-Me (eq 8) in the presence of H_2 (4 atm) afforded (^{t}Bu$_3$SiNH)$_3$ZrH (**1**-H), a consequence of dihydrogen addition across the imido ligand of

$$(^t\mathrm{Bu_3SiNH})_3\mathrm{ZrMe}\ (\mathbf{1}\text{-Me}) + H_2\ (4\ \mathrm{atm}) \xrightarrow[100\ ^\circ\mathrm{C},\ 8\ \mathrm{h}]{C_6H_{12},} (^t\mathrm{Bu_3SiNH})_3\mathrm{ZrH}\ (\mathbf{1}\text{-H},\ 62\%) + \mathrm{MeH} \quad (8)$$

putative intermediate **2**. The terminal hydride of **1**-H exhibited a resonance at δ 9.60 in its ^{1}H NMR spectrum, and an IR stretch at 1553 cm^{-1} (ν(ZrD) = 1117 cm^{-1}).[45] Hydride **1**-H could be similarly derived from (^{t}Bu$_3$SiNH)$_3$ZrPh (**1**-Ph) and H_2 in cyclohexane-d_{12}.

Thermolysis of (^{t}Bu$_3$SiNH)$_3$ZrMe (**1**-Me) at ~100 °C for 7 h in benzene or mesitylene afforded the respective phenyl, **1**-Ph, and mesityl, (^{t}Bu$_3$SiNH)$_3$Zr-CH$_2$C$_6$H$_3$Me$_2$ (**1**-Mes) derivatives (eq 9). A similar experiment in toluene led to a mixture of benzyl (**1**-CH$_2$Ph), and *para*- and *meta*-aryl products (eq 10)

$$(^t\mathrm{Bu_3SiNH})_3\mathrm{ZrMe}\ (\mathbf{1}\text{-Me}) \xrightarrow[100\ ^\circ\mathrm{C},\ 7\ \mathrm{h}]{\mathrm{RH}} (^t\mathrm{Bu_3SiNH})_3\mathrm{ZrR}\ (\mathrm{R} = \mathrm{Ph},\ \mathbf{1}\text{-Ph},\ 59\%;\ \mathrm{CH_2C_6H_3Me_2},\ \mathbf{1}\text{-Mes},\ 62\%) + \mathrm{MeH} \quad (9)$$

$$\mathbf{1}\text{-Me} \xrightarrow[100\ ^\circ\mathrm{C},\ 9\ \mathrm{h}]{C_7H_8} (^t\mathrm{Bu_3SiNH})_3\mathrm{ZrCH_2Ph}\ (\mathbf{1}\text{-CH}_2\mathrm{Ph}) + (^t\mathrm{Bu_3SiNH})_3\mathrm{ZrR'}\ (\mathrm{R'} = p\text{-}C_6H_4\mathrm{Me},\ m\text{-}C_6H_4\mathrm{Me};\ \mathbf{1}\text{-}C_6H_4\mathrm{Me}) + \mathrm{MeH} \quad (10)$$

whose relative composition changed with time (*vide infra*). Since the *para*:*meta* ratio of roughly 2:1 was relatively stable over the 9 h thermolysis, the aryl products were treated together (**1**-C$_6$H$_4$Me) in ensuing studies.

When the cyclohexyl or methyl derivatives **1**-Cy and **1**-Me were thermolyzed at ~100 °C in cyclohexane in the absence of added substrate, alkane extrusion ultimately led to the formation of ^{t}Bu$_3$SiNH$_2$, tetraamide (^{t}Bu$_3$SiNH)$_4$Zr (**1**-NHSi^{t}Bu$_3$), and an intramolecular C−H activation product, (^{t}Bu$_3$SiNH)$_2$ZrNHSi^{t}Bu$_2$CMe$_2$CH$_2$ (**3**), among other, uncharacterized products (eq 11). Attempts to activate ethane in cyclohexane produced similar results, a clear indication that activation of C−H bonds by the three-coordinate intermediate, (^{t}Bu$_3$SiNH)$_2$Zr=NSi^{t}Bu$_3$ (**2**), was quite selective. The cyclometalated derivative was most conveniently prepared via solid state

$$(^t\mathrm{Bu_3SiNH})_3\mathrm{ZrR} \xrightarrow[100\ ^\circ\mathrm{C},\ 3\ \mathrm{h}]{C_6D_{12},\ -\mathrm{RH}} (^t\mathrm{Bu_3SiNH})_2\mathrm{ZrNHSi^tBu_2CMe_2CH_2}\ (\mathbf{3}) + (^t\mathrm{Bu_3SiNH})_4\mathrm{Zr}\ (\mathbf{1}\text{-NHSi}^t\mathrm{Bu_3}) + {}^t\mathrm{Bu_3SiNH_2} + \ldots \quad (11)$$

$$(^t\mathrm{Bu_3SiNH})_3\mathrm{ZrMe}\ (\mathbf{1}\text{-Me}) \xrightarrow[10\ \mathrm{h}]{125\ ^\circ\mathrm{C}} (^t\mathrm{Bu_3SiNH})_2\mathrm{ZrNHSi^tBu_2CMe_2CH_2}\ (\mathbf{3}) + \mathrm{MeH} \quad (12)$$

thermolysis of the methyl (**1**-Me) at 125 °C in dynamic vacuum (eq 12). In this fashion the colorless "tuck-in" (**3**) formed with only ~5% of the tetraamide (**1**-NHSi^{t}Bu$_3$) as a byproduct.

(^{t}Bu$_3$SiNH)$_3$ZrPh (**1**-Ph) also proved to be a surprisingly good substrate for C−H bond activation when (^{t}Bu$_3$SiNH)$_3$ZrCy (**1**-Cy) was thermolyzed (~100 °C, ~3 h) in cyclohexane (eq 13).

$$(^t\mathrm{Bu_3SiNH})_3\mathrm{ZrCy}\ (\mathbf{1}\text{-Cy}) + (^t\mathrm{Bu_3SiNH})_3\mathrm{ZrPh}\ (\mathbf{1}\text{-Ph}) \xrightarrow[100\ ^\circ\mathrm{C},\ 3\ \mathrm{h}]{C_6D_{12},\ -\mathrm{CyH}} [(^t\mathrm{Bu_3SiNH})_3\mathrm{Zr}]_2(\mu_2{:}\eta^1,\eta^1\text{-1,4-}C_6H_4)\ (\mathbf{1}_2\text{-}C_6H_4) + (^t\mathrm{Bu_3SiNH})_2\mathrm{ZrNHSi^tBu_2CMe_2CH_2}\ (\mathbf{3}) \quad (13)$$

At ~80% conversion, the principal product (~90%) of the sealed NMR tube reaction was [(^{t}Bu$_3$Si-NH)$_3$Zr]$_2$(μ_2:η^1,η^1-1,4-C$_6$H$_4$) (**1**$_2$-C$_6$H$_4$), manifesting a di-*p*-activation of the benzene ring.[24,48] The colorless *para*-dizirconabenzene complex (**1**$_2$-C$_6$H$_4$) was sparingly soluble, partially crystallizing from the C_6D_{12} solution (0.65 mL) where the initial [Zr] ~ 0.05 mM.

Attempts to cleanly prepare (^{t}Bu$_3$SiNH)$_3$ZrCH=CH$_2$ (**1**-CH=CH$_2$) afforded similar results. In a sealed NMR tube, (^{t}Bu$_3$SiNH)$_3$ZrMe (**1**-Me) was exposed to 10 equiv of ethylene in cyclohexane-d_{12}. After sitting at 25 °C for 2 wk, the accumulation of a white precipitate was noted, but ^{1}H NMR spectroscopy indicated that **1**-Me and C_2H_4 were still present. Upon thermolysis at ~100 °C, **1**-CH=CH$_2$ appeared during the course of 1 h (~24%), but was accompanied by 6% [(^{t}Bu$_3$SiNH)$_3$Zr]$_2$(μ_2:η^1,η^1-*trans*-C$_2$H$_2$) (**1**$_2$-C$_2$H$_2$), the doubly activated dizirconaethylene complex. After ~8 h, the ratio (by metal) of **1**-CH=CH$_2$:**1**$_2$-C$_2$H$_2$ was 58:42, only 4% of the starting

$$(^t\mathrm{Bu_3SiNH})_3\mathrm{ZrMe}\ (\mathbf{1}\text{-Me}) + H_2C{=}CH_2\ (\text{excess}) \xrightarrow[100\ ^\circ\mathrm{C},\ 8\ \mathrm{h}]{C_6D_{12},\ -\mathrm{MeH}} [(^t\mathrm{Bu_3SiNH})_3\mathrm{Zr}]_2(\mu_2{:}\eta^1,\eta^1\text{-}\textit{trans}\text{-}C_2H_2)\ (\mathbf{1}_2\text{-}C_2H_2) + (^t\mathrm{Bu_3SiNH})_3\mathrm{ZrCH{=}CH_2}\ (\mathbf{1}\text{-CH{=}CH}_2) + \ldots \quad (14)$$

methyl complex remained, and the remaining ethylene had been completely converted to polyethylene, assumed to be the white precipitate (eq 14). Still seeking an alternative preparation of **1**-CH=CH$_2$, (^{t}Bu$_3$SiNH)$_3$ZrH (**1**-H) was treated with excess (4 equiv) acetylene in C_6D_6, and the vinyl complex (**1**-CH=CH$_2$) formed immediately with concomitant polyacetylene (eq 15). Its subsequent thermolysis (C_6D_{12}, 100 °C, 2 h) in another sealed NMR tube again produced the dizirconaethylene species **1**$_2$-

$$(^t\mathrm{Bu_3SiNH})_3\mathrm{ZrH}\ (\mathbf{1}\text{-H}) + HC{\equiv}CH\ (\text{excess}) \xrightarrow[25\ ^\circ\mathrm{C},\ 5\ \mathrm{min}]{C_6D_6} (^t\mathrm{Bu_3SiNH})_3\mathrm{ZrCH{=}CH_2}\ (\mathbf{1}\text{-CH{=}CH}_2) \quad (15)$$

$$\mathbf{1}\text{-}CH{=}CH_2 \xrightarrow[100\ ^\circ C,\ 2\ h]{C_6D_{12}} [(^tBu_3SiNH)_3Zr]_2(\mu_2{:}\eta^1,\eta^1\text{-}trans\text{-}C_2H_2) + \ldots \quad (16)$$
$$\mathbf{1}_2\text{-}C_2H_2$$

C_2H_2 (eq 16). Trace amounts of an olefin polymerization catalyst apparently coexist with the identifiable zirconium amides. When ethylene is released from **1**-CH=CH_2 in a 1,2-elimination event, transient imido ($^tBu_3SiNH)_2Zr{=}NSi^tBu_3$ (**2**) may recapture it or activate the *trans* vinylic position in **1**-CH=CH_2. Since the polymerization reaction drains away C_2H_4, the major product becomes $\mathbf{1}_2$-C_2H_2, which is assumed to be *trans* on the basis of molecular models.

Insertion of isobutylene into the zirconium−hydride bond of *in situ* generated ($^tBu_3SiNH)_3ZrH$ (**1**-H) occurred swiftly at 25 °C in hexane solution under 0.5 atm isobutylene to give the isobutyl complex ($^tBu_3SiNH)_3ZrCH_2CHMe_2$ (**1**-^{i}Bu), which was isolated in poor yield (eq 17). Although the reaction was clean

$$(^tBu_3SiNH)_3ZrH + Me_2C{=}CH_2\ (0.5\ atm) \xrightarrow[hexane]{25\ ^\circ C,\ 20\ min} (^tBu_3SiNH)_3ZrCH_2CHMe_2 \quad (17)$$
$$\mathbf{1}\text{-}H \qquad\qquad \mathbf{1}\text{-}^i\text{Bu},\ 15\%$$

$$\mathbf{1}\text{-}H + H_2C{=}C{=}CMe_2 \xrightarrow[benzene]{25\ ^\circ C,\ 3\ h} (^tBu_3SiNH)_3ZrCH_2CH{=}CMe_2 \quad (18)$$
$$\mathbf{1}\text{-dma},\ 24\%$$

(>90%) when conducted in a sealed NMR tube, the extreme solubility of **1**-^{i}Bu hampered crystallization and isolation efforts. Exposure of **1**-H to 3-methyl-1,2-butadiene (1,1-dimethylallene) yielded the highly soluble, hindered allyl derivative, ($^tBu_3SiNH)_3ZrCH_2CH{=}CMe_2$ (**1**-dma, dma = 3,3-dimethylallyl, 24%) (eq 18).

NMR spectra of allyl derivatives ($^tBu_3SiNH)_3Zr(CH_2CHCH_2)$ (**1**-allyl) and ($^tBu_3SiNH)_3$-$ZrCH_2CH{=}CMe_2$ (**1**-dma) differed significantly in appearance. The $^{13}C\{^1H\}$ NMR spectrum of **1**-allyl revealed shifts of δ 142.05 and δ 81.88 for the respective central and terminal η^3-allyl carbons. The central proton resonates as a quintet at δ 6.61 (J = 11 Hz) in the ^1H NMR spectrum, while the syn and anti protons appear as a doublet at δ 3.64 (J = 11 Hz), indicative of an η^3-allyl undergoing rapid syn/anti exchange.[49] In contrast, **1**-dma is best construed as an η^1-allyl, since its $^{13}C\{^1H\}$ spectrum exhibits olefinic resonances at δ 121.41 and 138.75, accompanied by the $ZrCH_2-$ carbon at δ 54.55, and methyl constituents at δ 18.24 and 26.39. In the ^1H NMR spectrum, methyl singlets at δ 1.83 and 1.90 are accompanied by a $ZrCH_2-$ doublet at δ 2.22 (J = 9 Hz) and a vinylic triplet at δ 6.08 (J = 9 Hz). An asymmetric η^3-allyl, even one dimethylated as in **1**-dma, is not expected to display signals of the dispersity noted in the ^{13}C NMR spectrum, and the resonances of the methylene are clearly more consistent with an η^1-, rather than η^3-allylic $ZrCH_2-$ unit. Moreover, molecular models strongly suggest that an η^3-disposition of the dma ligand could not be accommodated by the "pocket" formed by the probable C_3 disposition[45] of the amides in the ($^tBu_3SiNH)_3Zr$ moiety.

Correlations of NH shift vs R-substituent σ- and π-donation to zirconium were not evident in ^1H NMR spectra of ($^tBu_3$-$SiNH)_3ZrCl$ (**1**-Cl), ($^tBu_3SiNH)_3ZrR$ (**1**-R, R = H, BH_4, hydrocarbyl), and ($^tBu_3SiNH)_4Zr$ (**1**-$NHSi^tBu_3$), in contrast to a correspondence between downfield NH shifts and a more electrophilic metal center in a related titanium system.[23] Minor trends in NH stretching frequencies were provided by infrared studies of ($^tBu_3SiNH)_3ZrR$ (**1**-R), along with useful fingerprint information. The relatively wide range of ν(N-H) (3218−3280 cm^{-1}) was indicative of a subtle interplay between the N($p\pi$) → Zr($d\pi$) interaction and the R-substituent, whose steric bulk and electronegativity presumably influence the sp^2 character of the amide nitrogen. Partial disruption of N($p\pi$) → Zr($d\pi$) donation should lessen the stretching frequency of the NH by slightly diminishing its sp^2 character. Large hydrocarbyl ligands (e.g., $CH_2{}^tBu$ (3221 cm^{-1}), ^{i}Bu (3228), dma (3238), Cy (3230), Mes (3234), CH_2Ph (3238), Ph (3239)) possess roughly lower ν(N-H) than corresponding small substituents (e.g., H (3280 cm^{-1}), Me (3242), ^{c}Pr (3245), CH=CH_2 (3245), Et (3248), C_2-Ph (3258), $C_2{}^tBu$ (3265)). Subtle, yet significant steric influences on the ^{t}Bu periphery of the *tris*-amide coordination sphere may slightly distort the $ZrNHSi^tBu_3$ linkages, perhaps lessening amide π-bonding. More electronegative functionalities, such as Cl (3255 cm^{-1}) and the acetylides, may promote a slight increase in N($p\pi$) → Zr($d\pi$) donation relative to the hydrocarbyl ligands. Tetraamide **1**-$NHSi^tBu_3$ represents an anomaly; although more electronegative than the majority of the R groups, its tremendous size and competing amide π-donation are reflected in the lowest frequency observed, 3218 cm^{-1}. The hydride, **1**-H, manifests almost no steric influence and represents the highest member of the series (3280 cm^{-1}), despite the lesser electronegativity accorded H in respect to its hydrocarbyl cognates.

2. ($^tBu_3SiNH)_2LZr{=}NSi^tBu_3$. *Bis*-amidoimido adducts ($^tBu_3SiNH)_2LZr{=}NSi^tBu_3$ (**2**-L) were obtained via 1,2-elimination reactions of appropriate precursor complexes. Spectral characteristics of the compounds, some of which were only prepared *in situ* on an NMR tube scale, are listed in Table 1.

Thermolysis of ($^tBu_3SiNH)_3ZrMe$ (**1**-Me) at 100 °C for 10 h in THF, followed by precipitation from hexanes at −78 °C, afforded ($^tBu_3SiNH)_2$(THF)$Zr{=}NSi^tBu_3$ (**2**-THF) as a colorless

$$(^tBu_3SiNH)_3ZrMe \xrightarrow[100\ ^\circ C,\ \sim 1\ h]{THF} (^tBu_3SiNH)_2(THF)Zr{=}NSi^tBu_3 + MeH \quad (19)$$
$$\mathbf{1}\text{-Me} \qquad\qquad \mathbf{2}\text{-THF},\ 81\%$$

powder in 81% yield (eq 19). The reaction conditions are reminiscent of those observed in hydrocarbon metatheses involving **1**-R, suggesting that the THF ligand trapped transient ($^tBu_3SiNH)_2Zr{=}NSi^tBu_3$ (**2**) subsequent to 1,2-elimination of MeH. Adduct **2**-THF was also synthesized on a preparative scale from ($^tBu_3SiNH)_3ZrPh$ (**1**-Ph) and was routinely produced and isolated in surprisingly good purity starting from vestiges of the hydrocarbyl (**1**-R) syntheses.

Adduct formation appeared to occur in a distinctly different fashion when ($^tBu_3SiNH)_3ZrH$ (**1**-H)[45] was employed as the imide source. Exposure of **1**-H to L (L = THF, Et_2O, NMe_3, PMe_3) at 25 °C in sealed NMR tubes led to the immediate evolution of H_2, producing ($^tBu_3SiNH)_2LZr{=}NSi^tBu_3$ (**2**-L, L = THF, Et_2O, NMe_3, PMe_3) in near quantitative yields according to ^1H NMR (eq 20). The procedure was easily scaled up; using

$$(^tBu_3SiNH)_3ZrH + L \xrightarrow[25\ ^\circ C,\ <5\ m]{C_6D_6} (^tBu_3SiNH)_2LZr{=}NSi^tBu_3 + H_2 \quad (20)$$
$$\mathbf{1}\text{-H} \qquad\qquad \mathbf{2}\text{-L},\ L = THF,\ Et_2O,\ NMe_3,\ PMe_3$$

the dregs from a synthesis of **1**-H as starting material, the

(48) (a) Hunter, A. D.; Szigety, A. B. *Organometallics* **1989**, *8*, 2670−2679. (b) Chukwu, R.; Hunter, A. D.; Santarsiero, B. D.; Bott, S. G.; Atwood, J. L.; Chassaignac, J. *Organometallics* **1992**, *11*, 589−597.

(49) Collman, J. P.; Hegedus, L. S.; Norton, J. R.; Finke, R. G. *Principles and Applications of Organotransition Metal Chemistry*; University Science Books: Mill Valley, CA, 1987.

Table 2. Crystallographic Data for (^{t}Bu$_3$SiNH)$_2$(THF)Zr=NSi^{t}Bu$_3$ (**2**-THF)

formula: $C_{40}H_{91}N_3OSi_3Zr$	a = 13.312(5) Å
formula weight: 805.67	b = 18.268(6) Å
space group: $P2_1/n$	c = 20.551(7) Å
crystal dimensions: 0.3 × 0.3 × 0.3 mm	β = 92.30(3)°
μ = 3.14 cm^{-1} (no absorption correction)	V = 4994(3) Å^3
Nicolet R3m/V: 2θ range: 0−45° (±h, k, l)	Z = 4
reflections: 7135	T = 25 °C
independent reflections: 6557 (R_{int} = 3.64%)	λ = 0.71069 Å (Mo K$_\alpha$)
reflections ($F > 3\sigma(F)$): 4675	ρ_{calc} = 1.072 g/cm^3
R = 7.70%; R_w = 9.12% (4675 reflections)	
$w^{-1} = \sigma^2(F) + 0.0015F^2$)	GOF = 1.46 (4675 reflections)

addition of Et_2O produced **2**-OEt$_2$ in ∼45% isolated yield after crystallization. Unfortunately, since **1**-H remained one of the more difficult derivatives to prepare, the production of imido adducts via 1,2-dihydrogen elimination possessed limited utility. By monitoring a sealed NMR tube of **2**-OEt$_2$ and dihydrogen

$$(^t\text{Bu}_3\text{SiNH})_2(\text{Et}_2\text{O})\text{Zr}{=}\text{NSi}^t\text{Bu}_3 + \text{H}_2 \underset{25\ °C}{\overset{C_6D_6}{\rightleftharpoons}} (^t\text{Bu}_3\text{SiNH})_3\text{ZrH} + \text{Et}_2\text{O} \quad (21)$$

2-OEt$_2$ **1**-H

(∼3 atm), equilibration with **1**-H and Et_2O was noted over the course of 19 days (eq 21). Through direct integration of all components, a rough K_{eq}(25 °C) of 4.7 ($\Delta G°$ = −0.9 kcal/mol, all species 1 M standard states) was obtained.

The displacement of THF from **2**-THF by another ligand occurred with facility provided L was a stronger Lewis base. Exposure of **2**-THF in C_6D_6 to 1.0 of equiv pyridine in a sealed NMR tube (eq 22) caused the immediate formation of (^{t}Bu$_3$SiNH)$_2$(py)Zr=NSi^{t}Bu$_3$ (**2**-py) and concomitant free THF, as

$$(^t\text{Bu}_3\text{SiNH})_2(\text{THF})\text{Zr}{=}\text{NSi}^t\text{Bu}_3 + \text{py} \xrightarrow[25\ °C,\ <5\ m]{C_6D_6} (^t\text{Bu}_3\text{SiNH})_2(\text{py})\text{Zr}{=}\text{NSi}^t\text{Bu}_3 + \text{THF} \quad (22)$$

2-THF **2**-py

noted by ^{1}H NMR spectroscopy. In contrast, multiple exposures (∼10) of **2**-THF to diethyl ether solvent were needed to ensure the formation of (^{t}Bu$_3$SiNH)$_2$(Et$_2$O)Zr=NSi^{t}Bu$_3$ (**2**-OEt$_2$) in >98% purity (^{1}H NMR) upon isolation from Et_2O (eq 23).

$$\textbf{2}\text{-THF} \underset{}{\overset{Et_2O,\ 25\ °C}{\rightleftharpoons}} (^t\text{Bu}_3\text{SiNH})_2(\text{Et}_2\text{O})\text{Zr}{=}\text{NSi}^t\text{Bu}_3 + \text{THF} \quad (23)$$

2-OEt$_2$

3. Molecular Structure of (^{t}Bu$_3$SiNH)$_2$(THF)Zr=NSi^{t}Bu$_3$ (2-THF). A single-crystal X-ray structure determination (monoclinic, $P2_1/n$, R = 7.70%, R_w = 9.12%, Table 2) of (^{t}Bu$_3$SiNH)$_2$(THF)Zr=NSi^{t}Bu$_3$ (**2**-THF) confirmed its constitution and geometry. The molecular view of **2**-THF is shown in Figure 1, while selected interatomic distances (Å) and angles (deg) are listed in Table 3. The figures reveal a spiral, C_3 "propeller" arrangement of the sp^2-nitrogen-containing imide (Zr−N1−Si1) and amide (Zr−N2(H)−Si2, Zr−N3(H)−Si3) ligands, a feature reminiscent of the amide conformations about (^{t}Bu$_3$SiNH)$_3$ZrMe (**1**-Me)[45] and {(Me$_3$Si)$_2$N}$_3$MCl (M = Ti, Zr, Hf).[50] The O−Zr−N angles (105.3(24)° av) are significantly less than the N−Zr−N angles (113.2(14)° av), in accord with pseudotetrahedral symmetry and the greater repulsion between the imide/amide ligands. Both Zr−N(H)−Si planes and the Zr=N(1)−Si1 plane are canted such that the N−H/lone pair vectors (assuming sp^2-N-hybridization) are directed slightly toward the THF apex (dihedral angles: O−Zr−N2−H, 79.9°; O−Zr−N3−H, 90.4°; O−Zr−N1−(lone pair) = 83.4°), rendering each ^{t}Bu$_3$Si fragment approximately equatorial relative to the Zr−O bond. In this fashion, the distortion from approximate tetrahedral geometry is minimal, yet the amides/imide occupy a less sterically demanding region of space, just as observed for C_3 **1**-Me, whose H−N−Zr−C dihedral angles are ∼105°.[45]

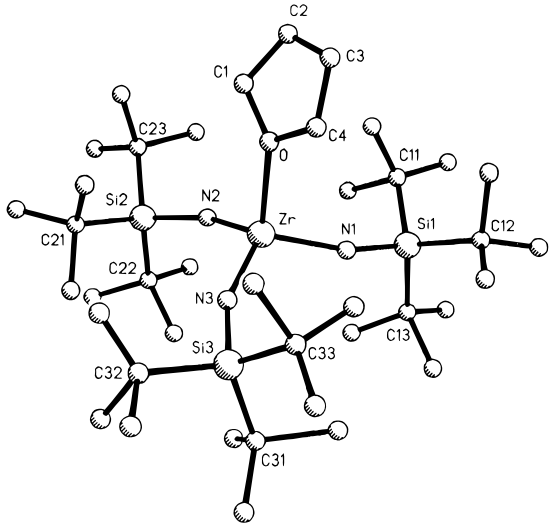

Figure 1. Molecular view of (^{t}Bu$_3$SiNH)$_2$(THF)Zr=NSi^{t}Bu$_3$ (**2**-THF).

Table 3. Selected Interatomic Distances (Å) and Angles (deg) for (^{t}Bu$_3$SiNH)$_2$(THF)Zr=N-Si^{t}Bu$_3$ (**2**-THF)

Zr−O	2.229(7)	N1−Si1	1.720(9)	O−C1 1.394(19)
Zr−N1	1.978(8)	N2−Si2	1.717(9)	O−C4 1.434(17)
Zr−N2	2.031(8)	N3−Si3	1.728(8)	C1−C2 1.435(26)
Zr−N3	2.028(8)	Si−C (av)	1.922(14)	C2−C3 1.400(28)
		C−C (av)	1.543(92)	C3−C4 1.435(23)
O−Zr−N1	102.9(3)	Zr−N1−Si1	156.9(5)	Zr−O−C1 129.0(9)
O−Zr−N2	105.3(3)	Zr−N2−Si2	154.7(5)	Zr−O−C4 123.5(7)
O−Zr−N3	107.7(3)	Zr−N3−Si3	158.1(5)	O−C1−C2 107.0(15)
N1−Zr−N2	112.3(3)	N−Si−C (av)	107.9(8)	O−C4−C3 108.0(13)
N2−Zr−N3	114.9(3)	Si−C−C (av)	111.9 (48)	C1−C2−C3 108.1(16)
N1−Zr−N3	112.5(3)	C−Si−C (av)	110.9(16)	C2−C3−C4 106.4(15)
		C−C−C (av)	106.5(42)	

The plane of the THF ligand is nearly aligned with the Zr−O vector (∠Zr−O−C = 123.5(7), 129.0(9)°), implicating strong O(pπ) → Zr(dπ) bonding, but the d(Zr−O) of 2.229(7) Å belies this argument. In Cp$_2$(THF)Zr=N^{t}Bu,[28] the plane of the THF lies approximately within the Cp$_2$Zr "wedge" with Zr−O−C angles of 124.3(4) and 127.3(6)°, and oxygen π-bonding is negligible because the perpendicularly oriented oxygen lone pair must π-donate into high energy, CpZr antibonding orbitals. Despite this factor, the Zr−O bond distance of 2.240(4) Å is essentially the same as that in **2**-THF, hence it is unlikely that either structure manifests significant oxygen π-donation. Contrast this data to the d(Zr−O) of 2.122(14) Å in Cp$_2$ZrMe(THF)$^+$,[51] where the THF plane is oriented perpendicular to the Cp$_2$Zr wedge, thereby ensuring O(pπ) → Zr(dπ) bonding, despite severe steric constraints.

The most striking feature of **2**-THF concerns the similarity of the imide and amide linkages. The imide Zr−N1−Si1 angle (156.9(5)°) is essentially the same as the amide Zr−N−Si angles (154.7(5)° and 158.1(5)°), while the Zr−N1 bond distance of 1.978(8) Å is ∼0.05 Å shorter than the amide 2.031(8) and 2.028(8) Å bond lengths of Zr−N2 and Zr−N3, respectively. Minimal lone pair N(pπ) → Zr(dπ) donation is implicated by

(50) Airoldi, C.; Bradley, D. C.; Chudzynska, H.; Hursthouse, M. B.; Malik, K. M. A.; Raithby, P. R. *J. Chem. Soc., Dalton Trans.* **1980**, 2010−2015.

(51) Jordan, R. F.; Bajgur, C. S.; Willett, R.; Scott, B. *J. Am. Chem. Soc.* **1986**, *108*, 7410−7411.

the similarity, *providing a structural basis upon which to predict its reactivity as in internal base in C−H bond activation processes*. The short amide distances, characteristic of low coordinate group 4 complexes,[45,50,52,53] manifest nitrogen π-donation that is nearly as strong as the formal π-bond of the imide functionality. The decidedly angular Zr═N−Si fragment represents a severe departure from typical M═N−R (R = hydrocarbyl) ligands, whose range of angles is 165−180°.[54] In complexes containing 18 e$^-$ (without inclusion of the imide lone pair) or hydrazido ligands, exceptions ($\angle$M═N−X < 165°) have been found, but known zirconium derivatives $Cp_2(THF)Zr{=}N^tBu$,[28] ((2,6-^{i}Pr$_2$C$_6$H$_3$)HN)$_2$(py′)$_2$Zr═N(2,6-^{i}Pr$_2$C$_6$H$_3$) and ((2,6-^{i}Pr$_2$C$_6$H$_3$)O)$_2$(py′)$_2$Zr═NPh (py′ = 4-pyrrolidinopyridine)[55] exhibit nearly linear Zr═N−C angles of 174.4(3), 174.9(3), and 175.5(8)°, respectively.

In view of the recent debunking of bond-stretch isomerism by Parkin *et al.*,[56] an imide/amide disorder in the structural model may be responsible for the unusually small difference in Zr−N imide and amide bond lengths; a weighted average of "normal" Zr═N− and Zr−N(H)− bond distances (typically ~0.2 Å apart) is plausible. However, the amide distances of **2**-THF are effectively the same as those in **1**-Me (2.039(7) Å av),[45] rendering this possibility considerably less appealing, since zirconium imide distances are substantially shorter than corresponding amides. In $Cp_2(THF)Zr{=}N^tBu$ (d(Zr═N) = 1.826(4) Å),[28] ((2,6-^{i}Pr$_2$C$_6$H$_3$)HN)$_2$(py′)$_2$Zr═N(2,6-^{i}Pr$_2$C$_6$H$_3$), and ((2,6-^{i}Pr$_2$C$_6$H$_3$)O)$_2$(py′)$_2$Zr═NPh (d(Zr═N) = 1.868(3), 1.844(9) Å, respectively),[55] the imide bond distances are significantly shorter despite ligation to higher-coordinate metal centers where longer imide bonds are expected. Given a hypothetical 1.86 Å Zr═N distance for **2**-THF, each amide would have to be an uncharacteristically long 2.09 Å for the structure to represent a weighted average of Zr−N bond lengths; furthermore, an explanation for the statistically different observed amide and imide distances would still be lacking.

Provided the structural characterization of **2**-THF is accurate, what factors contribute to the unusual imide disposition? In trigonal $(R_2N)_3M$ complexes (e.g., R_2N = N(SiMe$_3$)$_2$), the amides adopt a pinwheel dispostion about M, but the N lone pair is located principally in the N_3M plane. When restricted to this plane, the N(pπ)-based a_2' (assuming D_{3h}) ligand orbital is not of the appropriate symmetry to interact with any metal orbital. In d^2 Os(═NAr)$_3$ and related complexes,[57,58] these symmetry arguments have been used to rationalize apparent 20e$^-$ configurations. When the amides are disposed such that the N lone pairs are perpendicular to the N_3M plane, all three ligand orbitals possess the correct symmetry for interaction with the metal. Even in pseudo-C_3 tetrahedral molecules such as **2**-THF, these orbital arguments remain pertinent. As a consequence, there is an electronic, as well as steric, component to the orientation of the NHSi^{t}Bu$_3$ groups about zirconium in **1**-Me and **2**-THF. Since the THF oxygen is a poorer donor, the amides prefer an arrangement that aligns their lone pairs with the Zr−O vector, and the additional steric constraints cause each amide to be slightly tipped. Space-filling depictions of **2**-THF indicate that the orientation of the amides provide a strong impetus for bending of the imide linkage. In essence, the bent amide bonds permit only a similarly angular imide ligand to occupy the remaining space in the C_3 core. The amide hydrogens and imide lone pair reside in nearly equivalent positions. Based on the Zr−N−Si angles (156.6(17)° average), neither NH nor the lone pair is expected to engage an e set of metal orbitals in a significant agostic interaction or π-bonding, although correlations of $\angle$M−O−R and d(M−OR) have shown that such inferences can be misleading.[59]

Less well understood is the electronic influence of the ^{t}Bu$_3$-Si moiety on the conformation and d(Zr−N) of the imide. If N(pπ) → Si(dπ) bonding is significant, competition between Si and Zr for nitrogen π-bonding may partly explain the lengthened imide bond distance. However, the limited number of comparative M═N−R (R = CR′$_3$ vs SiR′$_3$) structures do not show a pronounced difference in bond length,[54] and the existence of significant, related O(pπ) → Si(dπ) interactions is a matter of some dispute.[60]

4. (^{t}Bu$_3$SiNH)$_2$(Et$_2$O)Zr═NSi^{t}Bu$_3$ Thermolysis. In a sealed NMR tube, diethyl ether adduct (^{t}Bu$_3$SiNH)$_2$(Et$_2$O)Zr═N-Si^{t}Bu$_3$ (**2**-OEt$_2$) decomposed at 120 °C (C_6D_6, 12 h) to generate (^{t}Bu$_3$SiNH)$_3$ZrOEt (**1**-OEt, ~90%) and concomitant ethylene, consistent with γ-CH activation (eq 24). Scale-up of the ethoxide derivative, **1**-OEt, was accomplished via a direct route

$$\underset{\textbf{2}\text{-OEt}_2}{(^t\text{Bu}_3\text{SiNH})_2\text{LZr}{=}\text{NSi}^t\text{Bu}_3} \xrightarrow[120\ ^\circ\text{C, 12 h}]{C_6D_6} \underset{\textbf{1}\text{-OEt}}{(^t\text{Bu}_3\text{SiNH})_3\text{ZrOEt}} + \text{H}_2\text{C}{=}\text{CH}_2 \quad (24)$$

$$\underset{\textbf{1}\text{-Cy}}{(^t\text{Bu}_3\text{SiNH})_3\text{ZrCy}} + \text{Et}_2\text{O (excess)} \xrightarrow[115\ ^\circ\text{C, 16 h}]{\text{heptane}} \underset{\textbf{1}\text{-OEt}}{(^t\text{Bu}_3\text{SiNH})_3\text{ZrOEt}}\ \mathbf{H}_2\text{C}{=}\text{CH}_2 \quad (25)$$

involving thermolysis of (^{t}Bu$_3$SiNH)$_3$ZrCy (**1**-Cy) in heptane at 115 °C for 16 h in the presence of ~10 equiv Et$_2$O (eq 25). The formal γ-CH-activation product was isolated in 79% yield upon crystallization from hexanes.

This apparently internal γ-CH activation is reminiscent of Parkin's recent studies of Cp*$_2$Zr(═O)py (Cp* = η^5-C$_5$Me$_5$), which reacts with ^{t}BuI and RCOMe (R = Me, ^{t}Bu, Ph) to give Cp*$_2$ZrI(OH) and Cp*$_2$Zr(OH)OCR═CH$_2$, respectively.[21] Scheme 2 illustrates plausible mechanisms for these transformations, highlighting a common, concerted six-atom rearrangement where the oxo or imido unit functions as an internal base in attacking the γ-CH bond.

1,2-RH-Elimination: Labeling Studies. The prevalence of σ-bond metatheses[8,9] in early transition metal chemistry prompted a series of labeling studies. Under standard thermolysis conditions, (^{t}Bu$_3$SiNH)$_3$ZrMe (**1**-Me) in C_6D_6 afforded (^{t}Bu$_3$-

(52) (a) Planalp, R. P.; Andersen, R. A.; Zalkin, A. *Organometallics* **1983**, *2*, 16−20 and references therein. See, also: (b) Andersen, R. A. *Inorg. Chem.* **1979**, *18*, 2928−2932. (c) Andersen, R. A. *J. Organomet. Chem.* **1980**, *192*, 189−193.

(53) (a) Fryzuk, M. D.; Williams, H. D.; Rettig, S. J. *Inorg. Chem.* **1983**, *22*, 863−868. (b) Fryzuk, M. D.; Carter, A.; Westerhaus, A. *Inorg. Chem.* **1985**, *24*, 642−648. (c) Fryzuk, M. D.; Rettig, S. J.; Westerhaus, A.; Williams, H. D. *Inorg. Chem.* **1985**, *25*, 4316−4325. (d) Fryzuk, M. D.; Haddad, T. S.; Rettig, S. J. *Organometallics* **1989**, *8*, 1723−1732.

(54) (a) Nugent, W. A.; Mayer, J. M. *Metal-Ligand Multiple Bonds*; Wiley-Interscience: New York, 1988. (b) Wigley, D. E. *Prog. Inorg. Chem.* **1994**, *42*, 239−482.

(55) Zambrano, C. H.; Profilet, R. D.; Hill, J. E.; Fanwick, P. E.; Rothwell, I. P. *Polyhedron* **1993**, *12*, 689−708.

(56) (a) Parkin, G. *Acc. Chem. Res.* **1992**, *25*, 455−460. (b) Parkin, G. *Chem. Rev.* **1993**, *93*, 887−912.

(57) (a) Schofield, M. H.; Kee, T. P.; Anhaus, J. T.; Schrock, R. R.; Johnson, K. H.; Davis, W. M. *Inorg. Chem.* **1991**, 3595−3604. (b) Williams, D. S.; Anhaus, J. T.; Schofield, M. H.; Schrock, R. R.; Davis, W. M. *J. Am. Chem. Soc.* **1991**, *113*, 5480−5481. (b) Williams, D. S.; Anhaus, J. T.; Schofield, M. H.; Schrock, R. R.; Davis, W. M. *J. Am. Chem. Soc.* **1991**, *113*, 5480−5481.

(58) (a) Covert, K. J.; Neithamer, D. R.; Zonnevylle, M. C.; LaPointe, R. E.; Schaller, C. P.; Wolczanski, P. T. *Inorg. Chem.* **1991**, *30*, 2494−2508. (b) Eppley, D. F.; Wolczanski, P. T.; Van Duyne, G. D. *Angew. Chem., Int. Ed. Engl.* **1991**, *30*, 584−585.

(59) Steffey, B. D.; Fanwick, P. E.; Rothwell, I. P. *Polyhedron* **1990**, *9*, 963−968.

(60) Shambayatei, S.; Blake, J. F.; Wierschke, S. G.; Jorgensen, W. L.; Schreiber, S. L. *J. Am. Chem. Soc.* **1990**, *112*, 697−703; 6155.

Scheme 2

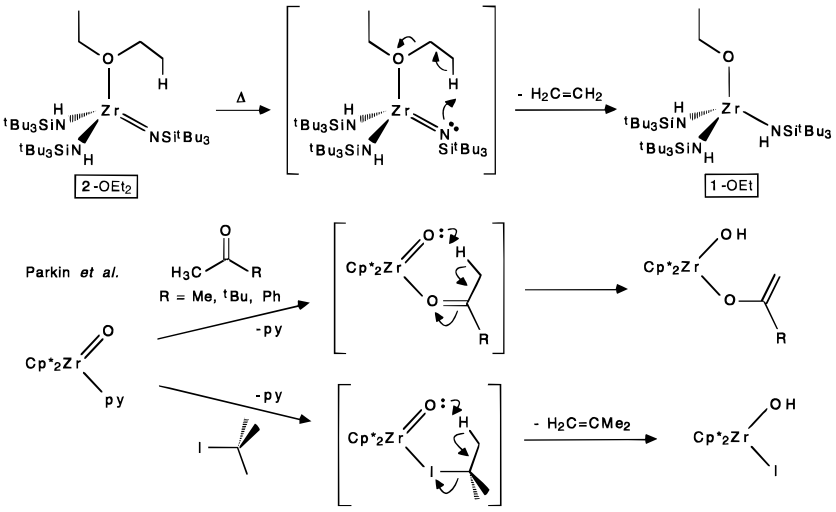

$SiND)_3ZrC_6D_5$ (**1**-$(ND)_3C_6D_5$) and CH_4, while (^{t}$Bu_3SiND)_3ZrMe$ in C_6H_6 provided **1**-Ph and CH_3D (0.9 equiv, >93% d_1 by ^{1}H

$$(^t\mathrm{Bu_3SiNX})_3\mathrm{ZrMe} \xrightarrow[100\ ^\circ\mathrm{C,\ 7\ h}]{\mathrm{C_6Y_6}} (^t\mathrm{Bu_3SiNY})_3\mathrm{ZrC_6Y_5} + \mathrm{X\text{-}CH_3} \quad (26)$$

X = H, **1**-Me; Y = D
X = D, **1**-$(ND)_3$-Me; Y = H

X = H; Y = D, **1**-$(ND)_3$-C_6D_5
X = D; Y = H, **1**-Ph

$$(^t\mathrm{Bu_3SiNH})_3\mathrm{ZrMe} + \mathrm{D_2\ (4\ atm)} \xrightarrow[100\ ^\circ\mathrm{C,\ 8\ h}]{\mathrm{C_6H_{12},}} (^t\mathrm{Bu_3SiND})_3\mathrm{ZrD} + \mathrm{CH_4} \quad (27)$$

1-Me

1-$(ND)_3$-D

NMR, IR) as shown in eq 26. In a related process, the ultimate products of deuteration (∼4 atm) of **1**-Me in C_6D_{12} were (^{t}Bu_3-$SiND)_3ZrD$ (**1**-$(ND)_3D$) and concomitant CH_4 (eq 27). σ-Bond metathesis pathways are convincingly obviated by these results, yet the riddle of amide H/D-exchange was introduced and solved by ensuing kinetics studies. The labeling experiments implicated the mechanism depicted in Scheme 1, where 1,2-RH-elimination from (^{t}$Bu_3SiNH)_3ZrR$ (**1**-R) produces transient three-coordinate imido, (^{t}$Bu_3SiNH)_2Zr{=}NSi^tBu_3$ (**2**), and 1,2-R′H-addition to its reactive Zr═N bond generates a new hydrocarbyl, **1**-R′.

Kinetics of 1,2-RH-Elimination. 1. Order and Activation Parameters. Kinetics investigations portray the 1,2-RH-elimination as the rate-determining step (Table 4). Thermolysis of (^{t}$Bu_3SiNH)_3ZrMe$ (**1**-Me) in C_6D_6 (eq 26), monitored by the loss of its NH resonances in ^{1}H NMR spectra, indicated that the reaction was first-order in **1**-Me and zero-order in C_6D_6 (k_{Me}-(av) = 1.02 (5) × 10^{-4} s^{-1}, 96.7 °C, eq 28). An Eyring plot for methane elimination (87.1−127.1 °C) from **1**-Me provided an activation enthalpy ($\Delta H^{\ddagger}$ = 25.9 (4) kcal/mol) indicative of

$$-\mathrm{d}[\mathbf{1}\text{-Me}]/\mathrm{d}t = k_{\mathrm{Me}}[\mathbf{1}\text{-Me}]^1[\mathrm{C_6D_6}]^0 \quad (28)$$

significant bond-breaking, and a small, negative activation entropy ($\Delta S^{\ddagger}$ = −7(1) eu). The latter portrays a rather constrained, unimolecular transition state[61−63] where amide reorganization is necessary to achieve the coplanar Zr(Me)−N(H) geometry that permits Me−H bond formation to occur.

With 50.0 equiv of C_6D_6 (2.00 M) in C_6D_{12} at 113.0 °C, k_{Me} = 4.99(5) × 10^{-4} s^{-1}, in comparison to the predicted k_{Me} of 4.91 × 10^{-4} s^{-1} in neat C_6D_6 (∼11.2 M), hence typical conditions manifest zero-order in benzene, and cyclohexane cannot have a pronounced solvent effect. As an additional check, rough monitoring of the conversion of **1**-Cy and methane (1, 2, 4, and 8 atm) to **1**-Me and cyclohexane in C_6D_{12} (eq 7)

$$\mathrm{d}[\mathbf{1}\text{-Me}]/\mathrm{d}t = -\mathrm{d}[\mathbf{1}\text{-Cy}]/\mathrm{d}t = k_{\mathrm{Cy}}[\mathbf{1}\text{-Cy}]^1[\mathrm{MeH}]^0 \quad (29)$$

revealed that neither disappearance of **1**-Cy (k_{Cy} (av) = 1.55 (8) × 10^{-3} s^{-1}) nor appearance of **1**-Me (k_{Me} (av) = 1.5 (1) × 10^{-3} s^{-1}) exhibited any order in methane (eq 29). When thermolyzed in THF-d_8, the rate (98.7 °C, k_{Me} = 6.27(9) × 10^{-4} s^{-1}) of MeH-elimination from (^{t}$Bu_3SiNH)_3ZrMe$ (**1**-Me) reflected a 5-fold increase relative to benzene-d_6, despite the difference in products (**2**-THF vs **1**-$(ND)_3$-C_6D_5). As a consequence of these experiments, preequilibrium binding of alkane or solvent is precluded as a significant factor in the 1,2-RH-elimination events; no further solvent studies were undertaken.

Note that some related reactions appear to be second-order. In eq 20, (^{t}$Bu_3SiNH)_3ZrH$ (**1**-H) is seen to be a ready precursor to (^{t}$Bu_3SiNH)_2LZr{=}NSi^tBu_3$ (**2**-L, L = THF, Et_2O, NMe_3, PMe_3) upon addition of L (<5 min), a process whose time scale is suggestive of second-order. Spin saturation transfer experiments revealed that the exchange of free THF with its bound counterpart in (^{t}$Bu_3SiNH)_2$(THF)$Zr{=}NSi^tBu_3$ (**2**-THF) is [THF]-dependent. The thermoneutrality of this swift exchange may help enable its observation; assuming a second-order process, k ∼55−85 M^{-1} s^{-1}.

2. 1,2-RH-Elimination Kinetic Isotope Effects. The large primary kinetic isotope effect (KIE)[64] for loss of CH_3H/D from **1**-Me vs **1**-$(ND)_3/CH_3$ (eq 30) at 96.7 °C was $k_H/k_D = z_{Me}$ = 6.27(8), a value consistent with a relatively linear H-atom transfer that implicated similar amounts of C−H bond-making and N−H bond-breaking[61,62] within the four-centered transition state. Kinetic isotope effects for $PhCH_3$ vs $PhCH_2D$ loss from **1**-CH_2Ph vs **1**-$(ND)_3$-CH_2Ph ($k_H/k_D = z_{Bz}$ = 7.1 (6), 96.8 °C),

(61) Carpenter, B. K. *Determination of Reaction Mechanisms*; Wiley-Interscience: New York, 1984.
(62) Lowry, T. H.; Richardson, K. S. *Mechanism and Theory in Organic Chemistry, Third Edition*; Harper and Row: New York; 1987.
(63) (a) Westaway, K. C. *Isotopes in Organic Chemistry, Volume 7: Secondary and Solvent Isotope Effects*; Buncel, E., Lee, C. C., Eds.; Elsevier, New York, 1987; pp 288−290. (b) *Isotope Effects in Chemical Reactions*; Collins, C. J., Bowman, N. S., Eds.; ACS Monograph 167; Van Nostrand Reinhold: New York, 1970. (c) Wolfe, S.; Kim, C.-K. *J. Am. Chem. Soc.* **1991**, *113*, 8056−8061 and references therein.
(64) Methane loss from **1**-Me vs **1**-$(ND)_3CH_3$ is considered solely a primary KIE; the assumption that the remaining ND positions do not exert a significant secondary KIE is implicit.

Table 4. First-Order Rate Constants,[a] Free Energies of Activation and Corresponding D(R−H) for 1,2-RH Elimination of RH from (^{t}Bu$_3$SiNH)$_3$ZrR (1-R) in C_6D_6, Producing (^{t}Bu$_3$SiND)$_3$ZrC$_6$D$_5$ (**1**-(ND)$_3$C$_6$D$_5$) (Exceptions Are Noted)

compound (solvent C_6D_6 or as noted)	k ($\times 10^4$ s^{-1})	T ($\pm$0.3 °C)	$\Delta G^{\ddagger}$ (kcal/mol)	[**1**-R] (M)	D(R−H) (kcal/mol)
(^{t}Bu$_3$SiNH)$_3$ZrCH$_2$Ph (**1**-CH$_2$Ph)	0.169(3)	96.7	29.9	0.036	88.5(15)
	0.130(6)[b]	96.8		0.036	
(^{t}Bu$_3$SiND)$_3$ZrCH$_2$Ph (**1**-(ND)$_3$-CH$_2$Ph)	0.0184(8)[b]	96.8		0.036	
(^{t}Bu$_3$SiNH)$_3$ZrCH$_2$C$_6$H$_3$Me$_2$ (**1**-Mes)	0.342(2)	96.7	29.4	0.035	88.5(15)
(^{t}Bu$_3$SiNH)$_3$ZrCH$_3$ (**1**-Me)	0.387(7)[c]	87.1		0.040	104.9(1)
	1.096(14)[c]	96.6		0.040	
	1.02(10)[d]	96.6		0.0050	
	0.980(4)[d]	96.6		0.025	
	0.968(6)[d]	96.6		0.050	
	1.06(2)	96.7	28.5	0.040	
(**1**-Me in THF-d_8; product **2**-THF)[e]	6.27 (9)	98.7		0.040	
	3.05(3)[c]	107.6		0.040	
(**1**-Me in C_6D_{12}, [C_6D_6] = 2.00 M)[f]	4.99(5)	113.0		0.040	
	7.00(4)[c]	116.9		0.040	
	16.3(2)[c]	127.1		0.040	
	1.104(7)[b]	96 .7		0.040	
	0.977(8)[g]	96.7		0.040	
	1.02(2)[h]	96.7		0.053	
(^{t}Bu$_3$SiND)$_3$ZrCH$_3$ (**1**-(ND)$_3$-CH$_3$)	0.176(2)[b]	96.7		0.040	
(^{t}Bu$_3$SiNH)$_3$ZrCD$_3$ (**1**-CD$_3$)	0.74(2)[g]	96.7		0.045	
((d_9-^{t}Bu)$_3$SiNH)$_3$ZrCH$_3$ (**1**-d_{81}-Me)	1.00(1)[h]	96.7		0.05	
(^{t}Bu$_3$SiNH)$_3$ZrCH$_2$^{t}Bu (**1**-CH$_2$^{t}Bu)	1.42(4)	96.7	28.3	0.037	101.1(4)
(^{t}Bu$_3$SiNH)$_3$ZrH (**1**-H)	1.51(6)	96.7	28.3	0.041	104.21(1)
	1.29(9)	96.7		0.041	
(^{t}Bu$_3$SiNH)$_3$ZrCH$_2$CH=CMe$_2$ (**1**-dma)	1.3(1)	96.7	28.3	0.037	88.2(21)
(^{t}Bu$_3$SiNH)$_3$Zr^{i}Bu (**1**-^{i}Bu)	3.2(1)	96.7	27.7	0.038	101.1(4)
(^{t}Bu$_3$SiNH)$_3$ZrEt (**1**-Et)	3.21(6)	96.7	27.7	0.039	101.1(4)
(^{t}Bu$_3$SiNH)$_3$ZrCy (**1**-Cy)	10.4(2)	96.7	26.9	0.031	98.2(5)
(^{t}Bu$_3$SiNH)$_3$ZrCH=CH2 (**1**-CH=CH$_2$)	13.2(4)	96.7	26.7	0.039	111.2(8)
(^{t}Bu$_3$SiNH)$_3$Zr^{c}Pr (**1**-^{c}Pr)	15.5(2)	96.7	26.6	0.038	
(^{t}Bu$_3$SiNH)$_3$ZrPh (**1**-Ph)	22.6(2)	96.7	26.3	0.043	111.2(8)
	21.4(10)[i]	96.7		0.040	
	22.4(4)[b]	96.7		0.037	
(^{t}Bu$_3$SiND)$_3$ZrPh (**1**-(ND)$_3$-Ph)	4.88(5)[b]	96.7		0.037	

[a] Determined from nonlinear, least-squares fitting of the differential form of the rate expression; D(RH) values are from ref 72. [b] Tandem measurement for obtaining primary isotope effect: k_H/k_D(PhCH$_2$H/D loss) = 7.1(6), from nonweighted fits; k_H/k_D(MeH/D loss) = 6.27(8); k_H/k_D(PhH/D loss) = 4.6(4). [c] Values used in the Eyring plot (87.1−127.1 °C) obtained from triplicate runs. From a weighted, nonlinear, least squares fit of the data: $\Delta H^{\ddagger}$ = 25.9(4) kcal/mol, $\Delta S^{\ddagger}$ = −7(1) eu. [d] Obtained from 0.05 M stock solution and dilutions. [e] Compare to MeH loss from **1**-Me in C_6D_6 (98.7 °C) calcd to be 1.24 × 10^{-4} s^{-1}; k(THF)/k(C_6D_6) = 5.1. [f] 50 equiv of C_6D_6. Compare to MeH loss from **1**-Me in C_6D_6 (113.0 °C) calcd to be 4.91 × 10^{-14} s^{-1}. [g] Tandem measurement for obtaining secondary isotope effect: k(CH$_3$)/k(CD$_3$) = 1.32 (8). [h] Tandem measurement for obtaining peripheral isotope effect: $k/k(d_{81})$ = 1.02(2). [i] Determined from monitoring the growth and subsequent loss of the NH protons of (^{t}Bu$_3$SiNH)$_2$(^{t}Bu$_3$SiND)ZrC$_6$D$_5$ (**1**-(ND)-C$_6$D$_5$) and (^{t}Bu$_3$SiNH)(^{t}Bu$_3$SiND)$_2$ZrC$_6$D$_5$ (**1**-(ND)$_2$C$_6$D$_5$) upon thermolysis of **1**-Me in C_6D_6 as consecutive, irreversible first-order processes; a k of 1.06 × 10^{-4} s^{-1} was used for MeH loss from **1**-Me.

$$\begin{array}{c}(^t\mathrm{Bu_3SiNX})_3\mathrm{ZrR} \\ \mathrm{X = H,\ \mathbf{1}\text{-}R} \\ \mathrm{R = CH_3,\ CD_3,\ Ph,\ CH_2Ph} \\ \mathrm{X = D,\ \mathbf{1}\text{-}(ND)_3\text{-}R} \\ \mathrm{R = CH_3,\ Ph,\ CH_2Ph}\end{array} \xrightarrow[100\ ^\circ\mathrm{C},\ 7\ \mathrm{h}]{C_6D_6} (^t\mathrm{Bu_3SiND})_3\mathrm{ZrC_6D_5} + \underset{\mathbf{1}\text{-}(ND)_3\text{-}C_6D_5}{\mathrm{X\text{-}R}}\ \begin{array}{c}\mathrm{X = H} \\ \mathrm{X = D}\end{array} \quad (30)$$

and PhH vs PhD loss from **1**-Ph vs **1**-(ND)$_3$Ph ($k_H/k_D = z_{Ph}$ = 4.6 (4), 96.7 °C), supported similar contentions, although the latter number hinted at a significantly less symmetric transition state for phenyl elimination. Multiple deuteration of the products was not detected, excluding reversible elimination/addition prior to RH loss. The α-secondary KIE for CH_4 vs CD_3H loss from **1**-Me vs **1**-CD$_3$ at 96.7 °C was $k_H/k_D = z'^3_{Me}$ = 1.32 (8) or z'_{Me} = 1.10 per D. A "normal" (i.e., $k_H/k_D > 1$) effect is traditionally interpreted as indicating a change from sp^3 to sp^2 character of the methyl group in the transition state.[61−63] Calculations by Cundari on methane elimination from (H$_2$N)$_3$ZrMe, a model of **1**-Me, portray the elimination as occurring with retention at carbon[43] and with minimal geometric changes in the transition state CH/D$_3$ fragment. The minor secondary KIE observed for **1**-Me vs **1**-CD$_3$ is consistent with this depiction.

In order for the critical atoms of the Zr−C···NH unit (H−N−Zr−C dihedral angle ~105°)[45] in **1**-Me to achieve coplanarity in the transition state, rotation about a Zr−N bond must occur, hence $\Delta G^{\ddagger}_{elim}(CH_4)$ can be considered to consist of two components: amide rotation ($\Delta G^{\ddagger}_{rot}$) and hydrogen abstraction ($\Delta G^{\ddagger}_{abs}$). Preliminary molecular mechanics calculations suggested that concomitant rotation of the remaining bulky amides exerts a steric influence on the Zr−Me, tipping it toward the N−H. Fully deuterated d_{27}-^{t}Bu$_3$SiNH$_2$, prepared from d_9-^{t}BuLi, was used to synthesize ((d_9-^{t}Bu)$_3$SiNH)$_3$ZrCH$_3$ (**1**-d_{81}-Me) in order to investigate the possibility of a steric isotope effect,[61] due to the 81 marginally shorter C−D bonds (by ~0.009 Å vs C−H). No evidence of a peripheral KIE was obtained (k_H(**1**-Me)/k_D(**1**-d_{81}-Me) = 1.02(2), 96.7 °C), and prudence dictated that other **1**-d_{81}-R remain uninvestigated.

3. Amide Deuteration in 1-(ND)$_x$C$_6$D$_5$ (x = 1−3). Thermolysis of **1**-R in C_6D_6 solutions resulted in the elimination of hydrocarbon RH and successive addition/elimination steps leading to the formation of (^{t}Bu$_3$SiND)$_3$ZrC$_6$D$_5$ (**1**-(ND)$_3$-C$_6$D$_5$) (eqs 31−33). Kinetics analysis of the conversion of (^{t}Bu$_3$SiNH)$_3$ZrCH$_3$ (**1**-Me) to **1**-(ND)$_3$-C$_6$D$_5$ was accomplished via monitoring the growth and subsequent decay of the NH resonances corresponding to the phenyl derivative (Figure 2).

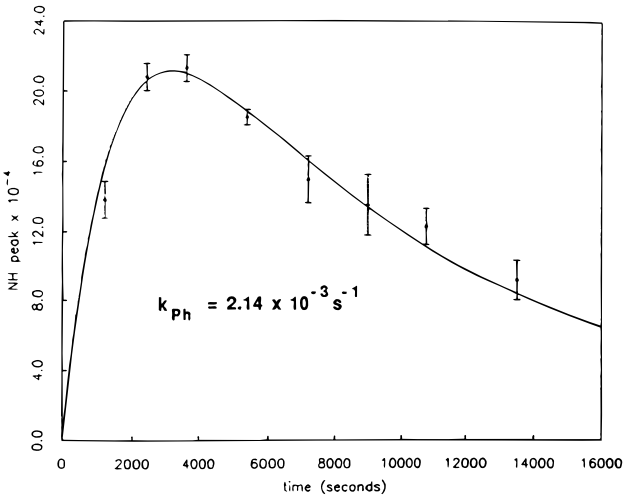

Figure 2. Upon thermolysis of **1**-Me in C_6D_6, the growth and subsequent loss of the intensity (^{1}H NMR spectra) of NH protons corresponding to (^{t}Bu$_3$SiNH)$_2$(^{t}Bu$_3$SiND)ZrC$_6$D$_5$ (**1**-(ND)C$_6$D$_5$) and (^{t}Bu$_3$SiNH)(^{t}Bu$_3$SiND)$_2$ZrC$_6$D$_5$ (**1**-(ND)$_2$C$_6$D$_5$) can be modeled as consecutive, irreversible first-order processes (eqs 31−33); a k_{Me} of 1.06×10^{-4} s^{-1} was used for MeH loss from **1**-Me.

$$(^t\text{Bu}_3\text{SiNH})_3\text{ZrCH}_3 \xrightarrow[C_6D_6]{k_{Me}} (^t\text{Bu}_3\text{SiNH})_2(^t\text{Bu}_3\text{SiND})\text{ZrC}_6\text{D}_5 + \text{CH}_4 \quad (31)$$

1-CH$_3$ → **1**-(ND)-C$_6$D$_5$

$$(^t\text{Bu}_3\text{SiNH})_3(^t\text{Bu}_3\text{SiND})\text{ZrC}_6\text{D}_5 \xrightarrow[C_6D_6]{2k_{Ph}/3} (^t\text{Bu}_3\text{SiNH})(^t\text{Bu}_3\text{SiND})_2\text{ZrC}_6\text{D}_5 + \text{C}_6\text{D}_5\text{H} \quad (32)$$

1-(ND)-C$_6$D$_5$ → **1**-(ND)$_2$-C$_6$D$_5$

$$(^t\text{Bu}_3\text{SiNH})(^t\text{Bu}_3\text{SiND})_2\text{ZrC}_6\text{D}_5 \xrightarrow[C_6D_6]{k_{Ph}/3} (^t\text{Bu}_3\text{SiND})_3\text{ZrC}_6\text{D}_5 + \text{C}_6\text{D}_5\text{H} \quad (33)$$

1-(ND)$_2$-C$_6$D$_5$ → **1**-(ND)$_3$-C$_6$D$_5$

Using a k_{Me} of 1.06×10^{-4} s^{-1} (eq 31) and modeling the deuteration as two subsequent first-order processes[65] that reflect the statistics of each event (eq 32, $2k_{Ph}/3$; eq 33, $k_{Ph}/3$), a rate constant of 2.14×10^{-3} s^{-1} for C$_6$D$_5$H elimination was obtained, consistent with the rate constant of $2.25(3) \times 10^{-3}$ s^{-1} generated from monitoring the loss of C$_6$H$_6$ from (^{t}Bu$_3$SiNH)$_3$ZrPh (**1**-Ph). The successful modeling of the deuteration supports the standard mechanism of Scheme 1.

4. Equilibria and C−H Bond Activation Selectivities. Inspection of the first-order rate constants for the elimination of hydrocarbons in Table 4, obtained at 96.7 °C, reveals a moderate distribution of reaction rates from (^{t}Bu$_3$SiNH)$_3$ZrCH$_2$-Ph (**1**-CH$_2$Ph, $k_{Bz} = 1.69(3) \times 10^{-5}$ s^{-1}) to (^{t}Bu$_3$SiNH)$_3$ZrPh (**1**-Ph, $k_{Ph} = 2.25(3) \times 10^{-3}$ s^{-1}). Of critical importance are the origins of these differences; do they reflect mostly disparate ground state energies, or do the deviations represent transition state energetics? Attempts to obtain crucial ground state information via equilibrium studies were thwarted by unanticipated difficulties. For example, thermolysis of **1**-Ph in the presence of MeH in C$_6$D$_{12}$ resulted in the precipitation of copius amounts of [(^{t}Bu$_3$SiNH)$_3$Zr]$_2$(μ_2:η^1,η^1-1,4-C$_6$H$_4$) (**1**$_2$-C$_6$H$_4$, eq 13). In other instances, cyclometalation of putative intermediate

(65) Benson, S. D. *The Foundations of Chemical Kinetics*; McGraw-Hill: New York, 1960.

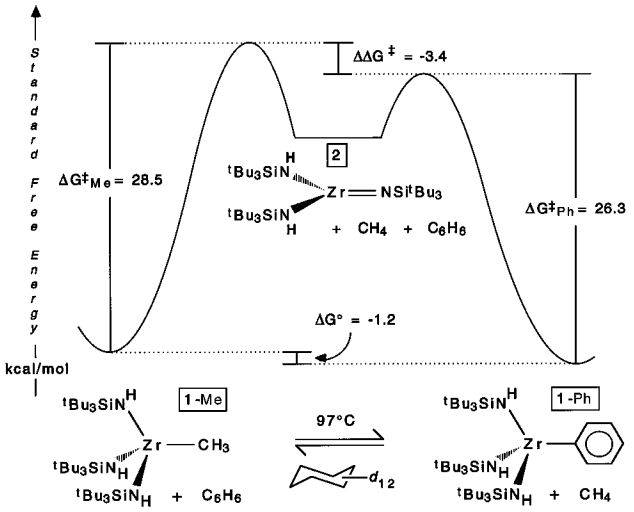

Figure 3.

(^{t}Bu$_3$SiNH)$_2$Zr=NSi^{t}Bu$_3$ (**2**) to (^{t}Bu$_3$SiNH)$_2$ZrNHSi^{t}Bu$_2$CMe$_2$CH$_2$ (**3**) proved competitive with C−H bond activation.

For some critical cases, these difficulties were circumvented through competition experiments designed to indirectly provide ground state information. Imido (^{t}Bu$_3$SiNH)$_2$Zr=NSi^{t}Bu$_3$ (**2**) was generated in the presence of methane (4 atm) and benzene (∼2 equiv) via irreversible loss of cyclohexane from **1**-Cy in C$_6$D$_{12}$ (eqs 34 and 35) at 97 °C. At early conversion (∼17%),

$$(^t\text{Bu}_3\text{SiNH})_3\text{ZrCy} \xrightarrow[\sim 97\ ^\circ\text{C}]{k_{Cy}} (^t\text{Bu}_3\text{SiNH})_2\text{Zr=NSi}^t\text{Bu}_3 + \text{CyH} \quad (34)$$

1-Cy → **2**

$$\mathbf{2} + \text{CH}_4 + \text{C}_6\text{H}_6 \xrightarrow[C_6D_{12},\ \sim 97\ ^\circ\text{C}]{k_{Me}\ \text{vs}\ k_{Ph}} (^t\text{Bu}_3\text{SiNH})_3\text{ZrMe} + (^t\text{Bu}_3\text{SiNH})_3\text{ZrPh} \quad (35)$$

1-Me + **1**-Ph

$$\mathbf{2} + \text{C}_7\text{H}_8 \xrightarrow[C_7H_8,\ \sim 97\ ^\circ\text{C}]{k_{Ar}\ \text{vs}\ k_{Bz}} (^t\text{Bu}_3\text{SiNH})_3\text{ZrC}_6\text{H}_4\text{Me} + (^t\text{Bu}_3\text{SiNH})_3\text{ZrCH}_2\text{Ph} \quad (36)$$

1-Ar + **1**-CH$_2$Ph

$$\mathbf{2} + \text{c-C}_3\text{H}_6 + \text{C}_6\text{H}_6 \xrightarrow[C_6D_{12},\ \sim 97\ ^\circ\text{C}]{k_{cPr}\ \text{vs}\ k_{Ph}} (^t\text{Bu}_3\text{SiNH})_3\text{Zr}^c\text{Pr} + (^t\text{Bu}_3\text{SiNH})_3\text{ZrPh} \quad (37)$$

1-^{c}Pr + **1**-Ph

where reversibility of R/R′H addition was considered minimal, the competition for H−Me vs H−Ph bond activation by the imide revealed that benzene was the favored substrate by $\Delta\Delta G^{\ddagger} = -3.4$ kcal/mol. Inclusion of this energy differential on a standard free energy vs reaction profile diagram enabled calculation of the free energy difference between **1**-Me + C$_6$H$_6$, and **1**-Ph + CH$_4$, which is favored by −1.2 kcal/mol, according to Figure 3.

This minor ground state free energy disparity is matched in related experiments involving activation of the aryl (*para* and *meta*) vs benzylic positions of toluene (eqs 34 and 36). Competition for **2** at 20% conversion revealed that only ∼1% **1**-CH$_2$Ph was observed relative to aryl-activated products, **1**-C$_6$H$_4$Me, indicating a preference for aryl activation by $\Delta\Delta G^{\ddagger} \leq -3.4$ kcal/mol. The products were then thermally equilibrated (∼97 °C), and a ground state energy difference of only

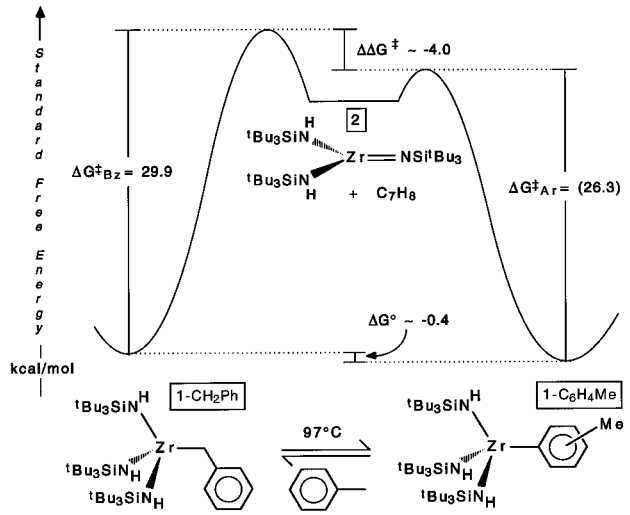

Figure 4.

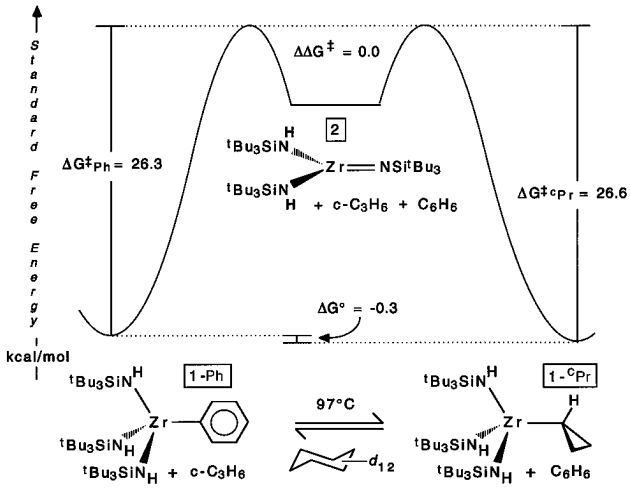

Figure 5.

~0.4 kcal/mol favoring **1**-C_6H_4Me over **1**-CH_2Ph was obtained. Once the activation energies for elimination of the respective groups were applied ($\Delta G^{\ddagger}_{Ar}$ for elimination of toluene from **1**-C_6H_4Me was assumed to be equal to $\Delta G^{\ddagger}_{Ph}$ for **1**-Ph), $\Delta\Delta G^{\ddagger}$ was determined by difference to be ~ −4.0 kcal/mol (Figure 4), consistent with the results of the competition.

Likewise, competition for (^{t}Bu$_3$SiNH)$_2$Zr═NSi^{t}Bu$_3$ (**2**) between cyclopropane and benzene revealed little selectivity (97 °C, $\Delta\Delta G^{\ddagger}$ ~0.0 kcal/mol) at early conversion (<15%). Equilibration afforded a ground state favoring **1**-^{c}Pr + C_6H_6 over **1**-Ph + c-C_3H_6 by −0.3 kcal/mol as depicted in Figure 5, a result fully consistent with the competition.

The data may be combined to infer that MeH activation is favored by −0.6 kcal/mol over $PhCH_2H$ addition or that cyclopropane activation is favored by −3.4 kcal/mol over that of methane and by −4.0 kcal/mol over benzylic activation, etc. Rough estimates[66] based on substrate competitions suggest that cyclometalation of (^{t}Bu$_3$SiNH)$_2$Zr═NSi^{t}Bu$_3$ (**2**) to (^{t}Bu$_3$SiNH)$_2$ZrNH-Si^{t}Bu$_2$CMe$_2$CH$_2$ (**3**) is disfavored by >5.1 kcal/mol relative to MeH activation. Likewise, various concentrations of ethane, neopentane, and cyclohexane have been shown to be uncompetitive substrates when compared with cyclometalation in cyclohexane, hence intramolecular C−H activation to form **3** is <−0.4, <−0.8, and <−2.7 kcal/mol more favorable than Et−H,[67] ^{t}BuCH$_2$−H,[68] and Cy−H addition.[69]

Calculation of a rough, relative C−H bond activation selectivity scale, with ^{c}Pr−H addition taken as the reference, follows ($\Delta\Delta G^{\ddagger}$ in kcal/mol, values in brackets are measured, values in parentheses are estimated): ^{c}PrH [0.0] ≈ ArH [0.0] > MeH [3.4] > $PhCH_2H$ [4.0] > cyclometalation (>8.5) > EtH (>8.9) > ^{t}BuCH_2H (>9.3) > CyH (>11.2). These measurements represent a rare quantitative assessment of selectivities for C−H bond activation,[3,9,11,25,34,70] but care must be taken not to place too much emphasis on the relative positions of the estimated substrates. Figure 6 illustrates relative transition state energies—and therefore the $\Delta\Delta G^{\ddagger}$'s corresponding to CH bond activation selectivity—for the appropriate 1,2-RH-eliminations from **1**-R, which were calculated by taking the standard free energy of **1**-^{c}Pr as reference (0.0 kcal/mol).

5. Thermochemistry and Relative *D*(Zr−R)′s. The general features of relative elimination rates (i.e., $\Delta H^{\ddagger}_{elim}(R) - \Delta H^{\ddagger}_{elim}(R')$) have previously been espoused.[24] Entropic factors—admittedly difficult to assess—are ignored, specifically because it is likely that significant entropic contributions from **1**-R + R′H vs **1**-R′ + RH are likely to cancel.[71] In addition, factors such as solvation energies, which can be important, will also be considered to essentially cancel, *thus our initial analysis will focus on critical bond enthalpies*. With these considerations, it can be shown that $[\Delta H^{\ddagger}_{elim}(R) - \Delta H^{\ddagger}_{elim}(R')] - [\Delta H^{\ddagger}_{addn}(R) - \Delta H^{\ddagger}_{addn}(R')]$ equals ΔH_{rxn}, which can be defined in terms of the respective metal−carbon and carbon−hydrogen bond energies[72] as shown in eq 38. The ΔH_{rxn} corresponding to Figures 3−5 can be estimated from each diagram, thus

$$\Delta H_{rxn} \approx [D(R-H) - D(R-H)] + [D(M-R) - D(M-R')] \quad (38)$$

comparisons of solution phase metal alkyl bond strengths with

(66) Even when fairly low concentrations of MeH (~0.025 M) are used in eq 7, no cyclometalation is evident. Taking the selectivity of (^{t}Bu$_3$SiNH)$_2$Zr═NSi^{t}Bu$_3$ (**2**, generated from **1**-Cy) for MeH vs cyclometalation to **3** to be at least 25 (an easily measurable quantity by ^{1}H NMR), then $r(CH_4)/r(\text{cyclomet}) \sim (k_{MeH}[\mathbf{2}][CH_4]/k_{cymet}[\mathbf{2}]) \sim (k_{MeH}[\mathbf{2}][0.025]/k_{cymet}[\mathbf{2}]) > 25$, and $k_{MeH}/k_{cymet} > 1000$ (1 M standard states). Since $k_{MeH}/k_{cymet} = \exp[(\Delta G^{\ddagger}_{cymet} - \Delta G^{\ddagger}_{MeH})/RT] > 1000$ M, then $\Delta G^{\ddagger}_{cymet} - \Delta G^{\ddagger}_{MeH} > 5.1$ kcal/mol at 370 K.

(67) In each estimate where cyclometalation is observed, other degradation products rendered NMR spectral measurements difficult. Taking the selectivity of (^{t}Bu$_3$SiNH)$_2$Zr═NSi^{t}Bu$_3$ (**2**, generated from **1**-Cy) for cyclometalation to **3** vs EtH activation to be at least 5 (assuming a <5:1 **3**:**1**-Et ratio could be detected by ^{1}H NMR spectroscopy; difficulties with byproduct formation prevented a more definitive estimate by ^{1}H NMR), then $r(\text{cyclomet})/r(\text{EtH}) \sim (k_{cymet}[\mathbf{2}]/k_{EtH}[\mathbf{2}][C_2H_6]) \sim (k_{cymet}[\mathbf{2}]/k_{EtH}[\mathbf{2}]\cdot[0.36]) > 5$, and $k_{cymet}/k_{EtH} > 1.8$ (1 M standard states). Since $k_{cymet}/k_{EtH} = \exp[(\Delta G^{\ddagger}_{EtH} - \Delta G^{\ddagger}_{cymet})/RT] > 1.8$, then $\Delta G^{\ddagger}_{EtH} - \Delta G^{\ddagger}_{cymet} > 0.4$ kcal/mol at 370 K. This analysis relies on the fact that **1**-Et eliminates about three times slower than **1**-Cy and could be reasonably observed under reaction conditions.

(68) Taking the selectivity of (^{t}Bu$_3$SiNH)$_2$Zr═NSi^{t}Bu$_3$ (**2**, generated from **1**-Cy) for cyclometalation to **3** vs ^{t}BuCH_2-H activation to be at least 25 (assuming a <25:1 **3**:**1**-$CH_2{}^t$Bu ratio could be detected by ^{1}H NMR spectroscopy), then $r(\text{cyclomet}/r(Me_4C) \sim (k_{cymet}[\mathbf{2}]/k_{NpH}[\mathbf{2}][Me_4C]) \sim (k_{cymet}[\mathbf{2}]/k_{NpH}[\mathbf{2}][0.12]) > 25$, and $k_{cymet}/k_{NpH} > 3$ (1 M standard states). Since $k_{cymet}/k_{NpH} = \exp[(\Delta G^{\ddagger}_{NpH} - \Delta G^{\ddagger}_{cymet})/RT] > 3$, then $\Delta G^{\ddagger}_{NpH} - \Delta G^{\ddagger}_{cymet} > 0.8$ kcal/mol at 370 K. This analysis relies on the fact that **1**-$CH_2{}^t$Bu eliminates about seven times slower than **1**-Cy and could be reasonably observed under reaction conditions.

(69) When **1**-Me is thermolyzed in cyclohexane-d_{12}, no deuteration of the amide positions of any products is observed, hence there is no evidence of C_6D_{12} activation. Assuming the density of C_6D_{12} (0.89 g/mL) is relatively insensitive to temperature, neat cyclohexane is ~9.3 M. Assuming a k_H/k_D for cyclohexane activation to be ~5, and that >5% deuteration could be detected by ^{1}H NMR spectroscopy, the selectivity of (^{t}Bu$_3$SiNH)$_2$Zr═NSi^{t}Bu$_3$ (**2**, generated from **1**-Me) for cyclometalation to **3** vs CyH activation would be at least 4; then $r(\text{cyclomet})/r(\text{CyH}) \sim (k_{cymet}[\mathbf{2}]/k_{CyH}[\mathbf{2}][C_6H_{12}]) \sim (k_{cymet}[\mathbf{2}]/k_{CyH}[\mathbf{2}][9.3]) > 4$, and $k_{cymet}/k_{CyH} > 37$ (1 M standard states). Since $k_{cymet}/k_{CyH} = \exp[(\Delta G^{\ddagger}_{CyH} - \Delta G^{\ddagger}_{cymet})/RT] > 37$, then $\Delta G^{\ddagger}_{CyH} - \Delta G^{\ddagger}_{cymet} > 2.7$ kcal/mol at 370 K.

(70) Periana, R. A.; Bergman, R. G. *Organometallics* **1984**, *3*, 508−510.

(71) (a) Jones, W. D.; Feher, F. J. *J. Am. Chem. Soc.* **1984**, *106*, 1650−1664. (b) Jones, W. D.; Feher, F. J. *Acc. Chem. Res.* **1989**, *22*, 91−100.

(72) Berkowitz, J.; Ellison, G. B.; Gutman, D. *J. Phys. Chem.* **1994**, *98*, 2744−2765.

those of *gas phase* carbon−hydrogen bonds (Table IV) can be made. Implicit in the discussion is the assumption that enthalpies and entropies of sublimation associated with the various metal−alkyl complexes (**1**-R) can be considered approximately equal.[71]

From Figure 3, $\Delta H_{rxn} \approx -0.9$ kcal/mol (~ -0.3 kcal/mol are attributed to the statistics favoring benzene (6H) vs MeH (4H) capture) and $[D(\text{Ph}-\text{H}) - D(\text{Me-H})] \approx 6.3$ kcal/mol, thus $[D(\text{Zr}-\text{Me}) - D(\text{Zr}-\text{Ph})] \approx -7.2$ kcal/mol. In essence, the origin of the minimal ground state difference between **1**-Me + C_6H_6 and **1**-Ph + MeH stems from the similar differences in Zr-C[73−76] vs C−H bond enthalpies (eq 39).[72] The diagram

$$\Delta H_{rxn} \approx [\text{D}(\text{Zr}-\text{Me}) - \text{D}(\text{Zr}-\text{Ph})] + [\text{D}(\text{Ph}-\text{H}) - \text{D}(\text{Me}-\text{H})] \quad (39)$$

(Figure 4) reflecting benzyl vs aryl elimination possesses related features according to eq 40: $\Delta H_{rxn} \approx -0.4$ kcal/mol (recall that the elimination rate for **1**-Ph was used), $[D(\text{Ar}-\text{H}) - D(\text{PhCH}_2-\text{H})] \approx 22.7$ kcal/mol, $[D(\text{Zr}-\text{CH}_2\text{Ph}) - D(\text{Zr}-\text{Ar})] \approx -22.3$ kcal/mol. Toluene is absent in the equilibrium, hence this analysis assumes that the aryl and benzylic C−H bonds do not

$$\Delta H_{rxn} \approx [\text{D}(\text{Zr}-\text{CH}_2\text{Ph}) - \text{D}(\text{Zr}-\text{C}_6\text{H}_4\text{Me})] + [\text{D}(\text{Ar}-\text{H}) - \text{D}(\text{ArCH}_2-\text{H})] \quad (40)$$

differ when $(^t\text{Bu}_3\text{SiNH})_3\text{Zr}$ is an aryl substituent. A similar analysis corresponding to Figure 5 suggests that $[D(\text{Zr}-\text{Ph}) - D(\text{Zr}-{}^c\text{Pr})] \approx 4.9$ kcal/mol, simplified in eq 41. Comparable free energy pictures are obtained for all of the substrate competitions (i.e., minor ground state differences that ultimately

$$\Delta H_{rxn} \sim [\text{D}(\text{Zr}-\text{Ph}) - D(\text{Zr}-{}^c\text{Pr})] + [\text{D}({}^c\text{Pr}-\text{H}) - \text{D}(\text{Ph}-\text{H})] \quad (41)$$

relate to large differences in $D(\text{Zr}-\text{R}) - D(\text{Zr}-\text{R}')$), thus the assumption that entropic factors and heats of solvation are either minimal, or essentially cancel in comparison, gains some credence for these specific cases. The data roughly suggest that the differences between metal−carbon,[73−76] and between corresponding carbon−hydrogen bond strengths,[72] are essentially the same for the substrates amenable to the equilibrium study; related conclusions were determined for the previously investigated tantalum system.[24]

6. The Nature of the Transition State for 1,2-RH-Elimination. Figure 7 illustrates a plot of the free energies of activation for 1,2-RH-elimination (96.7 °C) from **1**-R vs $D(\text{R}-\text{H})$, the bond dissociation enthalpies of the corresponding hydrocarbons.[72] According to the rudiments of the Hammond postulate, a basic assessment of the rates is proferred; the transition state of 1,2-RH-elimination is proposed to reflect varying degrees of reactant and product character.[78] Choosing the ordinate scale as $D(\text{R}-\text{H})$ leads to two potential interpretations: (1) a negative slope implicates a correlation with the strength of the C−H bond formed in the 1,2-RH-elimination event (i.e., $\Delta G^{\ddagger} \propto D(\text{R}-\text{H})$)—a late transition state; (2) a positive slope indicates a correlation with the strength of Zr−C bond broken in the 1,2-RH elimination process (i.e., $\Delta G^{\ddagger} \propto$ $D(\text{Zr-R})$; assuming $D(\text{Zr}-\text{R}) \propto D(\text{R}-\text{H})$[72−76]—an early transition state. Note that the $\Delta\Delta G^{\ddagger}_{elim}$ data span a moderate energy range (3.6 kcal/mol, ~13% of $\Delta G^{\ddagger}_{av} = 27.9$ kcal/mol), while the scope of bond enthalpies for the hydrocarbons in common is substantially greater (23 kcal/mol, ~23% of $D(\text{R}-\text{H})_{av} =$

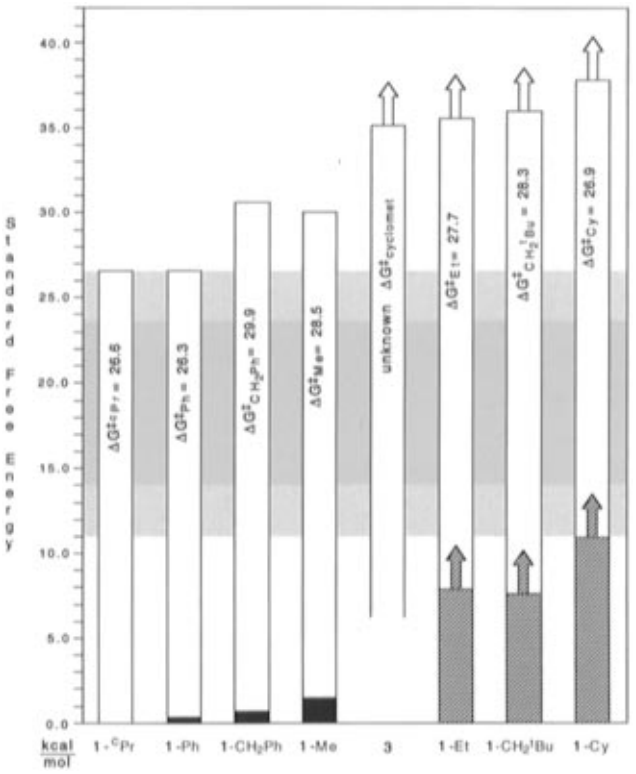

Figure 6. Relative ground state ($\Delta G°$ where $\Delta G°$ (**1**-^{c}Pr) = 0.0 kcal/mol) and transition state ($\Delta G°_{TS} = \Delta G° + \Delta G^{\ddagger}$(1,2-RH-elim)) energies for **1**-R obtained from kinetics studies (colorless), equilibrium (black) measurements, and estimated $\Delta G°$ data (lined) derived from competitive activations. The light and darked shaded background represents possible and most likely energetic positions of any intermediate(s). Arrows indicate that the energies are estimated minima.

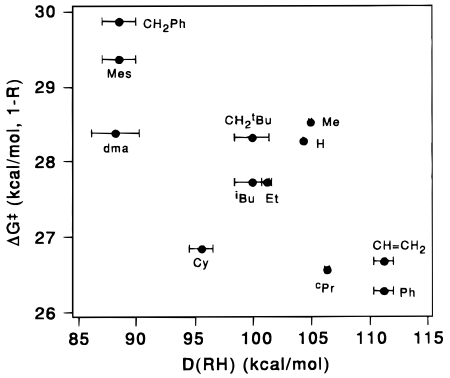

Figure 7. $\Delta G^{\ddagger}$ (1,2-RH-elim) for **1**-R vs bond dissociation enthalpy, $D(\text{R}-\text{H})$; $D(\text{M}-\text{R})$ is predicted to be proportional to the latter. A negative slope implicates a late transition state ($\Delta G^{\ddagger}$ decreases as $D(\text{R}-\text{H})$ increases) and a positive slope is indicative of an early transition state ($\Delta G^{\ddagger}$ increases as $D(\text{M}-\text{R})$ increases).

(73) (a) Schock, L. E.; Marks, T. J. *J. Am. Chem. Soc.* **1988**, *110*, 7701−7715. (b) Diogo, H. P.; de Alencar Simoni, J.; Minas da Piedade, M. E.; Dias, A. R.; Martinho Simões, J. A. *J. Am. Chem. Soc.* **1993**, *115*, 2764−2774.

(74) (a) Bryndza, H. E.; Fong, L. K.; Paciello, R. A.; Tam, W.; Bercaw, J. E. *J. Am. Chem. Soc.* **1987**, *109*, 1444−1456. (b) Bryndza, H. E.; Bercaw, J. E. *Polyhedron* **1988**, *7*, 1441−1452.

(75) Labinger, J. A.; Bercaw, J. E. *Organometallics* **1988**, *7*, 926−928.

(76) For an alternative viewpoint, see: Drago, R. S.; Wong, N. M.; Ferris, D. C. *J. Am. Chem. Soc.* **1992**, *114*, 91−98.

(77) The parabolic representations of the free energy surface arise from the usual ill-defined reaction coordinate that comprises Zr−R and N−H bond-breaking along with C−H and ZrN(π) bond-making and the geometric changes that accompany these events. In this model, the curvature of all **1**-R(R′) are considered equivalent (i.e., same dependence on x). While this is not rigorously true, only very minor deviations are expected in this energy region (i.e., the lower portion of each parabola is not consequential). The model also assumes that the reactant to product transition occurs adiabatically, with a facility that is independent of R. For the origin of such models, see: Thornton, E. R. *J. Am. Chem. Soc.* **1967**, *89*, 2915−2927. See, also: Hammond, G. S. *J. Am. Chem. Soc.* **1955**, *77*, 334−338.

(78) Cundari, T. R.; Matsunaga, N., submitted for publication.

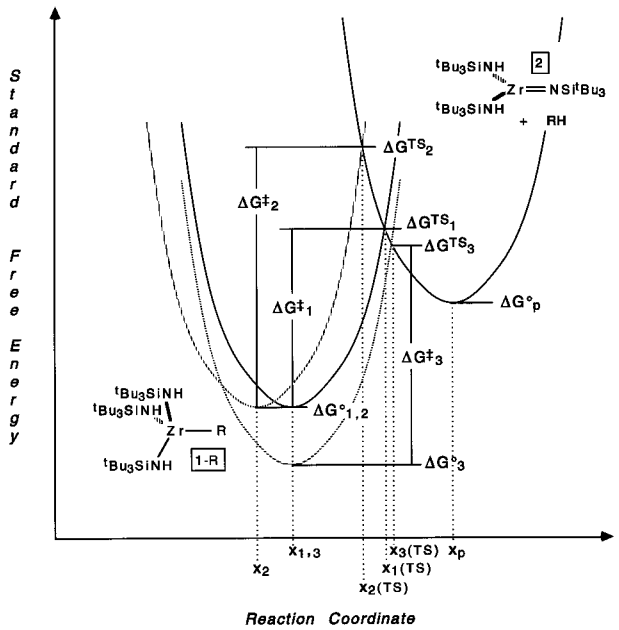

Figure 8. $\Delta G^{\ddagger}$ (1,2-RH-elim) for **1**-R values may be viewed as arising from disparate ground state energies (e.g., $\Delta G^{\circ}_{1,2}$ vs ΔG°_{3}), and differing positions ($x_{1,3}$ vs x_2) along the reaction coordinate.

100.4 kcal/mol). This disparity may portend transition states for 1,2-RH-elimination that possess a balanced character, consistent with the kinetic isotope effect data that portray the hydrogen/deuterium transfer as symmetric.

The data are roughly grouped into three regions. The first contains the benzylic hydrocarbyls, **1**-CH_2Ph and **1**-Mes, and the η^1-dimethylallyl derivative, **1**-dma, whose corresponding hydrocarbons possess similar bond dissociation energies. Data within a second group containing the alkyls, **1**-R (R = Cy, ^{i}Bu, Et, ^{t}BuCH_2, Me), and the hydride, **1**-H, are somewhat scattered, but a very rough positive correlation with D(R−H) can be inferred. Species containing Zr−C(sp^2) bonds, **1**-R (R = CH═CH_2, Ph, ^{c}Pr) comprise the third group of hydrocarbyls, assuming this description of the cyclopropyl derivative is apt.[62]

Figure 8 provides a textbook[62,77] parabolic view of **1**-R + R′H and an intermediate (elimination product) state of (^{t}Bu$_3$SiNH)$_2$Zr═NSi^{t}Bu$_3$ (**2**) + RH + R′H, enabling interpretation of the energetics in Figure 6 and Figure 7. Given the caveat of a common intermediate, the 1,2-RH-elimination data can be roughly explained with two variables: the disposition of the **1**-R + R′H (x_n) relative to **2** + RH + R′H (x_p) along the reaction coordinate and the relative standard free energies of **1**-R + R′H (ΔG°_{n}). The reaction coordinate is mostly comprised of Zr−C bond-breaking, C−H bond-making, ZrN(π) bond-making, and N−H bond-breaking. Figure 8 shows that late transition states are a general property of endothermic reactions comprised of similar parabolic surfaces for the reactant and product states, which are likely when D(Zr−R) approaches that of D(H−R). It is expected from the work of Schock and Marks *et al.* that the zirconium-carbon bonds are strong and that D(Zr−C) are in a regime where they correlate linearly with related hydrocarbon BDEs (e.g., D(Zr−R) ∼ αD(R−H) + β).[73]

For **1**-R + R′H with similar ground state energies, their respective $\Delta G^{\ddagger}_{elim}$ respond to a shift along the reaction coordinate. Note that $\Delta G^{\ddagger}_1 < \Delta G^{\ddagger}_2$ as a consequence of $x_1 > x_2$. As a corollary not easily grasped from the figure, $\{x_1(TS) - x_1\}/\{x_p - x_1\} > \{x_2(TS) - x_2\}/\{x_p - x_2\}$, i.e., x_1(TS) is further along than x_2(TS) on their respective reaction coordinates. Consequently, path 1 is *later* than path 2, thereby revealing the origin of the swifter rate, a situation applicable to **1**-Ph (or **1**-Ar, Figure 4) + C_7H_8 vs **1**-CH_2Ph + PhH (or ArH), where the respective ground states are of little consequence to the disparate elimination rates. Because of the minimal relative ground state differences of group representatives **1**-CH_2Ph ($k_{Bz} = 1.69(3) \times 10^{-5}$ s^{-1}), **1**-Me ($k_{Me} = 1.06(2) \times 10^{-4}$ s^{-1}), **1**-^{c}Pr ($k_{c\text{-}Pr} = 1.55(2) \times 10^{-3}$ s^{-1}) and **1**-Ph ($k_{Ph} = 2.26(2) \times 10^{-3}$ s^{-1}), these **1**-R manifest disparate 1,2-RH-elimination rates primarily as a consequence of differing positions along the reaction coordinate. For these complexes, use of transition state energies (e.g., define $\Delta G^{TS} = \Delta G^{\ddagger} + \Delta G^{\circ}$) naturally leads to the same conclusion—the later or more product-like the transition state, the faster the 1,2-RH-elimination rate. Note that the lowest primary KIE among the three measured (**1**-(ND)$_3$R, R = Me, CH_2Ph, Ph) is for **1**-Ph ($z_{Ph} = 4.6(4)$), where the transition state energy is likely to be near that of the intermediate state, consistent with a less symmetric N···H···Ph conformation that implicates a later position along the reaction coordinate.

Where ground state energies are significantly dissimilar, respective transition state energies are additionally effected. Note that $\Delta G^{\ddagger}_1 < \Delta G^{\ddagger}_3$ despite their identical ground state positions ($x_1 = x_3$) and despite the lower energy of ΔG^{TS}_3 relative to ΔG^{TS}_1. Furthermore, ΔG^{TS}_1 occurs *earlier* than ΔG^{TS}_3 (x_1(TS) < x_3(TS)), even though both pathways are generally "late". The ground state factor is particularly applicable to the alkyl and hydride group, whose **1**-R roughly correlates with the strength of the zirconium−carbon (−hydride) bond being broken, provided D(R−H) is an index of D(R−M). Figure 8 reveals why **1**-Me + EtH (e.g., ΔG°_3) has a slower methane elimination rate than 1,2-EtH-elimination from **1**-Et + MeH (e.g., ΔG°_1), despite a transition state energy that is lower by <−5.8 kcal/mol. Since the origins of the reaction coordinate will be similar, it is the ground state energy of **1**-Et + MeH, which is higher by >6.6 kcal/mol, that translates into an earlier, yet swifter alkane elimination.

Relative ground and transition state energies for selected **1**-R (Figure 6) show that the former must necessarily be coupled with positional changes in the reaction coordinate to adequately understand the correlation between $\Delta G^{\ddagger}_{elim}$ and D(R−H) (Figure 7). Ground state energetics pertaining to **1**-R (R = Et, $CH_2{}^{t}$Bu, Cy) suggest that greater reactant character is infused in the transition states for alkane (and possibly H_2) elimination, hence the positive correlation with D(Zr−C) (i.e., D(C−H)) for this subgroup, even though the process is still generally "late". Further inspection of Figure 6 reveals that the intermediate state (**2** + RH's) must be >11.3 kcal/mol (ΔG° for **1**-Cy relative to **1**-^{c}Pr at 0.0 kcal/mol) and <26.6 kcal/mol (ΔG^{TS} of **1**-^{c}Pr). From the energetics and the parabolic Hammond analysis, the character of the transition state with respect to Zr−C bond-breaking and C−H bond-making is likely to be balanced, although possessing more of the latter. *Ab initio* calculations (GAMESS) on the transition states of elimination from several models of **1**-R, (H_2N)$_3$Zr-R (**1′**-R), corroborate this postulation.[78,79]

The application of a Hammond analysis[62,77] to this system—and to the previously reported tantalum series,[24] which can be interpreted in similar fashion—is satisfying because conventional logic may be used to assemble a self-consistent depiction encompassing a variety of substrates. Furthermore, the nature of the 1,2-RH-elimination reaction is reminiscent of organic H−CH_2CH_2−X eliminations, where similar interpretive methods have proven useful. Given this analysis, it is pertinent to ask *why* a consistent picture can be obtained, i.e., why the necessary assumptions work, whether there are alternative explanations, and specifically why the ground states of **1**-Et, **1**-$CH_2{}^{t}$Bu, and **1**-Cy are relatively high.

(79) (a) Cundari, T. R.; Gordon, M. S. *J. Am. Chem. Soc.* **1993**, *115*, 4210−4217. (b) Cundari, T. R. *Organometallics* **1993**, *12*, 4971−4978.

If similar activation entropies for each 1,2-RH-elimination can be inferred from the data,[80] entropic contributions from rotation and alignment of the $^tBu_3SiNH$ ligand are probably dominant, since variation of R apparently has minor impact. Brown and Caffery's molecular mechanics analysis of the 1,2-RH-elimination events revealed little to moderate steric influence from variation of R.[81,82] As a corollary, entropic contributions by R to **1**-R and its transition state for 1,2-RH-elimination are effectively similar. Attempts to interdependently correlate D(C−H) (α D(Zr−C)) and appropriate steric factors to the $\Delta G^{\ddagger}_{elim}$ data failed.[82] Calculational treatments suggest that the eliminations can be assessed as a replacement of Zr by H at a carbon center that undergoes minimal distortion, hence the enthalpic correlations assessing bond-making and -breaking characteristics were anticipated.[43,78,79] Nonetheless, it is certainly plausible that some of the scatter in the data results from subtle deviations in $\Delta S^{\ddagger}_{elim}$.

An earlier, alternative explanation for the 1,2-RH-elimination vs D(R−H) data (Figure 7) ascribed the relative speed of elimination from the sp^2 substrates (**1**-Ph, **1**-^{c}Pr, and **1**-CH=CH$_2$) to a transition state stabilization[22] due to adjacent p-orbital participation in the H−C bond-forming process. Calculational support for p-orbital participation has not been uncovered (except for R = C≡CR, *vide infra*),[78] and the possibility of special ground state stabilization for **1**-CH$_2$Ph etc., is not supported by experiment. The $^1J_{CH}$ of 119 Hz for the Zr−CH$_2$− group of the benzyl complex, **1**-CH$_2$Ph, is typical for such fragments, and not particularly indicative of agostic[46] or allylic bonding. Low temperature ^{1}H NMR studies revealed no peculiar benzyl conformation or agostic effect that would prevent ready access to the geometry required for 1,2-elimination, but subtle energetic effects ($\sim$ <5 kcal/mol) would not be evident in these experiments, hence some ambiguity persists.

The most difficult aspect of the 1,2-RH-elimination rates to assess concerns the rather dramatic jump in relative ground state energies for the alkyl derivatives, especially the large difference between **1**-Me and **1**-Et. Steric arguments, augmented by the molecular mechanics study,[81] rationalize the destabilization of **1**-Cy and **1**-CH$_2$^{t}Bu relative to **1**-Me, but differentiation of methyl from ethyl on this basis is untenable in view of the stability of much bigger substituents such as benzyl, mesityl, and phenyl.

Attempts to correlate the 1,2-RH-elimination rates and transition state energies to gas phase[83,84] and solution acidities[85] met with little success but suggested a possible explanation for the ground state anomalies. For gas phase acidities, the addition of α-Me groups to CH$_4$ leads to an inductive acid-weakening effect that is compensated by an acid-strengthening polarization effect.[83] Methane is therefore a stronger acid than ethane, which is approximately the same as propane (2-position), while isobutane (2-position) is stronger than MeH. Solution acidity data show that increasing substitution at carbon results in a weakening of acidity. If the acidity data can be considered to reflect the ionic character of the bond, the data can be interpreted to mean that increasing substitution at carbon decreases the ionicity of a bond to that carbon. Electronegativity arguments support the contention that zirconium−carbon bonds possess a substantially stronger ionic component than their hydrocarbon congeners, and thus may be destabilized to a greater degree by inductive effects relative to RH. An inductive destabilization of **1**-R (R = Et, CH$_2$^{t}Bu, Cy) relative to **1**-Me would explain their higher ground states and corresponding greater influence on the respective transition state species. The drawback to this argument concerns its specificity; substantial acidity differences among the more acidic RH (R = ^{c}Pr, Ph, CH$_2$Ph) substrates must not generate equivalent inductive influences, perhaps due to a leveling effect, i.e., the Zr−C bond may have a maximum ionicity.

Existence of the Three-Coordinate Intermediate, (^{t}Bu$_3$SiNH)$_2$Zr=NSi^{t}Bu$_3$ (2), and Alkane Binding. 1. Proton Affinity and 1,2-RH-Elimination. The previous discussion of 1,2-RH-elimination rates assumed that a single intermediate, (^{t}Bu$_3$SiNH)$_2$Zr=NSi^{t}Bu$_3$ (**2**), mediated the process and its microcopic reverse, 1,2-RH-addition. Since arene[86] and, more recently, alkane complexes have been implicated as intermediates in the activation of C−H bonds by late metal d^8 complexes,[31−35] and as transients indirectly observed in reductive elimination reactions,[4,36] it is prudent to assess the viability of such species in this d^0 metal imido system.

Consider the binding of an alkane or arene to an electropositive, d^0 zirconium center to be analogous to protonation of RH, whose enthalpy change is −PA, where PA is the proton affinity of the hydrocarbon.[87,88] Figure 9 illustrates a plot of $\Delta G^{\ddagger}$ for 1,2-RH-elimination versus the proton affinity of the corresponding RH. When available, appropriate experimental PA values were utilized, but several were obtained from semiempirical AM1 calculations. In specific cases such as benzylic activation, calculations were necessary because experimental results reflect protonation of the arene ring, mimicking an unproductive reaction coordinate. In such instances, protonation was effected at the appropriate C−H bond, the structure minimized, and the proton affinity calculated. The hydride, **1**-H, was not considered because of the obvious orbital differences between H and an R fragment; its PA of 104.1(11) kcal/mol places it conspicuously off the curve.

A relatively smooth correlation is apparent; the greater the proton affinity of RH, the faster the 1,2-RH-elimination from

(80) 1,2-XH-elimination activation entropies are −10(3) eu in three distinct systems: see refs 23, 25 and this work.

(81) Caffery, M. L.; Brown, T. L., personal communication. Employing a fit to ln k(1,2-RH-elim) = aE_R' + bD(C−H) + c, where E_R' is a ligand repulsive energy, a correlation coefficient of 0.838 was found for α = 0.036, β = 0.18, and γ = −27.50. The results were consistent with a late transition state that manifests some steric acceleration of 1,2-RH-elimination. Mechanics calculations were performed using BIOGRAF, through an academic collaborators arrangement with Molecular Simulations, Inc. For a related study, see: Brown, T. L. *Inorg. Chem.* **1992**, *31*, 1286−1294.

(82) Attempts to establish a Thornton−More O'Farrell−Jencks type diagram using D(RH) (α D(Zr−C)) and PA (proton affinity) data as interdependent indicators of orthogonal reaction coordinates failed to converge to a solution where both were correlated with the $\Delta G^{\ddagger}$ values of **1**-R. In retrospect, these two data sets are probably not independent--they reflect similar features of each RH. Other efforts coupling D(RH) (α D(Zr−C)) and R steric factors (effective A-values) generated by Brown and Cafferty (ref 81), or PA and A-values also failed to elicit an interdependent correlation with the $\Delta G^{\ddagger}_{elim}$ (**1**-R) vlaues, possibly because the steric factors are of minor consequence in these reactions. (a) More O'Ferrall, R. A. *J. Chem. Soc. B.* **1970**, 274−277. (b) Jencks, W. P. *Chem. Rev.* **1972**, *72*, 705−718.

(83) DePuy, C. H.; Gronert, S.; Barlow, S. E.; Bierbaun, V. M.; Damrauer, R. *J. Am. Chem. Soc.* **1989**, *111*, 1968−1973.

(84) Current values have been compiled by John E. Bartmess, Department of Chemistry, University of Tennessee, Knoxville, TN 37996.

(85) Current values were obtained from Andrew Streitweiser, Jr., Department of Chemistry, University of California, Berkeley, Berkeley, California, 94720. See, also: Streitweiser, A., Jr.; Juaristi, E.; Nebenzahl, L. L. In *Comprehensive Carbanion Chemistry, Part A*; Buncel, E., Durst, T., Eds.; Elsevier: Amsterdam, 1980.

(86) For an interesting example, see: Jones, W. D.; Feher, F. J. *J. Am. Chem. Soc.* **1986**, *108*, 4814−4819.

(87) (a) McMahon, T. B.; Kebarle, P. *J. Am. Chem. Soc.* **1985**, *107*, 2612−2617. (b) Collyer, S. M.; McMahon, T. B. J. Phys. Chem. 1983, 87, 909−912. (c) Rosenstock, H. M.; Buff, R.; Ferreira, M. A. A.; Lias, S. G.; Parr, A. C.; Stockbauer, R. L.; Holmes, J. L. *J. Am. Chem. Soc.* **1982**, *104*, 2337−2345. (d) Cotter, R. J.; Rozett, R. W.; Koski, W. S. *J. Chem. Phys.* **1972**, *57*, 4100−4102.(e) Moylan, C. R.; Brauman, J. I. *Ann. Rev. Phys. Chem.* **1983**, *34*, 187−215. (f) Devlin, J. L.; Wolf, J. F.; Taft, R. W.; Hehre, W. J. *J. Am. Chem. Soc.* **1976**, *98*, 1990−1992. (g) Chong, S.-L.; Franklin, J. L. *J. Am. Chem. Soc.* **1972**, *94*, 6347−6351. (h) Walder, R.; Franklin, J. L. *Int. J. M. S. Ion. Phys.*, **1980**, *36*, 87.

(88) Lee, C. C.; Hass, E. C.; Obafemi, C. A.; Mezey, P. G. *J. Comput. Chem.* **1984**, 5, 190−196.

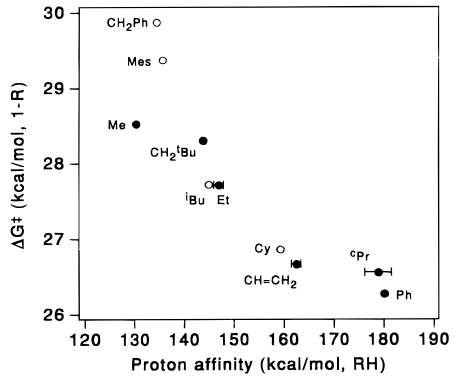

Figure 9. $\Delta G^{\ddagger}$ (1,2-RH-elim) for **1**-R vs the proton affinity, PA, from experiment (●) or from AM1 calculations (○).

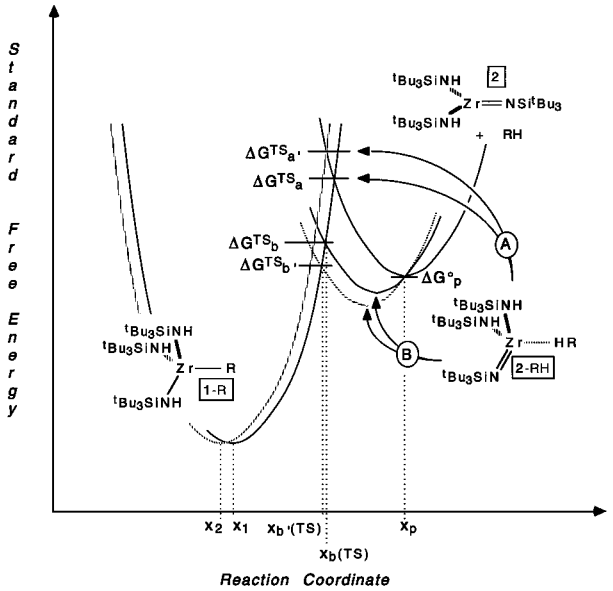

Figure 10. The proton affinity correlation may be viewed as reflecting a purely positional component (x_1 vs x_2, A), or indicating complexation of RH (i.e., **2**-RH, B). To highlight the latter possibility, note that **2** is no longer accorded a minimum in the free energy surface.

1-R. While the intrinsically enthalpic correlation substantiates the proposed minimal importance of entropic effects, the data are also consistent with the previous contention of a generally late transition state. Attempts to interdependently correlate PA and appropriate steric factors to the $\Delta G^{\ddagger}_{\text{elim}}$ data failed.[82] Consider the parabolic depiction in Figure 10, where the reaction coordinate again corresponds to the 1,2-elimination of RH to putative (^{t}Bu$_3$SiNH)$_2$Zr═NSi^{t}Bu$_3$ (**2**), affording (^{t}Bu$_3$SiNH)$_2$-(^{t}Bu$_3$SiN═)Zr(RH) as a transition state (**A**, **2**-RH‡). The correlation of $\Delta G^{\ddagger}_{\text{elim}}$ with PA implicates a stabilization of the transition state **A**. Figure 8 revealed that stabilization of ΔG^{TS} could occur via a later reaction coordinate for 1,2-RH-elimination (e.g., earlier for 1,2-RH-addition) and through lowering the ground state energy of **1**-R; the former results in a decrease in $\Delta G^{\ddagger}_{\text{elim}}$, but the latter actually results in an *increase*, and ΔG^{TS} reflects both components. Consequently, it must be inferred that the correlation of $\Delta G^{\ddagger}$ with PA stems from the change in $\Delta G^{\ddagger}_{\text{elim}}$ that *derives solely from a positional change* (e.g., $x_2 \rightarrow x_1$ results in $\Delta G^{\text{TS}}_{\text{a}} < \Delta G^{\text{TS}}_{\text{a}'}$) *along the reaction coordinate*. An RH substrate more tightly bound in the transition state would naturally have its R group and H atom nearer the Zr and N, respectively. As a corollary, note that PA would *not* be expected to correlate with ΔG^{TS} or $(x_{\text{n}}(\text{TS}) - x_{\text{n}})/(x_{\text{p}} - x_{\text{n}})$, the fractional position of the transition state along the reaction coordinate, because these are influenced by both $x_{\text{p}} - x_{\text{n}}$ and ΔG°_{n}(**1**-R).

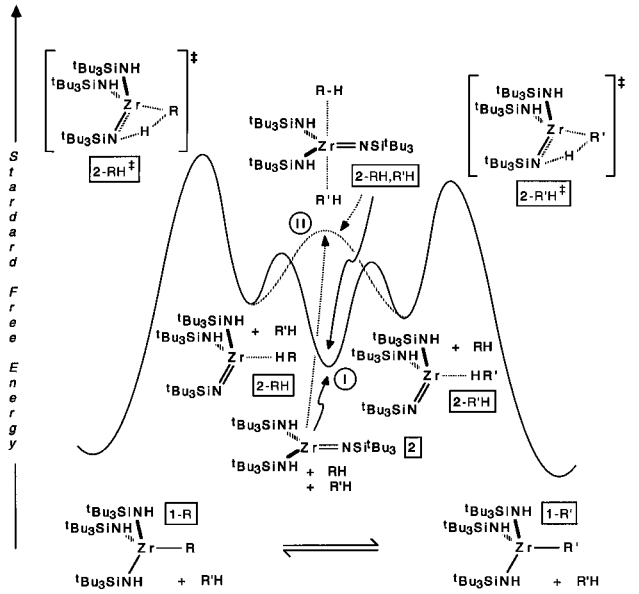

Figure 11. Standard free energy diagram illustrating a 1,2-RH-elimination/addition process mediated by RH-binding transients, **2**-RH and **2**-R′H, and dissociative (**I**) or associative (**II**) pathways between them.

Alternatively, RH-bound intermediates (**2**-RH, **B**) could play a role as indicated in Figure 10. The parabolas for **2**-RH are arbitrarily sketched to cross the surface ascribed to (^{t}Bu$_3$SiNH)$_2$-Zr═NSi^{t}Bu$_3$ (**2**) such that $\Delta G^{\circ}_{\text{p}}$ is no longer at a minimum, thereby showing that **2** need not be a viable intermediate in this system; hydrocarbon exchanges could occur between **2**-RH and **2**-R′H via dissociative or associative interchange pathways.[89] For intermediates **B**, it is clear that stronger binding of RH results in a lower transition state for elimination (i.e., $\Delta G^{\text{TS}}_{\text{b}'} < \Delta G^{\text{TS}}_{\text{b}}$) that can be considered independent from ground state or positional influences of **1**-R.

In either situation, transition state stabilization (**A**) or intermediate state (**B**) alternative, one common theme derives from the $\Delta G^{\ddagger}_{\text{elim}}$ vs PA correlation: the more tightly RH is bound in the transition state, the nearer ΔG^{TS} is to the reactant and product states. It is noteworthy that the swiftest **1**-R eliminations are observed for sp^2-hybridized hydrocarbyls, whose Zr−C bond lengths are shorter than corresponding sp^3-hybridized species, and are thereby positionally later in their respective reaction coordinates. Furthermore, the straightforward correlation depicted in Figure 9 illustrates that proton affinity can be used to predict the 1,2-RH-elimination rate of a new **1**-R but cannot assess the true "lateness" of its transition state because ground state contributions from **1**-R cannot be discerned.

Figure 11 presents a conventional depiction of a standard free energy surface where intermediate (^{t}Bu$_3$SiNH)$_2$(^{t}Bu$_3$SiN═)Zr-(RH) (**2**-RH) and **2**-R′H complexes reside at positions succeeding the respective 1,2-RH-elimination transition states (labeling experiments discount reversible elimination/addition prior to RH loss). Transients such as (^{t}Bu$_3$SiNH)$_2$Zr═NSi^{t}Bu$_3$ (**2**) or even five-coordinate (^{t}Bu$_3$SiNH)$_2$(^{t}Bu$_3$SiN═)Zr(RH)(R′H) (**2**-RH,R′H) may exist (**I**) or may simply be representative of transition states for RH for R′H exchange via dissociative or associative interchange pathways (**II**).[89]

2. Associative Exchange in (^{t}Bu$_3$SiNH)$_3$ZrC≡CR (1-C≡CR). Alkynyl derivatives, (^{t}Bu$_3$SiNH)$_3$ZrC≡CR (**1**-C≡CPh, **1**-C≡C^{t}Bu), are conspicuous by their absence in the previous mechanistic discussions. Thermolysis of **1**-C≡CPh or **1**-C≡

(89) Atwood, J. D. *Inorganic and Organometallic Reaction Mechanisms*; Brooks/Cole: Monterey, CA, 1985.

C^{t}Bu in benzene-d_6 at 96.7 °C for several days did not induce 1,2-elimination of the terminal acetylenes. Phenylacetylene loss from **1**-C≡CPh occurred in the presence of excess *tert*-butylacetylene, affording **1**-C≡C^{t}Bu rather than **1**-(ND)$_3$-C$_6$D$_5$, and the reaction rate was roughly first-order in [^{t}BuC≡CH] according to initial rate studies (<20% conversion, k_{CCPh} = 1.1-(4) × 10^{-3} M^{-1} s^{-1}). Likewise, elimination of ^{t}BuC≡CH from **1**-C≡C^{t}Bu occurred in the presence of excess PhC≡CH to provide **1**-C≡CPh, and rough initial rate measurements revealed a first-order dependence on [PhC≡CH], with k_{CCBu} = 1.2 (5)

$$(^t\mathrm{Bu_3SiNH})_3\mathrm{ZrC{\equiv}C}^t\mathrm{Bu} + \mathrm{PhC{\equiv}CH} \underset{96.7\ ^\circ\mathrm{C}}{\overset{\mathrm{C_6D_6}}{\rightleftharpoons}} (^t\mathrm{Bu_3SiNH})_3\mathrm{ZrC{\equiv}CPh} + {}^t\mathrm{BuC{\equiv}CH} \quad (42)$$

1-C≡C^{t}Bu **1**-C≡CPh

× 10^{-3} M^{-1} s^{-1} (eq 42). In support of the initial rate studies, equilibrium studies revealed that **1**-C≡CPh is slightly favored (K(eq 42) = 0.5, $\Delta G^\circ \sim 0.5$ kcal/mol). Since the rates of alkyne exchange appear to be second-order in both directions, an associative interchange pathway is tentatively proferred.[89] σ-Bond metathesis[9] represents an alternative pathway, but one difficult to reconcile with the lack of supporting evidence from the aforementioned studies of **1**-R.

On the basis of the bond strength (D(RC≡C−H) ∼ 120−135 kcal/mol) and proton affinity estimates, 1,2-alkyne elimination should be swift, provided the conventional mechanistic scheme is relevant. A pathway consistent with the other **1**-R complexes involves the intermediacy of azametallacyclobutene intermediates, (^{t}Bu$_3$SiNH)$_2$ZrC(R)=C(H)NSi^{t}Bu$_3$ (R = Ph, **2**-HC≡CPh; ^{t}Bu, **2**-HC≡C-^{t}Bu), formed via 1,2-RC$_2$H-elimination and subsequent 2+2 addition to the imide. Intermediate **2**-HC≡CR complexes can be considered the equivalent of the alkane or arene complexes (**2**-RH) previously proposed. The exchange in eq 42 can be accommodated by Figure 11 provided the transition states for 1,2-elimination of RH (i.e., HC≡CPh) and R′H (i.e., HC≡C^{t}Bu) are considered energetically lower than the transition state pertaining to associative interchange (**II**). In vanadium,[27] titanium,[25] and zirconium systems,[22] azametallacyclobutene (e.g., (^{t}Bu$_3$SiO)$_2$TiC(Me)=C(Me)N-Si^{t}Bu$_3$)[25] complexes have been isolated and characterized, suggesting that **2**-HC≡CR may be energetically near **1**-C≡CR (R = Ph, ^{t}Bu). Related oxametallacyclobutenes of Cp$_2$Ti have recently been equilibrated with corresponding hydroxide acetylide complexes.[90]

Some other comments about the relative free energy of **1**-C≡CR are germane. When either **1**-C≡CPh or **1**-C≡C^{t}Bu are thermolyzed in C$_6$D$_6$ for prolonged periods, their amide sites are not deuterated, precluding reversible addition of benzene-d_6. Thermolysis (C$_6$D$_6$, 100 °C) of (^{t}Bu$_3$SiNH)$_3$ZrPh (**1**-Ph) in the presence of HC≡C^{t}Bu afforded **1**-C≡C^{t}Bu among other products, proving that a pathway exists between **1**-Ph and **1**-C≡C^{t}Bu. Estimates place the ground state of **1**-C≡C^{t}Bu at least ∼8.6 kcal/mol lower than the ground state **1**-Ph,[91] hence the overall barrier of 1,2-RC≡CH elimination and alkyne dissociation from putative **2**-RC≡CH may be insurmountable. Calculations of 1,2-HC≡CH elimination from **1′**-C≡CH revealed a large activation energy, and a significant interaction of the C$_\alpha$ with the zirconium center as abstraction of the amide hydrogen occurs, suggesting that a low energy pathway toward 2 + 2 addition to the resulting imide is plausible.[78]

Thermolysis (C$_6$D$_6$, 96.5 °C) of (^{t}Bu$_3$SiNH)$_3$ZrCy (**1**-Cy) generated **2** in the presence of HC≡CPh and HC≡C^{t}Bu, providing a 1.5:1.0 ratio of **1**-C≡CPh to **1**-C≡C^{t}Bu at low conversion (∼6%). The amide resonances of the two products were again clearly resolved, indicative of no exchange with C$_6$D$_6$. While only limited exploration of the alkynyl derivatives proved possible, the reactivity can be rationalized via the associative or dissociative exchange processes involving **2**-RC≡CH and **2**-RH complexes in Figure 11 (**II**), where the transition state for HC≡CR exchange with benzene is at lower energy than the transition state for 1,2-PhH-addition to give **1**-Ph. In addition, the transition state(s) for HC≡CPh exchange with HC≡C^{t}Bu occurs at significantly lower energy than their respective exchanges with benzene, and formation of **1**-C≡CR from **2**-RC≡CH occurs at lower energy than alkyne exchange.

Conclusions

Mechanistic Overview. Quantitative aspects of the 1,2-RH-elimination/addition events have enabled a greater understanding of the free energy surface, albeit with some ambiguity regarding the true character of intermediate states. Figure 11 serves to summarize the mechanistic understanding of this deceptively simple process. (^{t}Bu$_3$SiNH)$_3$ZrR (**1**-R) complexes possess strong metal−carbon bonds whose energetic differences (i.e., D(Zr−R) − D(Zr−R′)) nearly correspond to their respective hydrocarbon differences for a select group of R (R = ^{c}Pr, Ph, Ar, CH$_2$Ph, Me). The remaining **1**-R derivatives (R = Et, CH$_2$^{t}Bu, Cy) have ground states that are higher, probably as a result of the inductive and minor steric effects of additional α-alkyls. A system with greater versatility will be needed to answer a broader spectrum of questions concerning ground state stability and therefore C−H bond activation selectivity.[25]

In the rate-determining 1,2-RH-elimination event, the large primary KIEs are consistent with a linear, rather symmetric transition state (**2**-RH‡, **2**-R′H‡), yet one that is somewhat loose. The secondary KIE on CD$_3$H elimination supports calculations that portray the methyl as relatively undeformed in the transition state,[43,78,79] hence the R group is envisioned as rotating its σ-orbital into alignment as the ^{t}Bu$_3$SiNH unit functions as a weak acid, a reasonable consideration in view of strong N(pπ) → Zr(dπ) bonding by the amide. Geometric considerations and the calculations depict the hydrogen transfer as linear between N and R, and within bonding distance of the zirconium via utilization of an appropriate, empty Zr(dπ)-orbital.[92] According to the Hammond analysis, the transition state is generally late, but possesses a mixed composition, hence the ground state energy of **1**-R and its position along the reaction coordinate can both dramatically influence the transition state energy and $\Delta G^‡_{elim}$.

The correlation of $\Delta G^‡_{elim}$ with RH proton affinity suggests that tight binding of RH in the transition state for 1,2-RH-elimination expedites the elimination process and evokes the possibility of intermediate alkane complexes (**2**-RH, **2**-R′H). Calculations of hypothetical (H$_2$N)$_2$(HN)Zr(η^2-CH$_4$) at 373 K indicate a binding enthalpy of ∼ −6.3 kcal/mol[44] at 373 K relative to (H$_2$N)$_2$Zr=NH + CH$_4$, but the free energy for binding may be >0 kcal/mol, hence possible **2**-RH species are likely to

(90) Polse, J. L.; Andersen, R. A.; Bergman, R. G. *J. Am. Chem. Soc.* **1995**, *117*, 5393−5394.

(91) Assume that the prolonged thermolysis (C$_6$D$_6$, 24 h, 96.7 °C) of **1**-C≡C^{t}Bu (0.036 M) yields equilibrium amounts of **1**-(ND)$_x$-Ph-d_5 and HC≡C^{t}Bu and that the latter can be confidently detected if present in >5% (>(0.05)(0.036 M)). No evidence for HC≡C^{t}Bu was observed. Assuming the density of C$_6$D$_6$ (0.95 g/ml) is relatively insensitive to temperature, neat benzene-d_6 is ∼11.2 M. At equilibrium: $K \geq$ [C$_6$D$_6$][**1**-C≡C^{t}Bu]/[**1**-(ND)$_x$-Ph-d_5][HC≡C^{t}Bu] = [11.2][0.0342]/[0.0018]^2; K > 1.2 × 10^5 and $\Delta G^\circ \leq$ −8.6 kcal/mol.

(92) For related *ab initio* calculations probing methane activations of a different type, see: (a) Schreiner, P. R.; von Ragué Schleyer, Schaefer III, H. F. *J. Am. Chem. Soc.* **1993**, *115*, 9659−9666. (b) Olah, G. A.; Hartz, N.; Rasul, G.; Surya Prakash, G. K. *J. Am. Chem. Soc.* **1995**, *117*, 1336−1343.

be energetically similar to (^{t}Bu$_3$SiNH)$_2$Zr=NSi^{t}Bu$_3$ (**2**) + RH. Provided the acetylide derivatives, **1**-C≡CR (R = Ph, ^{t}Bu) can be described by a related free energy surface, the associative terminal alkyne exchange can be considered a limiting case of **2**-RH + R′H ⇌ **2**-R′H + RH, providing tentative support for intermediate alkane and arene complexes as weak solvates.

If **2**-RH(R′H) transients exist, exchange of bound hydrocarbons may take place with an intermediate of lower (3) or higher (5) coordination number (Figure 11, **I**) or without (**II**). Like classic interchange substitutions,[89] the latter pathway can have dissociative (e.g.,the **2**···RH is virtually broken as the R′H enters the coordination sphere) or associative (e.g., substantial **2**···R′H bonding has incurred as **2**···RH is starting to break) character (**II**). It should be noted that **2** could internally solvate itself via coordination of a peripheral methyl agostic bond, a possible intermediate *en route* to (^{t}Bu$_3$SiNH)$_2$ZrNHSi^{t}Bu$_2$CMe$_2$CH$_2$ (**3**), but thermodynamic parameters associated with this intramolecular solvation are difficult to estimate. Calculations on (H$_2$N)$_2$Zr=NH (**2′**) and (Me$_3$SiNH)$_2$Zr=NSiMe$_3$ (**2″**) suggest that (^{t}Bu$_3$SiNH)$_2$Zr=NSi^{t}Bu$_3$ (**2**) is likely to distort toward a pyramidal structure; in fact, the zirconium in **2′** and **2″** lies 0.04 and 0.32 Å above the N$_3$ plane, and Zr=N−Si deviates from linearity (165°).[78] Through distortion, d_{z^2}/p_z mixing can occur to enhance the electrophilic character of the orbital oriented toward the incoming hydrocarbon. Given the potent electropositive nature of low-coordinate zirconium, it is unlikely that **2** exists as an unsolvated pseudotrigonal species, hence internal solvation via an agostic effect or external solvation via substrate or solvent binding is most reasonable.

In viewing the activation of a bound hydrocarbon, it is informative to use (^{t}Bu$_3$SiNH)$_2$(THF)Zr=NSi^{t}Bu$_3$ (**2**-THF) as a model. Envision the pair of electrons in the R−H σ-bond being drawn into the coordination sphere by the empty d_{z^2}/p_z hybrid orbital, eventually binding in the position of the THF. In **2**-THF, the lone pair of the imide nitrogen is not significantly involved in N(pπ) → Zr(dπ) bonding, thus it may also be free to act as an internal base in the scission of the C−H bond in **2**-RH. Use of the lone pair on nitrogen enables the formal Zr=N π-bond to essentially remain intact as the R−H bond is broken, since that specific π-interaction correlates with a N(pπ) → Zr(dπ) bond of an amide that subsequently rotates to afford ground state **1**-R.

Hydrocarbon Selectivities. The quantitative hydrocarbon kinetic selectivity data (i.e., ^{c}PrH ≈ ArH [0.0 kcal/mol] > MeH [3.4] > PhCH$_2$H [4.0] > RH (R = Et, CH$_2$^{t}Bu, Cy)), while limited, exhibits some correspondence to the selectivities for oxidative addition attributed to [HB(3,5-dimethylpyrazoyl)$_3$]Rh(CNCH$_2$^{t}Bu) at −15 °C (i.e., PhH [0.0 kcal/mol] > HCH$_2$-3,5-Me$_2$C$_6$H$_3$ [0.15] > MeH [0.4] > ^{n}PeH [0.80] > ^{c}PeH [1.7] > CyH [1.8]),[3] but the magnitudes of each $\Delta\Delta G^{\ddagger}$ (relative to Ph−H) are significantly greater. Both groups of data are consistent with qualitative results of Cp*M(PMe$_3$) (M = Rh, Ir) systems,[34] where activation of PhH ≫ primary alkyl > cycloalkyl, although the $\Delta\Delta G^{\ddagger}$ (−60 °C) for benzene vs cyclohexane activation where M = Rh is only 1.2 kcal/mol, and the selectivity is substantially less for M = Ir.[70] Current data for (^{t}Bu$_3$SiO)$_2$Ti=NSi^{t}Bu$_3$ (i.e., 25 °C; PhH [0.0 kcal/mol] > MeH [1.0] > PhCH$_2$H [2.6]) reveal somewhat less selectivity than the zirconium system,[25] but it is still greater than the late metal derivatives. Selectivity differences for second-order σ-bond metatheses in the Cp*$_2$ScR system are difficult to quantify; using Cp*$_2$ScMe as the benchmark, benzene activation is ∼0.8 kcal/mol easier than that of methane.[9] Carbon-hydrogen bond activations by Cp*$_2$ThCH$_2$CMe$_2$CH$_2$ qualitatively follow a trend similar to those above.[11]

Similar selectivity trends in systems as disparate as d^8, 16 e$^-$, Tp′Rh(CNCH$_2$^{t}Bu), and Cp*Rh(PMe$_3$) in comparison to putative d^0 solvates of (^{t}Bu$_3$SiNH)$_2$Zr=NSi^{t}Bu$_3$ (**2**) and (^{t}Bu$_3$SiO)$_2$Ti=NSi^{t}Bu$_3$ suggest that properties of each hydrocarbon dictate its activation, but the subtleties and varying degrees of selectivity imply that metal centers can tune this reactivity. In the Tp′Rh(CNCH$_2$^{t}Bu) system, the hydrocarbon selectivities parallel the thermodynamic stabilities of the product Tp′Rh(CNCH$_2$^{t}Bu)(H)R complexes. In the zirconium imido system, benzylic activation is kinetically less favored than predicted on the basis of ground state stabilities, but this apparent discrepancy may be due to an anomalous ground state stabilization of **1**-CH$_2$-Ph. A perusal of these systems suggest that steric factors can contribute to substrate discrimination. The *bis*(amido)imido ligand arrangement of **2** (or **2**-RH) is likely to hinder substrate approach more than in solvates of (^{t}Bu$_3$SiO)$_2$Ti=NSi^{t}Bu$_3$, where the linear siloxides provide a more open electrophilic pocket. Both systems are likely to be less open than Tp′Rh(CNCH$_2$^{t}Bu), which is in turn more congested than Cp*Rh(PMe$_3$).

The rate-determining capture of RH by the late metal d^8 systems leads to an alkane adduct, which subsequently adds to the metal center. This contrasts with 1,2-RH-addition to the transient imido, where proposed alkane/arene complexes precede rate-determining C−H bond activation, an event with intrinsically greater selectivity. Rate-determining 1,2-RH-addition across the Zr=N unit of the reactive intermediate clearly requires greater substrate-specific orientation than rate-determining formation of alkane/alkene adducts prior to oxidative addition of RH to d^8 metal centers.[93] A system in which a greater number of substrates may be assessed is greatly needed in order to zero in on the critical factors affecting selectivity.[25]

Uncompetitive β-H-Elimination. β-Hydride elimination in **1**-R (R = Cy, ^{i}Bu, Et, ^{c}Pr) was not evidenced, although insertions of isobutylene, acetylene and 1,1-dimethylallene into the Zr−H bond of **1**-H proved such a pathway exists. The barrier for CH$_2$=CMe$_2$ insertion into **1**-H is estimated to be ∼15 kcal/mol at 100 °C in view of the swift (<20 min) insertion under pseudo-first-order conditions at 25 °C. Provided the transition state for 1,2-RH-elimination ($\Delta G^{\ddagger}$ = 27.7 ≈ 28 kcal/mol) from **1**-^{i}Bu is at least 3 kcal/mol lower than the β-H-elimination transition state, ΔH° for insertion is ≤−16 kcal/mol. Previous arguments ascribe the relative paucity of β-H-elimination to steric congestion (i.e., Cr(^{t}Bu$_4$))[94] or the absence of vacant *cis* coordination sites in tetrahedral molecules. Chisholm *et al.*[95] has proposed that strong X(pπ) → M(dπ) interactions raise the level of metal-based empty orbitals critical to accommodating the eliminating alkene. The cycle expressed above suggests that there is a pronounced endothermicity to a β-H-elimination event leading to free olefin, hence the stability of related metal alkyls (i.e., Cp$_2$MX(^{t}Bu),[96] (Me$_2$N)$_4$Ta^{t}Bu,[95] (^{t}Bu$_3$SiNH)(THF)^{t}BuTi=NSi^{t}Bu$_3$[23]) may be predominantly thermodynamic in origin. From an enthalpy cycle using ΔH_f° estimates for (CH$_3$)$_2$CHCH$_2^{\cdot}$ (14 kcal/mol) and isobutylene (−3.6 kcal/mol),[61] the difference in zirconium−hydride and −alkyl bond strengths (i.e., D(Zr−H) − D(Zr−C)) in this system is ≤18 kcal/mol.

Experimental Section

General Considerations. All manipulations were performed using either glovebox or high vacuum line techniques. Hydrocarbon solvents containing 1−2 mL of added tetraglyme were distilled under nitrogen

(93) Cundari, T. R. *J. Am. Chem. Soc.* **1994**, *116*, 340−347.
(94) Kruse, W. *J. Organomet. Chem.* **1972**, *42*, C39−42.
(95) Chisholm, M. H.; Tan, L.-S.; Huffman, J. C. *J. Am. Chem. Soc.* **1982**, *104*, 4879−4884.
(96) (a) Büchwald, S. L.; Kreutzer, K. A.; Fisher, R. A. *J. Am. Chem. Soc.* **1990**, *112*, 4600−4601. (b) Büchwald, S. L.; Lum, R. T.; Fisher, R. A.; Davis, W. M. *J. Am. Chem. Soc.* **1989**, *111*, 9113−9114.

from purple benzophenone ketyl and vacuum transferred from same prior to use. Benzene-d_6 and cyclohexane-d_{12} were dried over activated 4 Å molecular sieves, vacuum transferred, and stored under N_2; THF and THF-d_8 were dried over sodium benzophenone ketyl. All glassware was base-washed and oven dried, and NMR tubes were additionally flamed under dynamic vacuum. Methane, ethane, ethylene, allene, cyclopropane, and isobutylene (Matheson) were typically passed through a −78 °C trap prior to use. ^{t}Bu$_3$SiNHLi, (^{t}Bu$_3$SiNH)$_3$ZrCl (**1**), (^{t}Bu$_3$SiNH)$_3$ZrMe (**1**-Me), and (^{t}Bu$_3$SiNH)$_3$ZrH (**1**-H) were prepared according to published procedures.[45]

^{1}H and ^{13}C {^{1}H} NMR spectra were obtained using Varian XL-200, XL-400, VXR-400S, and UNITY-500 spectrometers. Infrared spectra were recorded on a Mattson FT-IR interfaced to an AT&T PC7300 computer or a Perkin Elmer 299B spectrophotometer. Analyses were performed by Texas Analytical Labs, Stafford, TX or Oneida Research Services, Whitesboro, NY. We have had difficulty obtaining satisfactory analyses of the complexes containing the ^{t}Bu$_3$SiNH ligand,and they have been difficult to analyze; low carbon percentages (by 1−2%) are typical, while the hydrogen and nitrogen numbers are sporadic, despite use of various burning aids. The failures may be due in part from partial decomposition of the ^{t}Bu$_3$SiNH ligand to SiC and Si_3N_4 during combustion.[97]

Procedures. 1. General (^{t}Bu$_3$SiNH)$_3$ZrR (1-R) from 1-Cl and RMgX or RLi. To an appropriately sized flask containing a slurry of **1**-Cl in ethereal solvent at −78 °C was added a solution of RMgX or RLi by syringe under Ar counterflow. In certain cases, solid Grignard or lithium reagents were mixed with **1**-Cl in the flask, and the solvent, either ethereal or hydrocarbon, was added at −78 °C via distillation. The mixture was allowed to warm to 25 °C over the course of ∼2 h and stirred for an additional 8−12 h at 25 °C. Upon removal of the volatiles, hexane was added to the residue. The slurry was filtered, and the filter cake was washed repeatedly with hexanes and concentrated. Cooling to −78 °C afforded colorless, microcrystalline **1**-R in variable yields upon isolation by filtration; sometimes an additional crop was taken.

a. (^{t}Bu$_3$SiNH)$_3$ZrC$_2$H$_5$ (1-Et). **1**-Cl (1.556 g, 2.02 mmol) in 25 mL of Et$_2$O and 1.06 mL of EtMgBr in ether (2.0 M, 2.12 mmol) gave 882 mg of **1**-Et (57%); a second crop yielded 235 mg (77% total): IR (Nujol, cm^{-1}) 3248 (w), 1360 (m), 1060 (s), 1006 (m), 942 (m), 872 (w), 815 (s), 721 (w), 610 (s). Anal. Calcd for $ZrC_{38}H_{89}N_3Si_3$: C, 59.77; H, 11.75; N, 5.50. Found: C, 59.61; H, 11.86; N, 5.38.

b. (^{t}Bu$_3$SiNH)$_3$ZrC$_6$H$_{11}$ (1-Cy). **1**-Cl (500 mg, 0.649 mmol) in 10 mL of Et$_2$O and 0.36 mL of cyclohexyl magnesium chloride in ether (2.0 M, 0.715 mmol) gave 250 mg **1**-Cy (46%): IR (Nujol, cm^{-1}) 3230 (w), 1580 (w), 1360 (m), 1069 (s), 1008 (m), 960 (w), 939 (m), 861 (w), 810 (s), 720 (w), 612 (s). Anal. Calcd for $ZrC_{42}H_{95}N_3Si_3$: C, 61.69; H, 11.71; N, 5.14. Found: C, 65.21; H, 10.86; N, 4.83.

c. (^{t}Bu$_3$SiNH)$_3$ZrCH$_2$Ph (1-CH$_2$Ph). **1**-Cl (950 mg, 1.234 mmol) in 15 mL of THF and 0.65 mL of benzyl magnesium chloride in ether (2.0 M, 1.30 mmol) gave 356 mg **1**-CH$_2$Ph (35%): IR (Nujol, cm^{-1}) 3238 (w), 1655 (w), 1598 (m), 1365 (m), 1205 (m), 1165 (w), 1152 (w), 1068 (s), 1030 (m), 1011 (m), 990 (m), 932 (m), 872 (w), 810 (s), 742 (m), 721 (w), 695 (m), 610 (s). Anal. Calcd for $ZrC_{43}H_{91}N_3Si_3$: C, 62.55; H, 11.11; N, 5.09. Found: C, 61.18; H, 11.29; N, 5.27.

d. (^{t}Bu$_3$SiNH)$_3$ZrCH═CH$_2$ (1-CH═CH$_2$). **1**-Cl (510 mg, 0.662 mmol) in 20 mL of ether and 0.35 mL of vinyl magnesium bromide in ether (2.0 M, 0.695 mmol) gave 282 mg **1**-CH═CH$_2$ (56%): IR (Nujol, cm^{-1}) 3245 (w), 1550 (w), 1535 (w), 1360 (m), 1050 (s), 1010 (m), 930 (m), 870 (w), 810 (s), 715 (w), 610 (s). Anal. Calcd for $ZrC_{38}H_{87}N_3Si_3$: C, 59.93; H, 11.51; N, 5.52. Found: C, 59.77; H, 11.75; N, 5.50.

e. (^{t}Bu$_3$SiNH)$_3$Zr(η^3-CH$_2$CHCH$_2$) (1-allyl). **1**-Cl (514 mg, 0.667 mmol) in 10 mL of ether and 0.67 mL of allyl magnesium bromide in ether (1.0 M, 0.670 mmol) gave 163 mg of off-white **1**-allyl (32%): IR (Nujol, cm^{-1}) 3244 (w), 1608 (w), 1565 (w), 1545 (w), 1360 (m), 1069 (s), 1010 (m), 942 (m), 869 (w), 815 (s), 721 (w), 610 (s). Anal. Calcd for $ZrC_{39}H_{89}N_3Si_3$: C, 60.39; H, 11.56; N, 5.42. Found: C, 60.23; H, 11.65; N, 5.38.

f. (^{t}Bu$_3$SiNH)$_3$ZrC$_6$H$_5$ (1-Ph). **1**-Cl (560 mg, 0.729 mmol) in 20 mL of ether and 0.39 mL of phenyl magnesium bromide in ether (2.0 M, 0.76 mmol) gave 350 mg of **1**-Ph (59%). Typical syntheses involved C−H bond activation. Thermolysis of variable amounts of **1**-R at 100 °C in a glass bomb reactor containing C_6H_6 (the time was dependent on R) induced 1,2-RH-elimination to give **2**, which was subsequently trapped by benzene to give **1**-Ph in yields >75% when isolated as above: IR (Nujol, cm^{-1}) 3239 (w), 1358 (m), 1125 (m), 1065 (s), 1008 (m), 930 (m), 872 (w), 810 (s), 718 (m), 695 (m), 642-(w), 610 (s). Anal. Calcd for $ZrC_{42}H_{89}N_3Si_3$: C, 62.15; H, 11.05; N, 5.18. Found: C, 58.08; H, 10.92; N, 4.88.

g. (^{t}Bu$_3$SiNH)$_3$ZrCH$_2$^{t}Bu (1-CH$_2$^{t}Bu). **1**-Cl (510 mg, 0.662 mmol) and ^{t}BuCH$_2$Li (57 mg, 0.728 mmol) reacted in 20 mL of ether to afford 274 mg of **1**-CH$_2$^{t}Bu (51%): IR (Nujol, cm^{-1}) 3221 (w), 1360 (m), 1228 (m), 1210 (w), 1188 (w), 1065 (s), 1006 (m), 929 (m), 870 (w), 810 (s), 610 (s). Anal. Calcd for $ZrC_{41}H_{95}N_3Si_3$: C, 61.12; H, 11.88; N, 5.21. Found: C, 61.23; H, 11.95; N, 5.11.

h. (^{t}Bu$_3$SiNH)$_3$ZrCCPh (1-CCPh). **1**-Cl (478 mg, 0.621 mmol) and PhCCLi (73 mg, 0.675 mmol) reacted in 20 mL of THF to afford 210 mg of **1**-CCPh as an orange powder (41%): IR (Nujol, cm^{-1}) 3258 (w), 2082 (s), 1595 (w), 1574 (w), 1366 (m), 1208 (m), 1060 (s), 1010 (m), 1005 (m), 942 (m), 876 (w), 815 (s), 758 (w), 686 (m), 620 (s). Anal. Calcd for $ZrC_{44}H_{89}N_3Si_3$: C, 63.24; H, 10.73; N, 5.03. Found: C, 62.36; H, 10.86; N, 4.95.

i. (^{t}Bu$_3$SiNH)$_3$ZrCC^{t}Bu (1-CC^{t}Bu). **1**-Cl (344 mg, 0.446 mmol) and ^{t}BuCCLi (39 mg, 0.446 mmol) reacted in 15 mL of benzene, but a ^{1}H NMR spectrum of the mixture revealed 60% completion; 30 mg of ^{t}BuCCLi 0.341 mmol) was added to ultimately give 285 mg of **1**-CC^{t}Bu as a yellow powder (81%): IR (Nujol, cm^{-1}): 3265 (w), 2090 (m), 1367 (m), 1250 (m), 1207 (w), 1136 (w), 1055 (s), 1012 (m), 943 (m), 876 (w), 815 (s), 932 (w), 620 (s). Anal. Calcd for $ZrC_{42}H_{93}N_3Si_3$: C, 61.84; H, 11.49; N, 5.14. Found: C, 61.62; H, 11.58; N, 5.06.

j. (^{t}Bu$_3$SiNH)$_3$Zr(η^3-BH$_4$) (1-BH$_4$). **1**-Cl (318 mg, 0.413 mmol) and LiBH$_4$ (90 mg, 4.13 mmol) reacted in 6 mL of benzene to afford 274 mg of **1**-BH$_4$ (56%): IR (Nujol, cm^{-1}) 3228 (w), 2530 (m), 2150 (m), 2210 (m), 1360 (m), 1201 (m), 1061 (s), 1006 (m), 929 (m), 876 (w), 805 (s), 610 (s). Anal. Calcd for $ZrBC_{36}H_{88}N_3Si_3$: C, 57.70; H, 11.84; N, 5.61. Found: C, 57.58; H, 11.89; N, 5.56.

2. (^{t}Bu$_3$SiNH)$_3$Zr-^{c}C$_3$H$_5$ (1-^{c}Pr). To a 200 mL glass bomb containing **1**-Cy (333 mg, 0.407 mmol) was added 40 mL of cyclohexane via vacuum transfer. Cyclopropane was admitted (∼20 equiv, 1 atm), and the vessel was placed in a 95 °C bath for 4 h. After cooling to 25 °C, the volatiles were removed. The solid was dissolved in 5 mL of hexane, and the solution was filtered, concentrated, and cooled to −78 °C. White crystalline **6**-^{c}Pr was collected by filtration (110 mg, 35%, 5% impurities, chiefly (^{t}Bu$_3$SiNH)$_4$Zr (**3**)): IR (Nujol, cm^{-1}) 3245 (w), 1535 (w), 1358 (m), 1060 (s), 1008 (m), 928 (m), 860 (w), 810 (s), 717 (w), 610 (s). Anal. Calcd for $ZrC_{39}H_{90}N_3Si_3$: C, 60.31; H, 11.68; N, 5.41. Found: C, 60.22; H, 11.74; N, 5.38.

3. (^{t}Bu$_3$SiNH)$_3$Zr-CH$_2$C$_6$H$_3$-3,5-Me$_2$ (1-Mes). To a 50 mL glass bomb containing **1**-CH$_3$ (516 mg, 0.688 mmol) was added 7 mL of mesitylene via vacuum transfer. The vessel was placed in a 95 °C bath for 8 h and cooled to 25 °C. The volatiles were removed under vacuum, and the solid was dissolved in 5 mL of hexane and filtered. The solvent was removed, and the product was dissolved in ether. The solution was cooled to −78 °C, giving white, crystalline **1**-Mes, which was collected by filtration (371 mg, 62%): IR (Nujol, cm^{-1}) 3234 (w), 1600 (m), 1365 (m), 1295 (m), 1160 (m), 1075 (s), 1012 (m), 989 (w), 932 (m), 876 (m), 820 (s), 722 (w), 696 (m), 620 (s). Anal. Calcd for $ZrC_{45}H_{95}N_3Si_3$: C, 63.16; H, 11.19; N, 4.91. Found: C, 62.66; H, 11.16; N, 4.66.

4. (^{t}Bu$_3$SiNH)$_4$Zr (1-NHSi^{t}Bu$_3$). a. From 1-Me. To a flask containing **1**-Me (610 mg, 0.814 mmol) was added 25 mL of cyclohexane by vacuum distillation. The solution was brought to reflux for 10 h and then cooled. The volatiles were removed, and the yellow residue was taken up in pentane and filtered. The volatiles were again removed, and the residue was dissolved in 3 mL of THF. Cooling to −78 °C gave white microcrystals of **3**, which were collected by filtration (150 mg, 0.204 mmol, 25%). **b. From 1-Cl.** To a glass bomb

(97) Sample ^{1}H and ^{13}C{^{1}H} NMR spectra of selected derivatives are included in the supporting information for ref 21.

(98) *Solubility Data Series*; Kertes, A. S., Ed.; Pergamon Press, London; Vol. 27/28 (Methane).

(99) Cromer, D. T.; Mann, J. B. *Acta Crystallogr., Sect. A* **1968**, *A24*, 321−324.

(100) $R = \sum||F_o| - |F_c||/(\sum|F_o|)$; $R_w = \{\sum w(|F_o| - |F_c|)^2/\sum w(|F_o|)^2\}^{1/2}$; GOF = $\{\sum[\text{weight}(|F_o| - |F_c|)^2]\}/(M - N)$ where M = number of observations and N = number of parameters; 3257 (88.9%) reflections with $|F_o| \geq 3\sigma(F_o)$.

containing ^{t}Bu$_3$SiNHLi (0.175 g, 0.791 mmol) and **1**-Cl (0.607 g, 0.788 mmol) was distilled 25 mL of hexanes at −78 °C. The reactor was then heated at 145 °C for 48 h leading to the precipitation of LiCl. This white mixture was then filtered and extracted once with 10 mL of hexanes. The solution was then concentrated and cooled to −78 °C, giving a colorless crystalline **1**-NHSi^{t}Bu$_3$ which was collected by filtration (0.646 g, 86%): IR (Nujol, cm^{-1}) 3218 (w), 1360 (m), 1066 (s), 1008 (m), 930 (m), 790 (s), 722 (w), 620 (s). Anal. Calcd for $ZrC_{48}H_{112}N_4Si_4$: C, 58.95; H, 11.40; N, 5.73. Found: C, 58.32; H, 11.63; N, 4.74.

5. (^{t}Bu$_3$SiNH)$_2$ZrN(H)Si^{t}Bu$_2$C(Me)$_2$CH$_2$ (3). A vessel containing 209 mg of **1**-Me (0.279 mmol) was attached to a needle valve and heated at 125 °C under dynamic vacuum for 10 h. After cooling, white, powdered **3** was collected. ^{1}H NMR showed 5% **1**-NHSi^{t}Bu$_3$ as an impurity: IR (Nujol, cm^{-1}) 3250 (w), 3228 (w), 1365 (m), 1195 (w), 1172 (w), 1065 (s), 1010 (m), 942 (m), 810 (s), 725 (w), 620 (s). Anal. Calcd for $ZrC_{36}H_{84}N_3Si_3$: C, 58.95; H, 11.40; N, 5.73. Found: C, 55.46; H, 10.79; N, 4.47.

6. (^{t}Bu$_3$SiNH)$_3$ZrCH$_2$CHMe$_2$ (1-^{i}Bu). To a thick-walled vessel containing a frozen solution of **1**-Me (734 mg, 0.979 mmol) in 50 mL of cyclohexane was admitted 1 atm H_2 at −195 °C. The solution was thawed, and the bomb was placed in a 105 °C bath for 8 h to generate **1**-H. The volatiles were removed, and the residue was placed in a small flask and dissolved in 15 mL of hexanes. The flask was opened to the vacuum manifold and exposed to 0.8 atm isobutylene. The uptake of isobutylene (the gas pressure in the manifold was monitored by manometer) was complete after 20 min. After stirring for 3 h, the solvent volume was reduced to ∼3 mL, and a white powder was collected by filtration at 20 °C (116 mg, 15% overall yield): IR (Nujol, cm^{-1}) 3228 (w), 1360 (m), 1065 (s), 1010 (m), 929 (m), 870 (m), 810 (s), 721 (w), 610 (s). Anal. Calcd for $ZrC_{40}H_{93}N_3Si_3$: C, 60.76; H, 11.85; N, 5.31. Found: C, 60.30; H, 11.81; N, 4.93.

7. (^{t}Bu$_3$SiNH)$_3$Zr(η^1-CH$_2$CH=CMe$_2$) (1-dma). To a flask containing a frozen solution of **1**-H (270 mg, 0.367 mmol) in 15 mL of benzene was added 1.1 equiv of dimethylallene (36.7 mL at 204 Torr) by condensation. The needle valve was closed, and the solution was stirred at 25 °C for 3 h. Upon removal of the volatiles, the residue was dissolved in ∼10 mL hexanes, concentrated to ∼2 mL, cooled to −78 °C, and filtered to afford **1**-dma as a white powder (71 mg, 24%): IR (Nujol, cm^{-1}) 3228 (w), 1690 (w), 1638 (w), 1608 (w), 1360 (m), 1193 (w), 1065 (s), 1010 (m), 932 (m), 810 (s), 726 (w), 692 (w), 610 (s). Anal. Calcd for $ZrC_{41}H_{93}N_3Si_3$: C, 61.27; H, 11.66; N, 5.23. Found: C, 61.22; H, 11.61; N, 5.28.

8. (^{t}Bu$_3$SiNH)$_2$(THF)Zr=NSi^{t}Bu$_3$ (2-THF). To 730 mg of **1**-Me (0.975 mmol) in an 80 mL bomb (dried at 150 °C under vacuum for 8 h) was added 20 mL of benzene by vacuum transfer. The vessel was placed in a 100 °C bath for 10 h. After cooling, the volatiles were removed, and a crude ^{1}H NMR spectrum verified the residue was clean **1**-Ph. THF (20 mL) was added to the bomb by distillation, and the vessel was heated at 100 °C for 0.75 h. The cooled solution was transferred to a flask, and the solvent was removed and replaced with hexanes. Reducing the volume to ∼5 mL and cooling to −78 °C resulted in the precipitation of **2**-THF, collected as a white powder by filtration: IR (Nujol, cm^{-1}): 3260 (w), 1540 (w), 1365 (m), 1175 (w), 1045 (s), 1012 (m), 934 (m), 912 (w), 868 (m), 830 (s), 723 (w), 605 (s). Anal. Calcd for $ZrOC_{40}H_{92}N_3Si_3$: C, 59.63; H, 11.38; N, 5.22. Found: C, 58.79; H, 11.15; N, 4.93.

9. (^{t}Bu$_3$SiNH)$_2$(Et$_2$O)Zr=NSi^{t}Bu$_3$ (2-OEt$_2$). To a flask containing crude **1**-H (1.33 g, 1.80 mmol) was distilled 20 mL of ether at −78 °C; H_2 evolution immediately ensued. The reaction mixture continued to effervesce as it warmed to 25 °C and was maintained at 25 °C for 1 h. Upon removal of the volatiles, the residue was taken up in 12 mL of hexanes and filtered, and the solution volume was reduced to 5 mL. Cooling the solution to −10 °C gave colorless crystals of **2**-OEt$_2$ that were collected by filtration (0.602 g, 41%).

10. (^{t}Bu$_3$SiNH)$_3$ZrOCH$_2$CH$_3$ (1-OEt). To a glass bomb containing 225 mg of **1**-Cy (0.275 mmol) was distilled ∼3 mL of Et$_2$O and ∼12 mL of *n*-heptane. The reactor was heated at 115 °C for 16 h and cooled to 25 °C. The solvent was removed in vacuo leaving a crystalline solid that was dissolved in hexanes, filtered, and crystallized at −78 °C to afford 165 mg of colorless **1**-OEt (79%).

11. NMR Tube Reactions. Oven and flame-dried 5 mm NMR tubes were sealed onto 14/20 ground glass joints, charged with reagents in the dry box, and brought out on needle valve adapters. Deuterated solvents were distilled into the tubes under vacuum, and the samples were freeze−pump−thaw degassed (−196 °C). Any gases or volatile liquids were subsequently admitted via calibrated gas bulbs when exact amounts were needed (measured via manometer) or via lecture bottles. The tubes were then sealed using a torch. **Example: Equilibration of 1-Ph and 1-^{c}Pr.** An NMR tube sealed to a 14/20 ground glass joint was charged with **1**-Cy (24 mg, 29 mmol). The tube was attached to a gas bulb and evacuated. C_6D_{12} (0.7 mL) was vacuum transferred into the tube and freeze−pump−thaw degassed. Benzene was added (280 Torr in 12.7 mL, 0.194 mmol, 6.6 equiv), followed by cyclopropane (44 Torr in 12.7 mL, 0.030 mmol, 1.0 equiv), and the tube was sealed with a torch. Thermolysis of the mixture at 96.7 °C for 14 h gave equilibrium quantities of C_6H_6, **1**-Ph, C_3H_6, and **1**-^{c}Pr which were integrated to give $K = ([C_6H_6][\mathbf{1}\text{-}^c\text{Pr}]/[C_3H_6][\mathbf{1}\text{-Ph}] = 1.57(33)$.

General Kinetics. 1. 1,2-RH-Elimination from 1-R. Solutions of **1**-R in the appropriate deuterated solvent were prepared in 2-mL volumetric flasks. Three samples of about 0.6 mL each were transferred to flame-dried, 5-mm NMR tubes sealed to 14/20 joints and attached to 180° needle valves. The tubes were freeze−pump−thaw degassed three cycles (77 K) and flame-sealed under vacuum. The three sample tubes were simultaneously heated by immersion in a polyethylene glycol bath with a Tamson immersion circulator. The typical bath temperature of 96.7 °C was stable to ±0.2 °C. Rates of disappearance of amido NH peaks were monitored in all cases except for the benzene loss from **1**-Ph (see text) and the determination of k_H/k_D pertaining to (^{t}Bu$_3$SiNH)$_3$ZrMe (**1**-Me) vs (^{t}Bu$_3$SiND)$_3$ZrMe (**1**-(ND)$_3$Me). Separate tubes of these complexes were measured in tandem by the disappearance of the methyl resonance. Similarly, the isotope effect pertaining to (^{t}Bu$_3$SiNH)$_3$ZrPh (**1**-Ph) vs (^{t}Bu$_3$SiND)$_3$ZrPh (**1**-(ND)$_3$-Ph) was monitored by following the phenyl ortho hydrogens, and the k_H/k_D for (^{t}Bu$_3$SiNH)$_3$ZrCH$_2$Ph (**1**-CH$_2$Ph) vs (^{t}Bu$_3$SiND)$_3$ZrCH$_2$Ph (**1**-(ND)$_3$-CH$_2$Ph) was monitored by the disappearance of the methylene resonance. All runs were monitored for 5−6 half-lives. Single transient spectra were used to obtain the most reproducible integrals. The data collection, rates, and uncertainties were obtained by using weighted ($1/\sigma^2$, where σ was obtained from three simultaneous runs if available) or unweighted, nonlinear least-squares fitting to the exponential form of the rate expression.

2. Equilibrium of 1-CH$_2$Ph and 1-C$_6$H$_4$Me. A 0.033 M solution of (^{t}Bu$_3$SiNH)$_3$ZrMe (**1**-Me) in toluene was thermolyzed at 96.7 °C for 1 h (1,2-MeH elimination of **1**-Me was ∼20% complete). The solvent was removed, and a ^{1}H NMR spectrum revealed ∼1% **1**-CH$_2$-Ph and ∼99% **1**-C$_6$H$_4$Me as determined from the ratio of CH_2 to CH_3 integrals. The latter was identified as a mixture of *para* (^{1}H NMR (tentative assignments, C_6D_6) δ 2.55 (CH_3, s, 3H), 4.45 (NH, s, 1 H), 8.10, 8.24 (ArH, A_2B_2, J = 6.3 Hz, 4 H) and *meta* or *ortho* (^{1}H NMR (tentative assignments, C_6D_6) δ 2.28 (CH_3, s, 3H), 5.05 (NH, s, 1 H), 7.09 (ArH, m, 1H), 8.20 (ArH, m, 3H) isomers and was treated collectively (see text). Thermolysis for an additional 8 h (∼4 half-lives) resulted in a dramatic change in the product ratios, which remained constant with further heating (i.e., ∼38% **1**-CH$_2$Ph and ∼62% **1**-C$_6$H$_4$Me).

3. Competitive activation of C$_6$H$_6$ and CH$_4$. To each of three tubes was added 20 mg of **1**-Cy (0.024 mmol). The tubes were individually evacuated and C_6D_{12} condensed into each, followed by 2 equiv of C_6H_6 (0.048 mmol) as measured by gas bulb. Next, a known amount of CH_4 was condensed into each tube which then contained the following, according to ^{1}H NMR spectra: tube 1, 0.69 mL, [**1**-Cy] = 0.035 M, [C_6H_6] = 0.071 M, [CH_4] = 0.099 M; tube 2, 0.77 mL, [**1**-Cy] = 0.031 M, [C_6H_6] = 0.064 M, [CH_4] = 0.120 M; tube 3, 0.66 mL, [**1**-Cy] = 0.036 M, [C_6H_6] = 0.074 M, [CH_4] = 0.120 M. The methane concentration was calculated using its standard concentration in cyclohexane at a partial pressure of 1 atm at 100 °C[9,98] and Henry's law. Calculated methane concentrations at 25 °C were accurate in comparison to the ^{1}H NMR spectra. Thermolysis at 97.5 °C ensued, and the reaction was stopped after 17% conversion. The [**1**-Me]/[**1**-Ph] ratio at low conversion represents $k_{MeH}[\mathbf{2}][CH_4]/k_{PhH}[\mathbf{2}][C_6H_6]$, permitting calculation of k_{MeH}/k_{PhH} and $\Delta\Delta G^{\ddagger}$ = 3.4 kcal/mol as an average of the three trials.

Single-Crystal X-ray Diffraction Analysis of (^{t}Bu$_3$SiNH)$_2$(THF)-Zr=NSi^{t}Bu$_3$ (2-THF). A colorless needle (0.3 × 0.3 × 0.3 mm) of (^{t}Bu$_3$SiNH)$_2$(THF)Zr=NSi^{t}Bu$_3$ (**2**-THF), obtained from benzene solu-

tion, was sealed in a capillary. Preliminary X-ray diffraction photographs revealed monoclinic symmetry. Precise lattice constants, determined from a least-squares fit of 15 diffractometer-measured 2Θ values at 25 °C, were $a = 13.312(5)$ Å, $b = 18.268(6)$ Å, $c = 20.551(7)$ Å, $\beta = 92.30(3)°$. The cell volume was 4994(3) Å^3, with a calculated density of 1.072 g/cm, where $Z = 4$. The space group was determined to be $P2_1/n$, and the asymmetric unit consisted of $C_{40}H_{91}N_3OSi_3Zr$. All unique diffraction maxima ($+h,+k,\pm l$) with $2\Theta < 45°$ were measured on a Nicolet R3m/V automated diffractometer, by a variable-speed, $2\Theta-\Theta$ scan (2.00−29.30°/min in ω) with graphite-monochromated Mo-Kα radiation ($\lambda = 0.71069$ Å) at 25 °C. After correction for Lorentz, polarization, and background effects, 4675 (71.3%) of the unique data (3967) were judged observed ($|F_o| > 3\sigma|F_o|$).[99] All heavy atoms were located using direct methods (SHELXTL PLUS), and all non-hydrogen atoms were revealed by successive Fourier syntheses. Full-matrix, least-squares refinements (minimization of $\sum w(F_o - F_c)^2$, where w is based on counting statistics modified by an ignorance factor ($w^{-1} = \sigma^2(F) + 0.0015F^2$)), with anisotropic heavy atoms and all hydrogens included at calculated positions (Riding model, fixed isotropic U), converged (3967 reflections) to $R = 7.70\%$ and $R_w = 9.12\%$, with GOF = 1.46.[100] A final difference Fourier map revealed no peaks greater than 0.74 e$^-$/Å^3.

Calculations. 1. AM1 Calculations of Proton Affinities. AM1 calculations were performed using the AMPAC-IBM program on the Cornell National Supercomputer Facility. All bond lengths and angles were left unconstrained. A charge of +1 was used for the protonated alkanes, and GEO-OK conditions allowed the inclusion of five-coordinate carbon. Calculations were performed on both the protonated alkanes and the corresponding unprotonated alkanes (neopentane, isobutane, toluene, mesitylene; also, calculations were checked against literature values for methane, cyclopropane and cyclohexane).[87,88] The heats of formation were then used to determine the proton affinity by

$$PA = -[\Delta H_f°(RH_2^+) - \Delta H_f°(RH) - \Delta H_f°(H^+)] \qquad (43)$$

eq 43. In all cases protonation was site-specific; the carbon which would be bonded to the metal in the corresponding zirconium hydrocarbyl was chosen as the site of protonation (e.g., the benzylic carbon in toluene). The initial symmetry of the protonated carbon was assigned as C_{2v} for the benzyls, and C_s for all other cases.

Acknowledgment. Primary support from the National Science Foundation (CHE-9218270) is gratefully acknowledged as are contributions from the Air Force Office of Scientific Research (AFOSR-87-0103), Cornell University, and the NSF-REU Program (CCC). We thank Prof. Barry K. Carpenter, Prof. Alan S. Goldman, Dr. William Tumas, and Dr. Farad Abu-Hasanyan for helpful discussions. Dr. Jeffrey B. Bonanno, Dr. Steven M. Baxter, and Mr. David Fuller are thanked for experimental assistance and Dr. Gregory D. Van Duyne for aid in the crystallographic study. We thank Prof. Theodore L. Brown and Prof. Mary Caffery for sharing the results of molecular mechanics calculations prior to publication. Support for the Cornell NMR Facility from the NIH and NSF Instrumentation Programs is acknowledged.

Supporting Information Available: X-ray structural information pertaining to (^{t}Bu$_3$SiNH)$_2$(THF)Zr=NSi^{t}Bu$_3$ (**2**-THF): a summary of crystal data encompassing data collection and solution/refinement, atomic coordinates, isotropic and anisotropic temperature factors, hydrogen atom coordinates, bond lengths, and bond angles (9 pages); table of observed and calculated structure factors (24 pages). This material is contained in many libraries on microfiche, immediately follows this article in the microfilm version of the journal, can be ordered from the ACS, and can be downloaded from the Internet; see any current masthead page for ordering information and Inernet access instructions.

JA950745I